

DEVELOPMENT OF CONSTRUCTION AND DEMOLITION WASTE-BASED  
ENGINEERED GEOPOLYMER COMPOSITES WITH SELF-HEALING  
CAPABILITY

A THESIS SUBMITTED TO  
THE GRADUATE SCHOOL OF NATURAL AND APPLIED SCIENCES  
OF  
MIDDLE EAST TECHNICAL UNIVERSITY

BY

HÜSEYİN ULUGÖL

IN PARTIAL FULFILLMENT OF THE REQUIREMENTS  
FOR  
THE DEGREE OF DOCTOR OF PHILOSOPHY  
IN  
CIVIL ENGINEERING

SEPTEMBER 2021



Approval of the thesis:

**DEVELOPMENT OF CONSTRUCTION AND DEMOLITION WASTE-BASED ENGINEERED GEOPOLYMER COMPOSITES WITH SELF-HEALING CAPABILITY**

submitted by **HÜSEYİN ULUGÖL** in partial fulfillment of the requirements for the degree of **Doctor of Philosophy in Civil Engineering, Middle East Technical University** by,

Prof. Dr. Halil Kalıpçılar  
Dean, Graduate School of **Natural and Applied Sciences**

Prof. Dr. Ahmet Türer  
Head of the Department, **Civil Engineering**

Prof. Dr. İsmail Özgür Yaman  
Supervisor, **Civil Engineering, METU**

**Examining Committee Members:**

Prof. Dr. Murat Güler  
Civil Engineering, METU

Prof. Dr. İsmail Özgür Yaman  
Civil Engineering, METU

Assoc. Prof. Dr. Serdar Göktepe  
Civil Engineering, METU

Prof. Dr. Mustafa Şahmaran  
Civil Engineering, Hacettepe University

Assoc. Prof. Dr. Tahir Kemal Erdem  
Civil Engineering, Marmara University

Date: 01.09.2021

**I hereby declare that all information in this document has been obtained and presented in accordance with academic rules and ethical conduct. I also declare that, as required by these rules and conduct, I have fully cited and referenced all material and results that are not original to this work.**

Name Last name : Hüseyin Ulugöl

Signature :

## **ABSTRACT**

### **DEVELOPMENT OF CONSTRUCTION AND DEMOLITION WASTE-BASED ENGINEERED GEOPOLYMER COMPOSITES WITH SELF-HEALING CAPABILITY**

Ulugöl, Hüseyin  
Doctor of Philosophy, Civil Engineering  
Supervisor : Prof. Dr. İsmail Özgür Yaman

September 2021, 138 pages

Construction and demolition waste (CDW) has been a popular alternative to mainstream precursors (fly-ash, slag, metakaolin, etc.) for geopolymerization. Its chemical content also has a promising future for self-healing behavior, which is strikingly important for sustainability. Engineered Geopolymer Composites (EGCs) meet one of the important requirements of self-healing with its limited crack width.

In this thesis study, CDW-based materials were evaluated in the context of both geopolymer production and EGC development. Besides, the self-healing performance of EGCs has also been assessed. The first stage of this study was the development of the geopolymer paste with a single CDW content. Thus, the usability of each CDW material in geopolymer production was determined. After determining the optimum conditions for CDW-based materials, geopolymer pastes with multi-CDW based materials were developed as the second stage of this dissertation study. In the third stage, concrete waste was also utilized as recycled concrete aggregate in the production of geopolymer mortar. In the last part of the study, EGCs with fiber addition were developed. Optimum fiber content was set to obtain a deflection hardening behavior. Preloading EGCs were exposed to wetting-drying cycles to

perform a self-healing process in laboratory conditions. Electrical impedance and water absorption measurements and optical observations were used to assess the self-healing process. In addition, mechanical recoveries were determined at the end of the healing period. Optical observations and microstructural investigations were carried out to justify the findings.

All results showed that EGCs generated with CDW-based materials have the capability of self-healing. Optical observations and microstructural investigations exhibit that many cracks were filled with  $\text{CaCO}_3$ ,  $\text{Na}_2\text{CO}_3$  and geopolymerization reaction products. Line mapping analyses show that recycled concrete aggregate can participate in geopolymerization reactions and relatively higher interfacial transition zone characteristics can be obtained. According to the water absorption results, the pore volume of geopolymers may be increased with raising maturity, unlike cementitious systems. On the other hand, it was also found out that parameters that raise the rate of early geopolymerization may limit the self-healing performance.

Keywords: Engineered Geopolymer Composites, Self-healing, Alkali-activated Materials, Construction and Demolition Waste

## ÖZ

# KENDİ KENDİNİ İYİLEŞTİRME YETENEĞİNE SAHİP İNŞAAT YIKINTI ATIĞI BAZLI TASARLANMIŞ GEOPOLİMER KOMPOZİTLERİN GELİŞTİRİLMESİ

Ulugöl, Hüseyin  
Doktora, İnşaat Mühendisliği  
Tez Yöneticisi: Prof. Dr. İsmail Özgür Yaman

Eylül 2021, 138 sayfa

İnşaat ve yıkıntı atıkları (İYA), geopolimerizasyon için popüler olan hammaddelere (uçucu kül, cüruf, metakaolin, vb.) popüler bir alternatif olmuştur. Kimyasal içeriği, sürdürülebilirlik için son derece önemli olan kendi kendini iyileştirme davranışı için de gelecek vaat etmektedir. Tasarlanmış Geopolimer Kompozitler (TGK'lar), sınırlı çatlak genişliği ile kendi kendini iyileştirmenin en önemli gereksinimlerinden birini karşılar.

Bu tez çalışmasında İYA bazlı malzemeler hem geopolimer üretimi hem de TGK geliştirme amacıyla kullanılmıştır. Ayrıca TGK'ların kendi kendini iyileştirme performansı da değerlendirilmiştir. Çalışmanın ilk aşamasında, tek bir çeşit İYA'dan geopolimer hamurları geliştirilmiştir. Böylece İYA bazlı malzemelerin geopolimer üretiminde kullanılabilirliği çalışmanın en başında belirlenmiştir. İYA bazlı malzemeler için optimum koşullar belirlendikten sonra, bu tez çalışmasının ikinci aşaması olarak birden fazla İYA bazlı malzeme içeren geopolimer hamurlar geliştirilmiştir. Üçüncü aşamada beton atıkları da çalışmaya dahil edilerek geopolimer harç üretiminde geri dönüştürülmüş beton agregası olarak kullanılmıştır.

Çalışmanın son bölümünde, lif içerikli TGK'lar geliştirildi. Şekil değiştirme sertleşmesi davranışı elde etmek için optimum fiber içeriği tespit edildi. Ön yüklenmiş TGK'lar, ıslatma-kurutma döngülerine maruz bırakılarak laboratuvar koşullarında kendi kendini iyileştirme işlemi simüle edildi. Belirli zamanlarda elektriksel empedans ve su emme ölçümleri ve optik gözlemler gerçekleştirildi. Ayrıca iyileşme süresi sonunda mekanik iyileşmeler de belirlendi. Sonuçları desteklemek üzere mikroyapısal analizler de gerçekleştirildi.

Tüm sonuçlar, İYA bazlı malzemelerle üretilen TGK'ların kendi kendini iyileştirme kapasitesine sahip olduğunu gösterdi. Optik gözlemler ve mikroyapısal araştırmalar, birçok çatlağın  $\text{CaCO}_3$ ,  $\text{Na}_2\text{CO}_3$  ve geopolimerizasyon reaksiyon ürünleri ile dolduğunu göstermektedir. Çizgi haritalama analizleri, geri dönüştürülmüş beton agregasının geopolimerizasyon reaksiyonlarına katılabileceğini ve görel olarak daha iyi agrega arayüzey geçiş bölgesi özellikleri elde edilebileceğini göstermektedir. Su emme sonuçları, artan olgunluğun çimentolu sistemlerden farklı olarak geopolimerlerin boşluk hacmini arttırabileceğini göstermektedir. Diğer yandan erken geopolimerizasyon hızını arttıran unsurların kendi kendini iyileştirme performansını sınırlayabileceği görülmüştür.

Anahtar Kelimeler: Tasarlanmış Geopolimer Kompozitler, Kendiliğinden İyileşme, Alkali İle Aktive Edilmiş Malzemeler, İnşaat Ve Yıkıntı Atığı



To My Family,

## ACKNOWLEDGMENTS

First of all, I would like to express my gratitude to my thesis advisor, Prof. Dr. İsmail Özgür Yaman, who has supported me throughout my thesis studies. For me, being his student was a great privilege and honor. Likewise, with his academic and intellectual guidance, I will always remember his kindness and supporting character.

I would like to thank Prof. Dr. Mustafa Şahmaran, whose expertise was invaluable in solving the problems and building up methodology. His sophisticated knowledge and feedback pushed me to improve my thinking and brought my work to a higher level.

I also want to thank Prof. Dr. Murat Güler, Assoc. Prof. Dr. Serdar Göktepe, Assoc. Prof. Dr. Tahir Kemal Erdem and Assoc. Prof. Dr. Gürkan Yıldırım for their valuable time and recommendations to make my thesis better. I would also like to thank Dr. Burhan Aleessa Alam, who did not turn me down whenever I asked for his help, despite his busyness, and contributed significantly to completing my thesis.

My special thanks are for the help of my colleagues Muhammed Faruk Günal and Anıl Kul.

Last but not least, I wish to thank my wife, Özlem Ulugöl and my mother Elifhan Güneş, who gave me endless support, motivation and patience. I would have never accomplished this degree without their support.

This work is partially funded by Scientific and Technological Research Council of Turkey under grant numbers TÜBİTAK 218M102 and 117M447.

## TABLE OF CONTENTS

ABSTRACT.....	v
ÖZ .....	vii
ACKNOWLEDGMENTS .....	x
TABLE OF CONTENTS.....	xi
LIST OF TABLES .....	xiv
LIST OF FIGURES .....	xvi
LIST OF ABBREVIATIONS.....	xix
LIST OF SYMBOLS .....	xxi
CHAPTERS	
1 INTRODUCTION .....	1
1.1 General .....	1
1.2 Aim & Research Questions .....	4
1.3 Scope of the Study.....	4
2 LITERATURE REVIEW .....	5
2.1 Geopolymerization Reaction Mechanism .....	5
2.2 Environmental Advantages and Disadvantages .....	7
2.3 Alkaline Activators .....	8
2.3.1 Alkali Hydroxides .....	9
2.3.2 Alkali Silicates .....	10
2.4 Chemical content and crystal structure .....	11

2.5	Precursors of geopolymerization .....	13
2.5.1	Slag .....	13
2.5.2	Fly-ash .....	14
2.5.3	Natural pozzolans and metakaolin.....	15
2.5.4	Construction and demolition waste as a precursor .....	16
2.6	Self-healing capability of geopolymers and EGC .....	18
2.6.1	Self-healing in cementitious systems .....	19
2.6.2	Engineered cementitious composites .....	21
2.6.3	Engineered geopolymer composites.....	22
3	EXPERIMENTAL STUDY .....	25
3.1	Materials .....	25
3.1.1	Construction and demolition waste-based materials and slag.....	25
3.1.2	Sand .....	36
3.1.3	Alkaline activators.....	37
3.1.4	Fiber.....	40
3.2	Method.....	41
3.2.1	Determination of Si, Al and Ca ions availability .....	42
3.2.2	Geopolymer paste preparation with single CDW and testing .....	43
3.2.3	Geopolymer paste preparation with multi CDW and testing .....	45
3.2.4	Geopolymer mortar preparation and testing.....	46
3.2.5	Engineered geopolymer composite preparation and testing.....	48
4	RESULTS AND DISCUSSION.....	57
4.1	Geopolymer pastes with single CDW-based material .....	57
4.1.1	Compressive strength .....	57

4.1.2	Microstructural analyses of single geopolymers pastes.....	62
4.2	Geopolymer pastes with binary CDW-based material.....	71
4.2.1	Compressive strength.....	71
4.3	Geopolymer mortars with single CDW-based material and recycled concrete aggregate.....	78
4.4	Mechanical properties and self-healing capability of EGCs.....	84
4.4.1	Compressive strength.....	84
4.4.2	Transportation properties.....	85
4.4.3	Optical investigation.....	96
4.4.4	Mechanical properties after self-healing.....	99
4.4.5	Microstructural investigations.....	102
5	SUMMARY, CONCLUSIONS AND RECOMMENDATIONS.....	111
	REFERENCES.....	117
	CURRICULUM VITAE.....	137

## LIST OF TABLES

### TABLES

Table 3.1 Chemical content of CDW-based materials and slag .....	28
Table 3.2 Particle size specifications of slag and CDW-based materials.....	29
Table 3.3 Definitions of minerals existing XRD diffractograms .....	30
Table 3.4 Physical properties of recycled concrete aggregate .....	37
Table 3.5 Chemical content of NaOH in pellet form .....	38
Table 3.6 Specifications of calcium hydroxide .....	39
Table 3.7 Chemical content and specifications of sodium silicate solution.....	40
Table 3.8 Specifications of fibers .....	41
Table 3.9 Dissolution rate of CDW-based materials.....	42
Table 3.10 Geopolymer paste compositions with single precursor.....	44
Table 3.11 Geopolymer paste compositions with binary precursor .....	45
Table 3.12 Geopolymer mortar compositions .....	47
Table 3.13 EGC Mixture Designs .....	50
Table 4.1 Compressive strength results of geopolymer pastes (28 days) with single CDW-based precursor content .....	59
Table 4.2 Optimum curing temperatures according to maximum compressive strength results.....	60
Table 4.3 Single geopolymer paste strength's Pearson correlations with curing period, temperature and concentration .....	62
Table 4.4 Compressive strength results of geopolymer pastes (28 days) with binary CDW-based precursor content .....	72
Table 4.5 Binary geopolymer paste strength's Pearson correlations with curing period, temperature and molarity .....	77
Table 4.6 Compressive strength results of geopolymer mortars (28 days) with CDW-based precursors and recycled concrete aggregate .....	79
Table 4.7 Geopolymer mortar strength's Pearson correlations with aggregate size, curing temperature, molarity and water to binder ratio .....	80

Table 4.8 Compressive strength results of EGCs .....	85
Table 4.9 Electrical impedance results .....	88

## LIST OF FIGURES

### FIGURES

Figure 1.1. Binder classifications according to aluminum and calcium content.....	2
Figure 2.1. Graphical illustration of simplified geopolymerization mechanism (van Deventer <i>et al.</i> , 2007) .....	6
Figure 2.2. Relationship between viscosity, concentration and molar ratio of sodium silicate solution (Vail and Wills, 1952) .....	10
Figure 2.3. Structure with network formers and network modifiers .....	12
Figure 2.4. Alkali-activated fly-ashes' ternary diagram showing the relationship between compressive strength and chemical content (Provis and Bernal, 2014)....	15
Figure 2.5. Reasons for autogenous self-healing of cementitious systems (Reinhardt <i>et al.</i> , 2013).....	21
Figure 2.6. Strain-hardening behavior of ECC (Heiman and Koerstz, 1991) .....	22
Figure 3.1. CDW-based materials in bulk, crushed and ground form red clay brick (a), roof tile (b), hollow brick (c), glass waste (d), concrete waste (e).....	26
Figure 3.2. Particle size distributions of CDW-based materials .....	29
Figure 3.3. Crystallographic structures of red clay brick waste (a), hollow brick waste (b), roof tile waste (c), glass waste (d), .....	32
Figure 3.4. Scanning electron microscopy images of red clay brick waste (a), hollow brick waste (b) and roof tile waste (c), (images on left and right side have magnifications of 1000× and 5000× respectively) .....	34
Figure 3.5. Scanning electron microscopy images of glass waste (a), concrete waste (b) and slag (c), (images on left and right side have magnifications of 1000× and 5000× respectively) .....	35
Figure 3.6. Particle size distribution of recycled fine aggregate utilized in EGC ...	36
Figure 3.7. Alkaline activators (a) NaOH, (b) Na <sub>2</sub> SiO <sub>3</sub> and (c) Ca(OH) <sub>2</sub> .....	37
Figure 3.8. Fibers tested in the thesis work .....	40
Figure 3.9. Preparing ICP-OES specimens .....	42
Figure 3.10. Cubic geopolymer paste specimens .....	44



Figure 3.11. Preloading of (a) prismatic- and (b) disc specimens, and (c) cracks formed after preloading.....	52
Figure 3.12. Electrical impedance testing device .....	54
Figure 3.13. 1 – time curve (ASTM C1585-11, 2011) .....	55
Figure 3.14. Midpoint displacement recording with deflectometer.....	56
Figure 4.1. XRD patterns of HB raw material (rm) and alkali-activated HB for 12% Na and 24 h of curing at different temperatures .....	63
Figure 4.2. XRD patterns of RCB raw material (rm) and alkali-activated RCB with 12% Na for different curing conditions .....	64
Figure 4.3. SEM images and EDX results of alkali-activated HB cured for 24 h, temperatures and Na ratio of (a) 85 °C and 10% (b) 115 °C and 10% (c) 115 °C and 12% (d) 125 °C and 12% .....	66
Figure 4.4. SEM images and EDX results of alkali-activated HB cured for 72 h, temperatures and Na ratio of (a) 85 °C and 10% (b) 115 °C and 10%.....	67
Figure 4.5. SEM images and EDX results of alkali-activated RCB activated with 12% Na and cured at temperatures and curing period of (a) 105 °C and 24 h (b) 105 °C and 72 h (c) 115 °C 24 h (d) 115 °C 72 h.....	68
Figure 4.6. TGA & DTA graphics of single geopolymer pastes .....	70
Figure 4.7. SEM images of aggregate paste connection.....	82
Figure 4.8. (a) Zoomed area of previous figure [2000×] (b) mapping analysis of line through both aggregate, interfacial transition zone and paste.....	83
Figure 4.9. Graphical representation of electrical impedance results .....	89
Figure 4.10. Typical misleading efflorescence on specimen (a) before and (b) after sprinkling water .....	91
Figure 4.11. Absorption results of EGCs.....	95
Figure 4.12. Optical images of specimens (S1, S2 and S3) on the 7 <sup>th</sup> , 28 <sup>th</sup> , 56 <sup>th</sup> , and 90 <sup>th</sup> days .....	97
Figure 4.13. Optical images of specimens (S4, S5 and S6) on the 7 <sup>th</sup> , 28 <sup>th</sup> , 56 <sup>th</sup> , and 90 <sup>th</sup> days .....	98

Figure 4.14. Mechanical recovery of EGCs (1 – preloading, 2 – reloading, 3 – reference).....	100
Figure 4.15. XRD diffractograms of matrix (black) and healed cracks (gray) .....	104
Figure 4.16. (a) SEM image of healed crack, (b) line-scan analysis images with (c) 5000× and (d) 40000× magnification of red dashed marked area, and (e) EDX analysis .....	107
Figure 4.17. SEM images of S2 specimen showing formations of (a) sodium carbonate, (b) calcium carbonate, (c) sodium carbonate and calcium carbonate together, and (d) unreacted brick particle .....	109

## LIST OF ABBREVIATIONS

### ABBREVIATIONS

AAM	Alkali-activated material
C	Concrete waste
CDW	Construction and demolition waste
DTA	Differential thermal analysis
ECC	Engineered cementitious composite
EDX	Energy dispersive x-ray analysis
EGC	Engineered geopolymer composite
EI	Electrical impedance
FRC	Fiber-reinforced concrete
FRCA	Fine recycled concrete aggregate
G	Glass waste
HB	Hollow brick waste
HPFRC	High-performance fiber-reinforced concrete
ITZ	Interfacial transition zone
NM	Nylon-mono
PE	Polyethylene
PVA	Polyvinyl alcohol
RCB	Red clay brick waste
RT	Roof tile waste

S	Slag
SEM	Scanning electron microscopy
SSA	Specific surface area
TGA	Thermogravimetric analysis
WA	Water absorption
XRD	X-ray diffraction analysis

## LIST OF SYMBOLS

### SYMBOLS

A	Aluminum oxide
C	Calcium oxide
H	Water molecule
J	Joule
K	Potassium oxide
M	Alkali ion
N	Sodium oxide
Q	Quartz
S	Silicon dioxide
$\Omega$	Ohm



## **CHAPTER 1**

### **INTRODUCTION**

#### **1.1 General**

With the increasing population and industrialization, the use of concrete and consequently the production of it has increased all over the world. There are many reasons that make it one of the best choices as a construction material, such as high compressive strength, being easy to shape, durability, being affordable and easily reachable. Low tensile strength, brittleness and lack of ductility are considered conventional concrete's weak points. Different types of concrete, such as Fiber-reinforced Concrete (FRC), High-performance Fiber-reinforced Concrete (HPFRC), Reinforced Ultra-high Performance Concrete (RUHP), Engineered Cementitious Composites (ECCs), have been developed to overcome these weak points. Strain-hardening and strain-softening characteristics of these special types of concretes make them more ductile and increase their toughness. Although these special types of concretes are called concrete, these materials generally do not contain coarse aggregate, and the aggregate portion consists of completely fine materials. As a result, the volume of binder need increases that induces a rise in cement production demand.

Globally, the carbon dioxide emission of the cement industry is the third largest one among all industries that release carbon into the atmosphere (Andrew, 2017). Local raw material consumption of cement production emerges as a problem, such that production of 1 tonne of portland cement clinker requires 1.7 tonnes of raw materials (Zhang and Xu, 2010). Also, it is reported that there is a 6% of increment in cement demand yearly (UNEP Global Environmental Alert Service, 2012). This situation

makes researchers consider developing environmentally friendly binders. Geopolymer, which is a subset of alkali-activated materials (AAMs), has become a popular alternative to cement. As shown in Figure 1.1, geopolymer is a type of alkali-activated material with low or no calcium content. However, the term ‘geopolymer’ is rarely used for all types of alkali-activated materials in the literature.

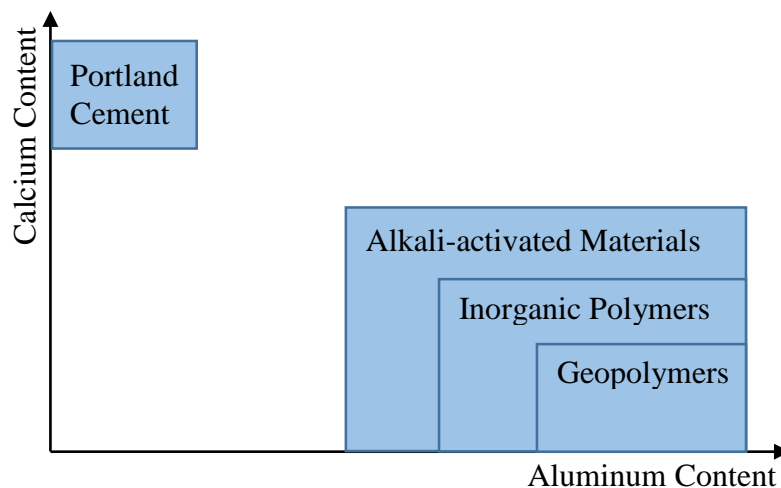


Figure 1.1. Binder classifications according to aluminum and calcium content

Alkali-activated materials are formed by the reaction between a raw material called precursor and an alkaline solution. The most popular precursors for alkali-activation are fly ash (Ding, Dai and Shi, 2016; Zhao, Liu, Wang, *et al.*, 2019), ground granulated blast furnace slag (Manjunath, Narasimhan and Umesha, 2019), metakaolin (Poulesquen, Frizon and Lambertin, 2011) and natural pozzolans (Ibrahim *et al.*, 2017). The aforementioned materials are already utilized in the cement industry. However, environmental awareness and sustainable production require the utilization of idle materials and the protection of raw materials. Construction and Demolition Waste (CDW) is one of the significant problems that the construction industry faces. In this context, alkali-activation of CDW-based materials is very important in terms of both carbon dioxide emission reduction and raw material consumption.



Demolition, renovation or repairing of construction generates inert (metals, timber, wood and plastics) and non-inert (soil, concrete and brick) waste materials that must be disposed of or utilized. In 2016, 374 Mt of CDW were generated in European Union (EU) countries (Wahlstrom, Bergmans, Teittinen, Bacher, Smeets and Anne Paduart, 2020). Turkey, an associated member of the EU, has above 6.5 million structures to be renovated and demolished through urban transformation. CDW is not only a problem for EU countries, but also is trouble for other countries, such as 100 Mt of CDW were generated each year in United States (Mills, Showalter and Jarman, 1999). Such a large amount of CDW-based material needs to be disposed off. CDW has already been utilized in landfilling for subgrades (Zhang *et al.*, 2020), soil applications (Suluguru *et al.*, 2019), road foundations (Tavira *et al.*, 2020) in non-selected form. In these applications, CDW-based materials are used in the form that exists in the demolition area, i.e., going through without any selection. However, the selection of these materials makes their utilization more specific. For example, it was shown in the literature that alkali-activation of concrete (Robayo-Salazar, Rivera and Mejía de Gutiérrez, 2017; Mahmoodi *et al.*, 2021), glass (Vafaei and Allahverdi, 2017), brick (Robayo-Salazar, Rivera and Mejía de Gutiérrez, 2017; Mahmoodi *et al.*, 2020b) and ceramic tile (Mahmoodi *et al.*, 2020a) is very feasible.

Despite the fact that most geopolymers have higher durability properties, the cracking tendency is one of the drawbacks. The crack filling and sealing capability of binders is called self-healing in the literature. Self-healing is not limited to cementitious materials (Engineered Geopolymer Composites – ECC); the self-healing capability of geopolymers was studied in the literature (Kan *et al.*, 2019; Guo and Yang, 2020; Zhang, Suleiman and Nehdi, 2020). Fiber containing geopolymer with the self-healing capability is called Engineered Geopolymers Composites (EGC).

## **1.2 Aim & Research Questions**

The aim of this thesis is threefold:

- To develop a geopolymer based binder using CDW
- To utilize the binder in the production of EGC
- To assess the self-healing performance of EGC

Research questions at the beginning of the study were:

- Is it possible to produce geopolymers entirely using construction and demolition waste?
- How to design geopolymer composites with fibers to achieve controlled multiple micro crack formation?
- How to provide to the geopolymer the ability of self-healing?
- Even if there is a complete crack healing, to what extent does self-healing improve the mechanical properties?

## **1.3 Scope of the Study**

The problem that this study focuses on is explained in chapter 1. Chapter 2 presents a detailed literature review about the thesis study's scope under six sections. The first section describes the reaction mechanism of geopolymerization. The second one is about alkaline activators and commonly used ones are detailed in this section. Chemical content and crystalline structure are explained in the fourth section. Chapter five presents detailed information about CDW-based precursors. Studies concentrated on EGC and their self-healing performance are presented in chapter six.

Chapter 3 presents experimental studies under four sections containing paste, mortar, EGC productions and self-healing process. Chapter 4 presents results obtained from pastes, mortars and EGCs, separately. Chapter 5 summarizes the facts and findings of the study. Also, it gives recommendations for future studies.

## **CHAPTER 2**

### **LITERATURE REVIEW**

As mentioned before, geopolymers and alkali-activated materials are considered as an alternative binder for concrete. Unlike the cementitious systems, parameters that affect geopolymer performance are much more complex, such as type and molarity of alkaline activator, curing conditions and precursor content. For this reason, the literature review is presented in five sections.

#### **2.1 Geopolymerization Reaction Mechanism**

Inorganic alkali aluminosilicate polymer, briefly called geopolymer, is a binder material consisting of a raw material called precursor, and an alkali activator, which attracts attention with its potential to be an alternative to cement or cementitious materials in general. The reaction that forms the binding material takes place between a solid aluminosilicate and a highly concentrated aqueous solution. Being an alternative is not only in the context of being a complete binder but also being a replacement material to the cementitious systems. While cement hydration starts with the water, geopolymerization is triggered by the alkaline solution, which can be in different forms and molarities, as detailed in section 2.2. The formation mechanism of geopolymers is generally divided into two according to their chemical content related to calcium availability. While the alkali-activation reaction mechanism of aluminosilicate precursors with low or no calcium content is easy to understand, the calcium-containing precursor's reaction is more complex.

Geopolymerization of aluminosilicate-containing precursors is started by the dissolution of this solid phase. Higher pH provided by the alkaline solution dissolves

and depolymerizes aluminosilicate species in the precursor. Silica ( $\text{SiO}_4$ ) and alumina ( $\text{AlO}_4$ ) tetrahedrals in precursor react with hydroxyl ions ( $\text{OH}^-$ ) coming from alkaline activator and generate silica  $[\text{Si}(\text{OH})_4^-]$  and alumina  $[\text{Al}(\text{OH})_4^-]$  monomers. The releasability of monomers is largely dependent on Si/Al ratio (Duxson, Provis, *et al.*, 2005) and amorphicity of the precursor, such that, the solubility of amorphous silicate structure is 45 times higher than those of crystalline ones (Iler, 1979). Monomers combine with each other and result in oligomer formation. Afterwards, some of these oligomers form an amorphous aluminosilicate structure depending on the environmental properties and chemical content, while the other part forms a zeolite-like crystal structure. High Si/Al ratio changes crystalline structure to an amorphous form (Provis, Lukey and van Deventer, 2005). Figure 2.1 illustrates the simplified model of geopolymerization. It should be noted that this reaction mechanism is an entirely simplified conceptual model for geopolymers with low/no calcium content.

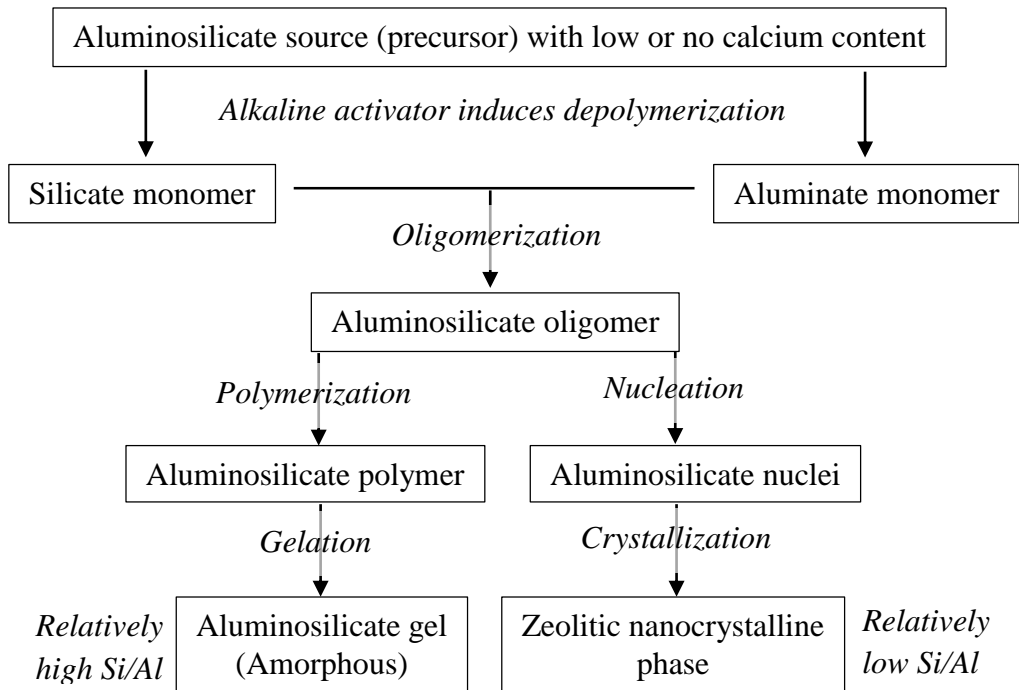


Figure 2.1. Graphical illustration of simplified geopolymerization mechanism (van Deventer *et al.*, 2007)

## 2.2 Environmental Advantages and Disadvantages

Geopolymers are referred to have the potential to compensate for the environmental disadvantageous of portland cement and concretes. According to the literature, up to 80% of CO<sub>2</sub> emissions can be inhibited by utilizing geopolymers as a binding material (Duxson, Provis, *et al.*, 2007). However, life cycle analysis is preferable to assess the environmental effect of geopolymers. In this context, it is hard to compare geopolymers and conventional concretes because of their chemical content variety, such as different alkaline activators and precursors of geopolymers and several pozzolanic materials that can be used in cement production. Habert *et al.* (2011) showed that fly ash- and slag-based geopolymers with sodium hydroxide and sodium silicate as activators have a less global warming effect than conventional concrete. However, replacing metakaolin with fly ash and slag further increases the global warming effect because of the thermal processing of metakaolin and finally exceeds the effect of conventional concrete. Another parameter that affects the environmental issues of geopolymers is the alkaline activator. Sodium hydroxide and sodium silicate are the most common activators, while the first one requires electricity consumption and the latter needs processing at higher temperatures, ~1400 °C (Myers, 2003). Consequently, it can be said that LCA analysis of geopolymers has more complexity than conventional concrete. Because of the variance in parameters of geopolymers (i.e., several activators with different concentrations, various precursors and curing regimes), LCA results are affected so much. When LCA is evaluated, the parameters below were used in the literature:

- Abiotic Depletion for Fossil Fuels (ADPF) [kg Sb eq.]
- Climate Change (Global Warming Potential - GWP) [kg CO<sub>2</sub> eq.]
- Acidification Potential (AP) [kg SO<sub>2</sub> eq.]
- Eutrophication Potential (EP) [kg PO<sub>4</sub> eq.]
- Photochemical Oxidants Formation (POF) [kg C<sub>2</sub>H<sub>4</sub> eq.]
- Ozone Depletion (ODP) [kg CFC-11 eq.]

Salas et al. (2018) conducted a study comparing the LCA of both conventional concrete and geopolymer concrete. LCA results of these concretes, which both aimed at 15 MPa of compressive strength, showed that conventional concrete has lower AP, ODP and POF results than geopolymer. However, geopolymer concrete has lower ADPF, EP and GWP results than conventional concrete. While Salas et al. (2018) exhibit that a higher difference between ADPF results of conventional concrete and geopolymer concrete. However, Weil et al. (2009) inferred that difference between ADPF of geopolymer and conventional concrete is incredibly slight.

### **2.3 Alkaline Activators**

Unlike the hydration of cementitious systems, which are induced by the presence of water, geopolymers need an alkaline species in aqueous form. In this context, an alkaline activator can be simply defined as the solution that dissolves the aluminosilicate-containing precursor. In the literature, alkaline activators are grouped into six different classes seen below (Shi, Krivenko, Pavel and Roy, 2005). Here, ‘M’ indicates the alkali component.

- Alkali hydroxides [or caustic alkali solutions] (MOH)
- Alkali silicates ( $M_2O.nSiO_2$ )
- Aluminosilicates ( $M_2O.Al_2O_3.(2-6)SiO_2$ )
- Aluminates ( $M_2O.nAl_2O_3$ )
- Strong acids without silicate ( $M_2SO_4$ )
- Weak acids without silicate ( $M_2CO_3, M_2SO_3, M_3PO_4, MF$ )

Although six different types of activators exist, the most commonly used ones are the first and second types (caustic alkali solutions such as NaOH, KOH, etc. and silicates such as  $Na_2SiO_3$ , etc.).

### 2.3.1 Alkali Hydroxides

Despite the fact that cesium, rubidium and lithium hydroxides, which are rare substances, can be used in large-sized structural members (Provis, 2009), NaOH and KOH are the most popular ones with their dissolution heat and viscosity (Provis and Bernal, 2014). Geopolymers activated with hydroxides have higher workability than counterparts activated with silicates, under favor of lower viscosity of hydroxides. Also, higher dimensional stability of fly ash activated with hydroxide is reported (Provis *et al.*, 2009). However, the production process of alkali hydroxides, consisting of electrolytic reactions of chloride salts, requires energy and is responsible for carbon dioxide emissions (Weidema, 2000). Moreover, the necessity of high-temperature curing is seen as a technical constraint (Criado, Palomo and Fernandez-Jimenez, 2005) for hydroxide-activated fly ash, which has a relatively low reactivity unless molarity is up to 14 M (Somna *et al.*, 2011). Alkali hydroxide activation results in higher porosity in the context of both pore volume and average pore radius than sodium silicate and sodium carbonate activated geopolymers (Shi, 1996). The phenomenon of efflorescence is also an adverse outcome of NaOH activation. Efflorescence is generated from the carbonation of alkali species in the pore solution with CO<sub>2</sub> from the atmosphere (Djobo *et al.*, 2017). White deposits on the specimen surface indicate the formation of Na<sub>2</sub>CO<sub>3</sub> as a result of efflorescence. Although it has been reported that the sodium amount should not exceed 4% to mitigate the efflorescence (Allahverdi, Mehrpour and Najafikani, 2008), as abovementioned such low concentration is not enough for sufficient geopolymerization, especially for air curing. To overcome this situation, many researchers prefer to use NaOH together with Na<sub>2</sub>SiO<sub>3</sub> (Razak *et al.*, 2015; Mohseni, 2018).

### 2.3.2 Alkali Silicates

Although alkali silicates mostly refer to sodium silicates or potassium silicates in the literature; the former is seen much more than the latter. Sodium silicate ( $\text{Na}_2\text{SiO}_3$ ) is obtained as a lump by heating  $\text{Na}_2\text{CO}_3$  (soda ash) and silica sand together, while commercial sodium silicate ( $\text{Na}_2\text{SiO}_3 \cdot \text{H}_2\text{O}$ ) is obtained by dissolving these lumps in water under pressure at elevated temperatures (Fawer, Concannon and Rieber, 1999). In the literature,  $\text{Na}_2\text{SiO}_3$  is, therefore, generally refers to sodium silicate solution, also called water glass. Reactivity of sodium silicates originated from the presence of  $\text{Si}(\text{OH})_4$  monomers (Provis and van Deventer, 2007) which introduce higher alkalinity into the system than alkali hydroxides. While numbers of linked monomers are increased, silica species are called  $\text{Q}^0$  [ $\text{SiO}_4$  monomer],  $\text{Q}^1$  [ $(\text{SiO}_4)_2\text{O}$  dimer],  $\text{Q}^2$  [ $(\text{SiO}_4)_3$  trimer],  $\text{Q}^3$  [ $(\text{SiO}_4)_4$  tetramer],  $\text{Q}^4$  [ $(\text{SiO}_4)_5$  pentamer] (Lunevich *et al.*, 2016).

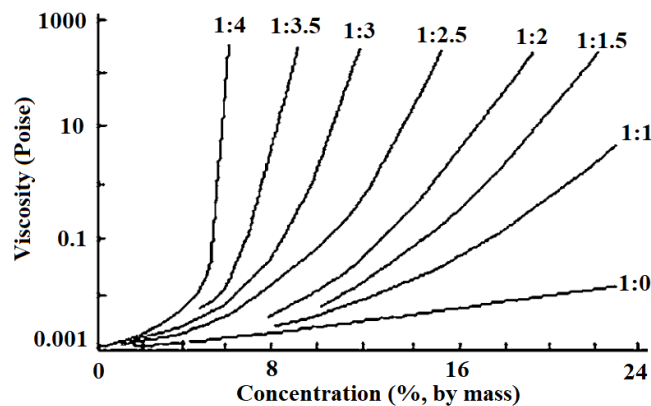


Figure 2.2. Relationship between viscosity, concentration and molar ratio of sodium silicate solution (Vail and Wills, 1952)

One of the significant problems facing researchers who want to use sodium silicate as an activator is their higher viscosity. Although potassium silicates have lower viscosity than sodium silicates, both of them have higher viscosity than sodium hydroxides. Figure 2.2 reveals the change in viscosity of sodium silicate solution depending on the concentration and molar ratio. As can be seen, different solutions



with identical modulus ( $\text{SiO}_2/\text{M}_2\text{O}$  molar ratio, where M refers to alkali metal such as Na or K) values have a threshold concentration, above which the slope of the graphic is rapidly increasing.

## 2.4 Chemical content and crystal structure

One of the most significant differences of geopolymers from cementitious systems and one of the problematic points of designing materials for geopolymers is that there are many factors affecting the chemical composition of the system. Because of the existence of various types of activators, as mentioned in the previous section, the ultimate composition of geopolymer may be varied. While hardened properties of geopolymers are affected by chemical content and crystal structure, fresh properties and strength development characteristics are also dependent on these parameters.

The chemical variety of alkali-activated systems are sourced from both different alkaline activators and various precursors. Therefore, rather than the chemical content percentages, an evolution parameter called modulus is often defined. One of the most used is the silica modulus that refers to the molar ratio of  $\text{SiO}_2$  to  $\text{Na}_2\text{O}$  exist in the activator. In the context of workability, increasing silica modulus may result in an increment in viscosity and consequently leads to a reduction in workability (Vail and Wills, 1952).

Si/Al is another crucial ratio that generally takes values between 1.15 and 2.15 (Duxson, Provis, *et al.*, 2005). It has been reported that Si/Al lower than 1.40 results in the formation of a highly porous structure. However, an increase in Si/Al ratio make pore structure homogenous and reduce the pore volume (Duxson, Fernandez-Jimenez, *et al.*, 2007) and consequently raise strength. The reason for this situation is the higher energy of Si-O-Si (siloxo) bonds than Al-O-Al and Si-O-Al (sialate) (Jong and Brown, 1980). However, Si/Al higher than 1.90 interrupts the strength development because the unreacted species behave like defects.

Al is known to have a great effect on geopolymerization reactions. Both amount and solubility of aluminum are parameters that affect the strength development property, setting specifications, durability and microstructure. As mentioned before, alkali activation is affected by many parameters because of its kinetically controlled mechanism. Such as solubility of ions are dependent on pH of the solution, free ions released from other components and temperature. Therefore, the solubility of aluminum, which affects geopolymerization, is not only dependent on itself but also depends on other factors.

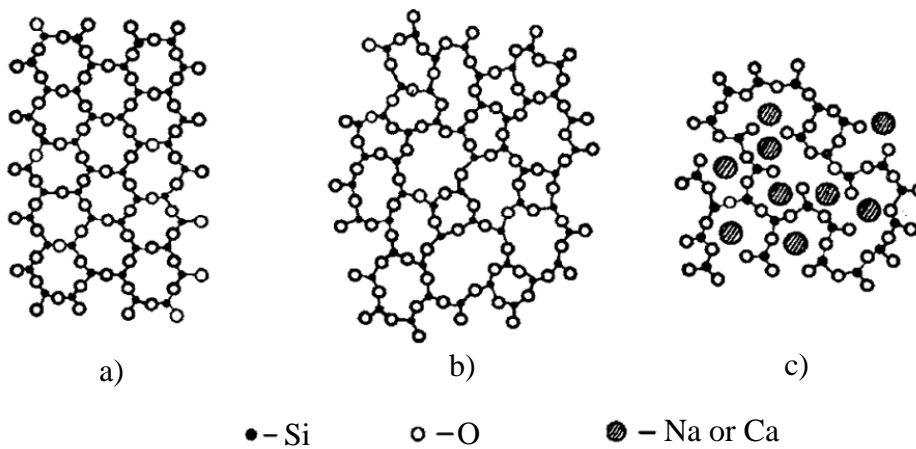


Figure 2.3. Structure with network formers and network modifiers [crystalline structure (a), amorphous structure (b) and amorphous structure with network modifiers (c)] (Shi, Krivenko, Pavel and Roy, 2005)

The structure of alkali-activated binders essentially contains network formers, network modifiers and intermediates. As the name suggests, network formers are surrounded by oxygen. Such as one molecule of  $\text{SiO}_4$  tetrahedra comprises one Si atom as a network former and four oxygen atoms around Si at the center. Network formers have relatively higher binding energies, and therefore they raise the condensation degree. However, network modifiers have a reasonably sizeable ionic radius with somewhat less nuclear charge and low bonding energies. Engagement of network modifiers promotes the disordered structure and depolymerizes it. Na, K and Ca are acting as network modifiers. Figure 2.3 illustrates the crystalline and

amorphous structure of silica vitreous structure. Intermediates, for example, Al and Mg, may behave like network modifiers or formers.

## **2.5 Precursors of geopolymerization**

The precursor is the solid raw material that is activated by an alkali activator solution. According to the literature, precursors are defined under three classes: fly ash, clays and metallurgical slags (Duxson, 2009). However, different materials with similar chemical and mineralogical content to mentioned materials have also been used, such as natural pozzolan (Haddad and Alshbuol, 2016), rice husk ash (Detphan and Chindaprasirt, 2009) and silica fume (Brew and Mackenzie, 2007). Although the chemical content is important for the efficiency of the precursor, the crystalline structure of precursor (amount of amorphous portions) is also essential for its reactivity.

### **2.5.1 Slag**

Although slag is the by-product of several metallurgical production processes, the most common type used in the cement industry is the blast furnace slag which is the by-product of the iron industry. Slag is a latent hydraulic material and already is utilized in the production of blended cements.

The first studies that concentrated on the alkali activation of slag date back to 1940 (Purdon, 1940). Various studies on alkali-activated slag-cements and -concretes were conducted in Ukraine in the 1980s (Glukhovsky and Pakhomov, 1978; Glukhovsky, 1980, 1983). Then, alkali-activation of slag started to gain attention in Europe (Belitsky, 1993; Hong S Y, 1993) and the world (Pu, 1991; Wang, 1991). Slag has great potential for alkali-activation with its ability to release cations (network modifying cations:  $\text{Ca}^{+2}$ ,  $\text{Mg}^{+2}$  and network forming cations:  $\text{Al}^{+3}$  and  $\text{Si}^{+4}$ ). In this context, reaction products of alkali-activated slag tend to be C-A-S-H type of gel. Although MgO does not directly participate in the gel formation, it promotes

strength development by accelerating the hydrotalcite formations (Haha *et al.*, 2011). The most striking property of alkali-activated slags is that they have relatively higher early strength and acid durability than geopolymers with fly-ash and metakaolin content (Singh *et al.*, 2015).

### **2.5.2 Fly-ash**

Fly-ash is a thermal power plant by-product that can already be utilized in the cement and concrete industry as a pozzolanic material. The reactivity of fly-ash is dependent on its chemical content, amorphous fraction, carbon residue content and particle size distribution (Provis and Bernal, 2014). While their amount varied with the type and source of fly-ash, chemical content of fly-ash comprising almost of Si, Al, Fe and Ca; latter determines that fly-ash is high- or low-lime type. Accordingly, while calcium together with silicon and aluminum determine the reactivity of fly ash and the structure of the geopolymerization gels, the factors controlling the reactivity of the amorphous phase of fly-ash are much more complex (Provis and Bernal, 2014). Alkali metals such as Na, K and alkaline earth cations such as Ca, Mg can behave as network modifiers in the amorphous phase in aluminosilicate structure. Thus, their presence is preferable to provide reactive amorphous phase in fly ash rather than non-reactive quartz or mullite. Figure 2.4 establishes the relationship between the compressive strength of geopolymers with various fly-ashes, which are compared with blast furnace slag. Direct effect of network modifier cations on the maturity of geopolymerization clearly can be seen.

Fly ash is a complex multiphase material that is affected by many parameters during alkali-activation. The ratio of silicon to aluminum in reactive amorphous portions can vary between similar sources due to the crystallization of mullite. Slow cooling of fly ash can result in the formation of large quantities of mullite crystals. Therefore, the method of cooling fly-ash can also affect the products that will be formed as a result of geopolymerization.

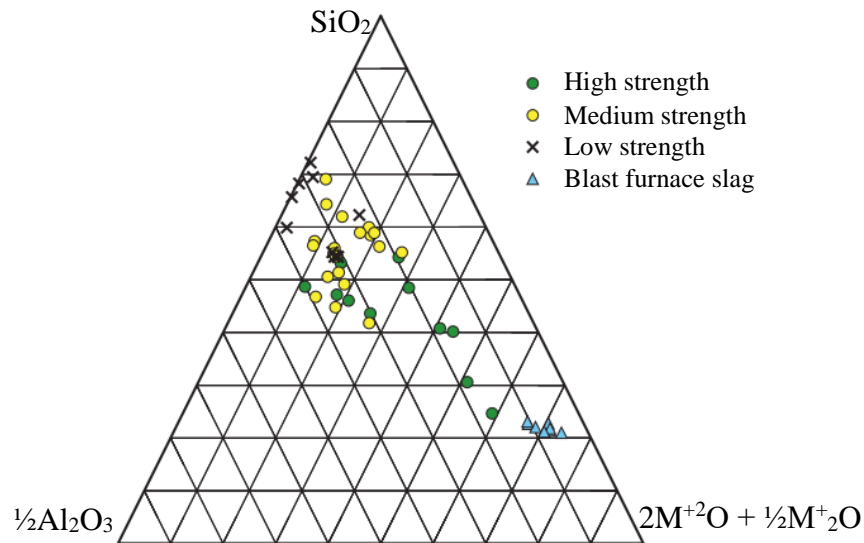


Figure 2.4. Alkali-activated fly-ashes' ternary diagram showing the relationship between compressive strength and chemical content (Provis and Bernal, 2014)

Strength development of fly-ash activated systems is highly dependent on curing temperature. While NaOH activated and ambient cured fly ash gives approximately 10 MPa of compressive strength on the 28<sup>th</sup> day (Somna *et al.*, 2011), curing at 65 °C for 24 hours, increase the strength result up to 20 MPa (Görhan and Kürklü, 2014).

### 2.5.3 Natural pozzolans and metakaolin

Natural pozzolans, a rich source of aluminosilicate, are volcanic materials. They are utilized in the cement industry by means of their Al<sub>2</sub>O<sub>3</sub> and SiO<sub>2</sub> content. However, the chemical content of natural pozzolans is highly varied. Due to magma content, eruption conditions and cooling parameters such as temperature and humidity (Siddique, 2011).

Metakaolin is a material derived by the calcination of kaolinite clay at temperatures between 500 – 850 °C. It comprises a considerable amount of SiO<sub>2</sub> (55-45%) and Al<sub>2</sub>O<sub>3</sub> (45-40%) is a complete aluminosilicate source material. Alkali-activation of

metakaolin dates back to 1982 (Davidovits, 1982). The amorphous structure of metakaolin together with its chemical composition provides an advantage for geopolymerization. Although the structure of metakaolin is mainly amorphous, it may have partially crystalline portions due to the removal of hydroxyl groups from the layered kaolinite structure, while the kaolinite clay is calcined at temperatures between 500 – 850 °C. If the chemical structure is considered, Al becomes more critical in terms of the reactivity of the material while the kaolin is transformed into metakaolin. According to the literature (Duxson, Mallicoat, *et al.*, 2007), metakaolin geopolymers with Si/Al ratio higher than 1.9 have a tendency to have higher strength results. This situation indicates that alkali silicates are more appropriate for alkali-activation of metakaolin.

#### **2.5.4 Construction and demolition waste as a precursor**

Construction and demolition wastes (CDWs) containing brick, concrete, wood, timber, metal and plastic are inert or non-inert materials resulting from the demolition, repair and renewal of constructions. In 2016, 374 million tons of CDW emerged in EU countries (Wahlstrom, Bergmans, Teittinen, Bacher, Smeets and A. Paduart, 2020). Turkey is an associate member of the EU as we take into account infrastructure and urban renewal because of the new action of infrastructure and urban transformation is expected to more than 6.5 million demolitions of the structure. In Turkey, where the total building stock is 19-20 million, this situation emerges as a problem that needs to be solved. In addition, the waste problem stands out as an essential problem in non-European countries, such that CDW production in the United States is about 100 million tons per year (Arslan, Coşgun and Salgın, 2012). Therefore, the need for methods that can dispose of such high amounts of construction and demolition waste without harming the environment is increasing day by day.

Although pozzolanic materials are successfully utilized in geopolymerization, the use of inert materials for geopolymer production has recently become the focus of

research projects. In parallel with this, as environmental awareness increases, the evaluation of waste materials becomes more important. In this context, the disposal of construction and demolition waste (CDWs) is one of the tough challenges facing the construction industry.

Researchers focusing on environmental savings, sustainable production and conservation of raw materials are trying to use construction and demolition wastes for geopolymerization while also reducing the problems of disposal of these waste materials.

Although construction and demolition waste can be processed in recycling facilities (Coelho and de Brito, 2013), the location, capacity and some other parameters of the facility can affect the recycling efficiency and make the efficiency of these facilities interrogable. However, selective demolition, in which all materials are separated at the demolition site and made ready for re-use, is a method that enables more efficient use of waste materials. In this way, it is possible and supported to use all materials in CDW in different forms. Not-selected CDW is being evaluated for applications such as landfilling subgrades (Zhang *et al.*, 2020), soil improvement (Suluguru *et al.*, 2019).

Concrete waste is one of the selected CDW-based materials. It has been reported that there is no spectacular strength development when concrete waste is used individually for alkali-activation; replacement of concrete waste with fly-ash is feasible in the context of strength development (Ahmari *et al.*, 2012). With the addition of pozzolanic material, the strength increment of geopolymer with concrete waste content is higher in the case of metakaolin use. In this way, the strength value of 25 MPa in the case of geopolymer with concrete waste content increased to 46 MPa with metakaolin (10%) substitution (Vásquez *et al.*, 2016).

Another CDW-based material is glass waste which is a suitable material to replace with calcium aluminate cement (Vafaei and Allahverdi, 2017). With the 57.8 MPa of compressive strength, tile may also be utilized in alkali-activation under the curing temperature of 80 °C for seven days (Komnitsas *et al.*, 2015). Ceramic, which is a

glass similar material, results in 71.1 MPa of compressive strength when it is activated with a combination of NaOH and KOH and cured at 60 °C for 28 days (Sun *et al.*, 2013).

Red clay brick, which is clayey material similar to tile, is shown to have excellent performance under the conditions of both ambient and high temperature (70 °C) curing (Robayo-Salazar, Rivera and Mejía de Gutiérrez, 2017). 30 MPa of compressive strength is reported from thermally cured (65 °C) NaOH-activated clay brick (Reig *et al.*, 2013). While there are different results for different activator and curing conditions, Silva *et al.* (2019) conducted a series of studies and determined the optimum conditions for alkali-activation of fire clay brick. Accordingly, optimum silica modulus, Na<sub>2</sub>O content, water to binder ratio are defined as 0.60, 8% and 0.27 for specimens cured between 65 and 80 °C for seven days.

It is also possible to produce composite materials comprising cement and geopolymer, such as eco-efficient hybrid cement consist of cement (30%) and geopolymer with red clay brick waste, resulting in 102 MPa of compressive strength (Robayo-Salazar, Mejía-Arcila and Mejía de Gutiérrez, 2017). Ouda and Gharieb (2020) reported that incorporation with waste concrete powder and alkali-activated brick waste have very satisfactory results in the context of strength development.

## **2.6 Self-healing capability of geopolymers and EGC**

Although geopolymers have unique mechanical specifications, durability is still a challenging issue. Considering the calcium content, geopolymers containing low calcium have less crack formation tendency under favor of little or no amount of ettringite and gypsum formation. Contrarily alkali-activated materials with a higher amount of calcium are susceptible to crack formation (Chindaprasirt *et al.*, 2013). While mechanical loading may cause crack formation, water is one of the significant reasons for crack formation. Unlike cement hydration, water participating in the geopolymerization may be released back to the system after the reaction take place



(Provis and van Deventer, 2009) and geopolymers may have free moisture content in later times of geopolymerization. Fang and Kayali (2013) exhibited that mature geopolymer specimens may contain 36.1% evaporable water of their total mass. The fact that water participates in geopolymerization and release after reactions. Taking part in the geopolymerization of water and then releasing it causes water loss and consequently shrinkage in the system. Therefore shrinkage and cracking are some of the drawbacks of alkali-activated binders. Cracking increases the permeability of the binder and makes the penetration of water, harmful acidic solutions and aggressive agents easy. As a result, a deterioration process initiate and durability problems occur. Incorporating fiber into the binder is a feasible way to suppress the crack formation that is not desired, considering the durability problems. Fiber bridging enables cracking control and the effect of cracking through fiber bridging. Accordingly, self-healing is an effective method both to prevent wider crack formation and heal cracks that already exist.

### **2.6.1 Self-healing in cementitious systems**

Self-healing is the ability of the material to repair and seal cracks on its own. Several self-healing methods for cementitious systems exist in the literature, such as the utilization of empty fibers, capsules containing chemical agents, bacteria-based healing, expansive additives, shape-memory materials (Sisomphon, Copuroglu and Koenders, 2012; Vijay, Murmu and Deo, 2017) and controlled microcracking, which is obtained by autogenous self-healing (Şahmaran and Li, 2008). Autogenous self-healing is particularly appealing in that it does not require external interference to trigger the mechanism, unlike other self-healing techniques. Therefore, the majority of self-healing studies available in the current literature focuses on autogenous self-healing.

Figure 2.5 presents the various reasons for autogenous self-healing of cementitious systems. As can be seen here, there are three main types of healing processes that exist. Although mechanical causes are presented in Figure 2.5, their effect is not

dependent on the chemical composition of the binder. However, continuing hydration is clearly dependent on the chemical content of binder material and environmental conditions. The reason for the continued hydration is that the cement, which has not reacted yet due to insufficient curing and lack of water, reacts with the water in the environment and becomes hydrated. Newly formed hydration products move into the crack and reduce the void volume. The volume of cement doubles when it hydrates, but continued hydration cannot completely heal a crack. Continued hydration can almost completely fill only cracks with a width of less than 100  $\mu\text{m}$ , but the healing ability decreases as the crack width increases (Reinhardt *et al.*, 2013).

Calcium carbonate formation is the second type of chemical reason. The calcium ions ( $\text{Ca}^{+2}$ ), present in the concrete pore water, react with the carbonate ions ( $\text{CO}_3^{-2}$ ) in the crack and a phenomenon called carbonation occurs.  $\text{CaCO}_3$  formed after the carbonation is highly effective for autogenous self-healing capacity of cementitious systems (Edvardsen, 1996).

As abovementioned, crack width should be limited to generate a complete self-healing process. However, lower crack width may hinder the penetration of  $\text{CO}_2$  in the atmosphere to the crack and hinder the calcium carbonate formation. Because of this reason, optimum crack width is defined as 5-10  $\mu\text{m}$  (Jacobsen, Marchand and Homain, 1995), 53  $\mu\text{m}$  (Ismail *et al.*, 2004), 100  $\mu\text{m}$  (Reinhardt and Jooss, 2003), 200  $\mu\text{m}$  (Edvardsen, 1996), 205  $\mu\text{m}$  (Aldea, Song and Popovics, 2000) and 300  $\mu\text{m}$  (Clear, 1985).

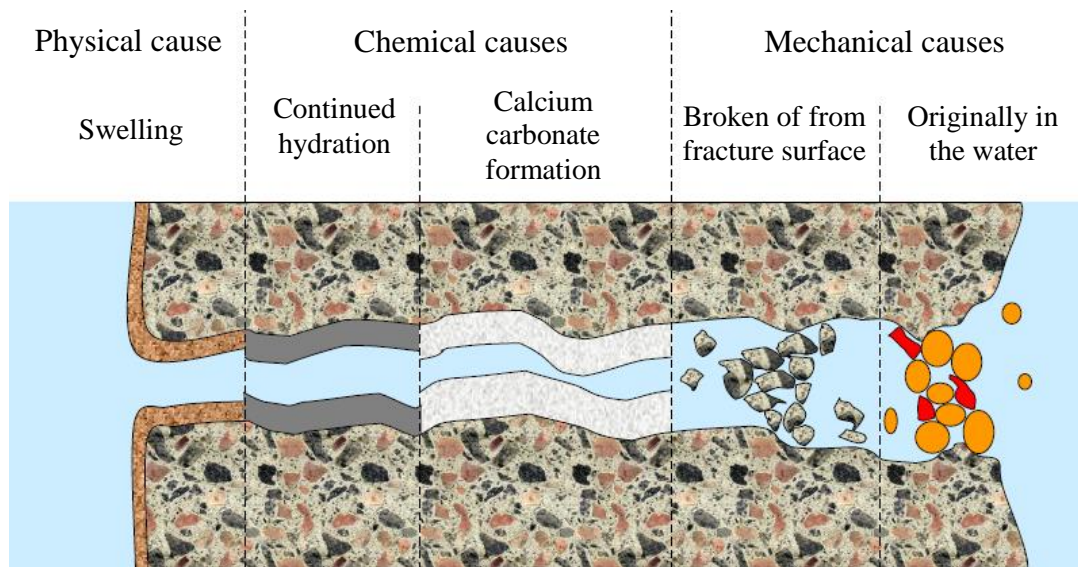


Figure 2.5. Reasons for autogenous self-healing of cementitious systems (Reinhardt *et al.*, 2013)

## 2.6.2 Engineered cementitious composites

Engineered Cementitious Composites (ECCs) are such materials capable of restricting the widths of their cracks by exhibiting a strain-hardening response similar to many common metals (Sahmaran and Li, 2007; Sahmaran, Li and Li, 2007). This behavior of ECCs is therefore significantly advantageous in favoring the autogenous self-healing capability. Multiple crack formation with lower widths is originated from the ability of fibers to bridge cracks. Fiber also introduces a toughness increment by energy absorption resulted from de-bonding and pull-out of the fiber, which bridges cracks (Sun and Wu, 2008). Polyethylene (PE) fibers were used in early studies on ECC (Li, Lim and Chan, 1998), then poly-vinyl alcohol (PVA) fibers were used (Li and Yang, 2007; Zhu, Yang and Yao, 2012). Thanks to the micromechanical design, cement paste and fiber interaction provides high ductility and toughness in parallel with the multiple microcrack formation. Figure 2.6 shows multiple microcracking behaviors and multiple microcracking formations of ECCs.

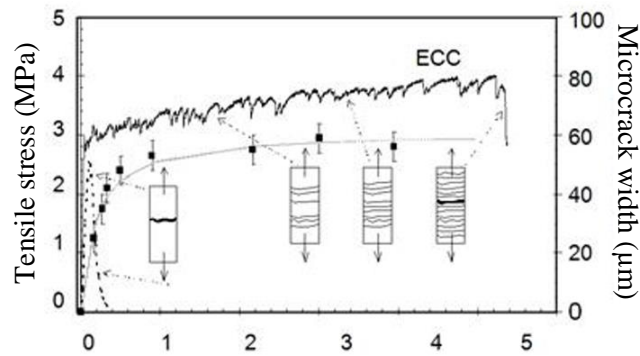


Figure 2.6. Strain-hardening behavior of ECC (Heiman and Koerstz, 1991)

### 2.6.3 Engineered geopolymer composites

With the successful applications of ECCs and the growing popularity of geopolymer, curiosity arises about Engineered Geopolymer Composites (EGCs). EGC is the geopolymer composite reinforced with fiber content that has strain-hardening characteristics. One of the early studies concentrated on fiber-reinforced geopolymer assessed utilization of wollastonite microfibers in geopolymers (Silva and Thaumaturgo, 2003). This study revealed that fracture toughness might be highly improved by utilization of fiber in the geopolymer. Dias and Thaumaturgo (2005) also establish that basalt fiber can be utilized in geopolymer to increase fracture toughness. Zhao et al. (2007) reinforced geopolymer with steel mesh and depict that steel mesh reinforced geopolymer has a yielding behavior similar metal materials. Considering the fibers mostly used in ECCs, PVA is used by Sun and Wu (2008) in fly-ash (Type F and C) based geopolymer activated with NaOH. While fiber content higher than 1% decreases workability, optimum PVA fiber content is determined as 1%, which increases the ductility six times. Yunsheng et al. (2008) investigated the impact toughness of metakaolin and fly-ash based geopolymer composites with PVA fiber content. While metakaolin-based geopolymer has an impact toughness of 209 mJ, 1% and 2% PVA fiber addition increase this result to 1177 and 1833 kJ, respectively. As can be seen here, optimum PVA content is 2% when the precursor is metakaolin. For this optimum design, fly-ash was replaced with metakaolin with percentages of 10, 20 and 30%. While 10% fly-ash replacement further increases

impact toughness to 2108 kJ, 20% and 30% fly-ash replacement decrease toughness to 1587 and 1307 kJ, respectively. This complexity is attributed to the fact that spherical, fine fly-ash particles both fill the pores and act as nucleation sites. As a result a highly denser structure is obtained. However, when fly-ash replacement becomes 20% or more, decreasing metakaolin leads to the lack of geopolymerization. It is clearly seen that from the last two studies mentioned (Sun and Wu, 2008; Yunsheng *et al.*, 2008), fly-ash lags behind metakaolin in terms of the efficiency of PVA.

Lin *et al.* (2008) investigated the utilization of carbon fiber in metakaolin-based geopolymer activated with KOH. The amount of carbon fibers used is 5% by volume, and three types of carbon fibers with lengths of 2, 7 and 12 mm are utilized. While the flexural strength of metakaolin-based geopolymer is 15 MPa, flexural strengths of geopolymer containing fiber with lengths of 2, 7 and 12 mm are 60, 90 and 83 MPa, respectively.

Lee *et al.* (2012) studied the fiber-reinforced alkali-activated slag mortar activated with a combination of calcium hydroxide, sodium sulfate and sodium silicate. Ingredient selection and mix design are made to get strain-hardening behavior when 2% PVA fiber is used. Accordingly, a large portion of aggregate is not included the mixture and unlike the studies mentioned so far, the necessary step was taken for EGC design in this study. Under tension, 4.7% of ductility and strain hardening behavior is clearly attained for mixtures activated with a combination of  $\text{Ca}(\text{OH})_2$  and  $\text{Na}_2\text{SO}_4$ . Similar to previously mentioned study, micro-mechanical modeling is applied for geopolymer with fly-ash content activated with a combination of sodium silicate and sodium hydroxide and 2% PVA fiber is used (Ohno and Li, 2014). Tensile behavior was evaluated through tensile tests on dogbone-shaped specimens. Multiple crack formation, which is one of the fundamental profits of micro-mechanical modeling, is obtained with maximum crack width of 117  $\mu\text{m}$  and average crack width of 45  $\mu\text{m}$ . It demonstrated that fly ash-based EGC could attain a tensile ductility of 4%. This amount of ductility is slightly lower than the slag-containing EGC in the previously mentioned study (Lee *et al.*, 2012).

The number of studies in the literature that concentrated on the autogenous self-healing behavior of EGCs is very few. According to Kan et al. (2019), who evaluated the self-healing performance of metakaolin and fly ash containing PVA fiber-reinforced EGC mixtures through wet-dry cycles on dog-bone-shaped specimens, tensile strain capacities in the range of 6–8% were achievable. In this study, where crack widths did not exceed 25  $\mu\text{m}$  after preloading levels reaching tensile strains of 1.0%, 2.0%, and 3.0%, self-healing sourced from continuing geopolymerization provided excellent strain-hardening behavior. Guo and Yang (2020) showed that slag addition to fly ash increases the tensile strength and ductility of the EGC specimens. However, slag addition caused wider widths and a lower number of cracks through higher toughness. They also mentioned that  $\text{Na}_2\text{CO}_3$  formation on the surface near the crack reflects the crack healing. Using only slag as a precursor leads to the formation of  $\text{CaCO}_3$  as a healing material in alkali-activated composites (Zhang, Suleiman and Nehdi, 2020) owing to the high  $\text{Ca}^{+2}$  concentration.  $\text{CaCO}_3$  can also be obtained from bacteria-based self-healing of geopolymers (Jadhav *et al.*, 2018).

EGC studies in the literature concentrated on dog-bone-shaped specimens preloaded under tensile loading. However, many types of bearing members are also subjected to flexural loads. Therefore, in this thesis study, flexural preloading is examined. Additionally, in the literature, no study focused on the changes in the transport and electrical properties of CDW-based geopolymers. This study aims to assess the autogenous self-healing performance of 100% CDW-based EGC specimens subjected to flexural preloading. During the assessment, the acquirement of deflection hardening behavior from the alkali-activated CDW was evaluated. Another goal was to determine if geopolymers from CDW-based materials have self-healing capability. Thus, these wastes, which have negative environmental issues, can be used in geopolymer binders with self-healing behavior. For these purposes, the self-healing performances of specimens exposed to wetting-drying cycles were essentially assessed through transport and electrical properties. Microstructural investigations were used to support the obtained results.

## CHAPTER 3

### EXPERIMENTAL STUDY

#### 3.1 Materials

Within the scope of this thesis, some of the materials used as raw materials were obtained from construction demolition wastes (CDW-based precursors and waste concrete-based sand), and some of them are commercial alkaline-activators. Detailed information about these materials is presented below.

##### 3.1.1 Construction and demolition waste-based materials and slag

In order to prevent uncertainties in the results caused by the variations in the chemical content of the materials taken from different demolition worksites, construction demolition waste-based materials were supplied from a large urban transformation area. These materials were received in selected form but were not crushed or ground. First, all the CDW-based materials were separately crushed in a jaw breaker with a 1 mm of spacing and made ready for grinding. When the grinding process is considered, the grindability indices of the CDW-based materials are different. Consequently the optimum ball configurations and grinding time required for the ideal grinding process change. However, since one of the aims of the study conducted within the scope of this thesis is to encourage recycling and utilization of CDW-based materials, the ball configuration and optimum grinding time determined for clayey materials (1 hour) were used for all materials in order to facilitate the process. Thus, in the studies to be carried out after this thesis, it will be possible to crush, grind and use the CDW-based materials together without selection. There are five types of CDW-based materials which are red clay brick waste (RCB), hollow brick waste (HB), roof tile waste (RT), concrete waste (C) and glass waste (G). Also,

ground granulated blast furnace slag (S) is utilized as a replacement material. These materials in bulk, crushed and ground form can be seen in Figure 3.1.



Figure 3.1. CDW-based materials in bulk, crushed and ground form red clay brick  
(a), roof tile (b), hollow brick (c), glass waste (d), concrete waste (e)



### 3.1.1.1 Chemical content of precursors

The chemical contents of these materials are determined by X-ray fluorescence (XRF) analyses and the results are presented in Table 3.1. Clay originated CDW-based materials (RCB, RT, and HB) are very close to each other in the context of chemical content, with the maximum amount of  $\text{SiO}_2$  followed by  $\text{Al}_2\text{O}_3$ . Since bricks and tile are rich in  $\text{SiO}_2$  and  $\text{Al}_2\text{O}_3$ , they seem feasible for alkali-activation in the context of chemical content with  $\text{SiO}_2/\text{Al}_2\text{O}_3$  ratios of 2.41, 2.84, and 2.88 for RCB, RT, and HB respectively. Since mechanical performance and stability of molecular structure reduce with raising  $\text{SiO}_2/\text{Al}_2\text{O}_3$  ratio (Wang *et al.*, 2020) RCB is seen as more appropriate than HB and RT for alkali-activation. Chen-Tan *et al.* (2009) reported that iron content tends to suppress the dissolution process and consequently geopolymerization reactions. According to McIntosh *et al.* (2015), iron content with a concentration higher than 15% reduces the strength development of geopolymers. RCB, RT and HB have iron oxide contents of 11.3%, 11.6%, and 11.8%, respectively. These values are a bit high but lower than the limit defined by McIntosh *et al.* (2015). Although suppressing the strength development is unfavorable, considering the autogenous self-healing process with continued hydration, slow-dissolving aluminosilicates at early ages may contribute to later reactions. RCB, RT, and HB have CaO content of 7.7%, 10.7%, and 11.6%, respectively. Accordingly, geopolymer composites produced with these precursors may be called geopolymer rather than a high-calcium alkali-activated binder.

Concrete waste with CaO content of 21.2% has the highest CaO content among all CDW-based precursors. Unlike other precursors, concrete waste has 19.7% of  $\text{CO}_2$  content generated from carbonation during the service life of the concrete.

Glass waste has the maximum percentages of  $\text{SiO}_2$  among all precursors. Since Si species can be network formers, glass waste is curious about to what extent it will contribute to geopolymerization with its high silica content. The efficiency of geopolymerization reactions is not only dependent on chemical content but also crystalline structure.

Table 3.1 Chemical content of CDW-based materials and slag

Oxide Composition (%)	Red Clay Brick (RCB)	Roof Tile (RT)	Hollow Brick (HB)	Concrete (C)	Glass (G)	Slag (S)
SiO <sub>2</sub>	41.7	42.6	39.7	37.4	53.8	32.1
CaO	7.7	10.7	11.6	21.2	17.8	36.1
CO <sub>2</sub>	8.0	7.5	7.8	19.7	8.6	9.1
Al <sub>2</sub> O <sub>3</sub>	17.3	15.0	13.8	10.7	4.4	11.2
Fe <sub>2</sub> O <sub>3</sub>	11.3	11.6	11.8	3.8	0.7	0.6
K <sub>2</sub> O	2.7	1.6	1.6	2.2	0.5	0.8
Na <sub>2</sub> O	1.2	1.6	1.5	2.0	8.7	0.3
MgO	6.5	6.3	6.5	1.3	4.2	5.6
MnO	0.2	0.2	0.2	0.1	0.3	0.1
SO <sub>3</sub>	1.4	0.7	3.4	0.9	0.2	1.2

### 3.1.1.2 Particle size distributions of precursors

Figure 3.2 illustrates the particle size distributions of CDW-based materials. Since the ball configuration of the mill is adjusted for clayey materials, which are the softest ones among all precursors, the bricks and tiles have become very fine-grained. Since glass waste is the hardest among all precursors, its particle size distribution graph is clearly to the right of the other graphs.

Particle size properties of slag and CDW-based precursors can be seen in Table 3.2. Here, specific surface area (SSA), surface weighted mean diameter (D[3,2]), volume-weighted mean diameter (D[4,3]) are presented. Diameter values, through which 10% [d(0.1)], 50% [d(0.5)] and 90% [d(0.9)] of the materials pass, are also presented. Results demonstrate that roof tile has the finest particles. Although glass has the largest grain size of all materials, the amount of particles larger than 50

microns in concrete is more than glass. This situation can be seen from d(0.9) results of glass and concrete which are 75.7  $\mu\text{m}$  and 79.6  $\mu\text{m}$ , respectively.

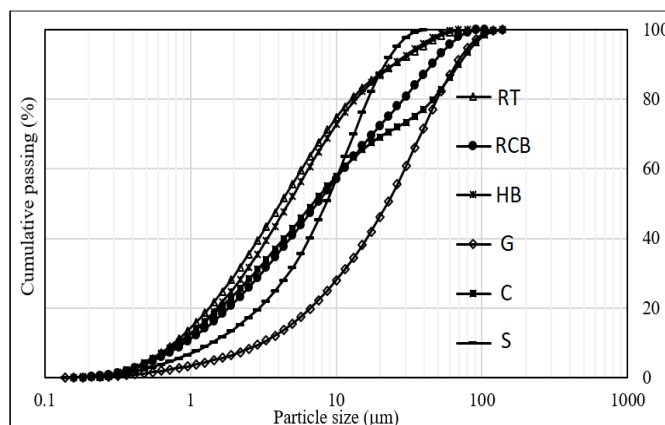


Figure 3.2. Particle size distributions of CDW-based materials

Table 3.2 Particle size specifications of slag and CDW-based materials

	Red Clay Brick (RCB)	Roof Tile (RT)	Hollow Brick (HB)	Concrete (C)	Glass (G)	Slag (S)
SSA ( $\text{m}^2/\text{kg}$ )	2.08	2.59	2.45	2.25	0.87	1.63
D[3.2] ( $\mu\text{m}$ )	2.89	2.32	2.45	2.67	6.93	3.68
D[4.3] ( $\mu\text{m}$ )	18.0	10.3	10.5	24.9	33.4	11.7
d(0.1) ( $\mu\text{m}$ )	1.06	0.89	0.97	0.94	3.55	1.62
d(0.5) ( $\mu\text{m}$ )	8.50	4.75	5.39	7.95	25.7	9.78
d(0.9) ( $\mu\text{m}$ )	51.9	28.4	28.4	79.6	75.7	11.7

D[3.2] and D[4.3] indicate the surface and volume-weighted mean diameters  
d(0.1), d(0.5) and d(0.9) indicate sieve aperture sizes through which 10%, 50% and 90% of the sample passes

### 3.1.1.3 Crystalline structure of precursors

The crystalline structures of precursors were analyzed by X-ray diffraction method (XRD) and XRD diffractograms of all precursors are seen in Figure 3.3. Although precursors except for slag and glass waste have pronounced peaks indicating the

presence of crystal structure, halos of these materials are also seen. Therefore it can be stated that all precursors have an amorphous structure which is vital for geopolymerization reactions (Iler, 1979). Minerals seen in those diffractograms are presented in Table 3.3.

Table 3.3 Definitions of minerals existing XRD diffractograms

Mineral	Symbol	Chemical formula	PDF Number
Quartz	Q	$O_2 Si$	96-101-1160
Calcite	C	$C Ca O_3$	96-900-9669
Magnesium silicate	M	$H_6 Mg O_6 Si$	69-901-6369
Analcime	A	$Al_2 H_4 Na_{1.8} O_{13.6} Si_4$	96-900-9956
Pyrope	P	$Al_2 Mg_3 O_{12} Si_3$	96-900-6559
Ferrosilite	F-S	$Fe O_3 Si$	96-900-0479
Dialuminium silicate oxide	A-S	$Al_2 O_5 Si$	96-101-0330
Potassium alumino silicate	K-A-S	$Al K O_6 Si_2$	96-153-7810
Ferrite	F	$Fe_2 O_3$	96-154-6384
Calcium alumino silicate	C-A-S	$Ca Al_2 Si_2$	96-153-0000

XRD diffractograms of clayey materials infer the presence of high quartz peaks. As expected, silica species in the clayey materials exist in both crystal and amorphous form. Although the solubility of amorphous silicate species is higher than silicate species in crystalline form, crystal structure does not entirely prevent the dissolution of these species. However a completely amorphous structure does not guarantee the maximum dissolution performance of precursor material. As an example, glass waste has a completely amorphous structure and relatively higher amount of  $SiO_2$  content; however, its alkali-activation may not be as efficient as alkali-activation of clayey materials. The reason for this is silicate species have relatively higher bonding energies (Shi, Krivenko, Pavel and Roy, 2005) and consequently lower solubility than network modifiers ( $Ca^{+2}$ ,  $Na^{+1}$ ,  $K^{+1}$  etc.) and lack of network modifiers in glass

may prevent the solubility of it. Therefore the amorphous structure is not enough for satisfactory alkali-activation performance.

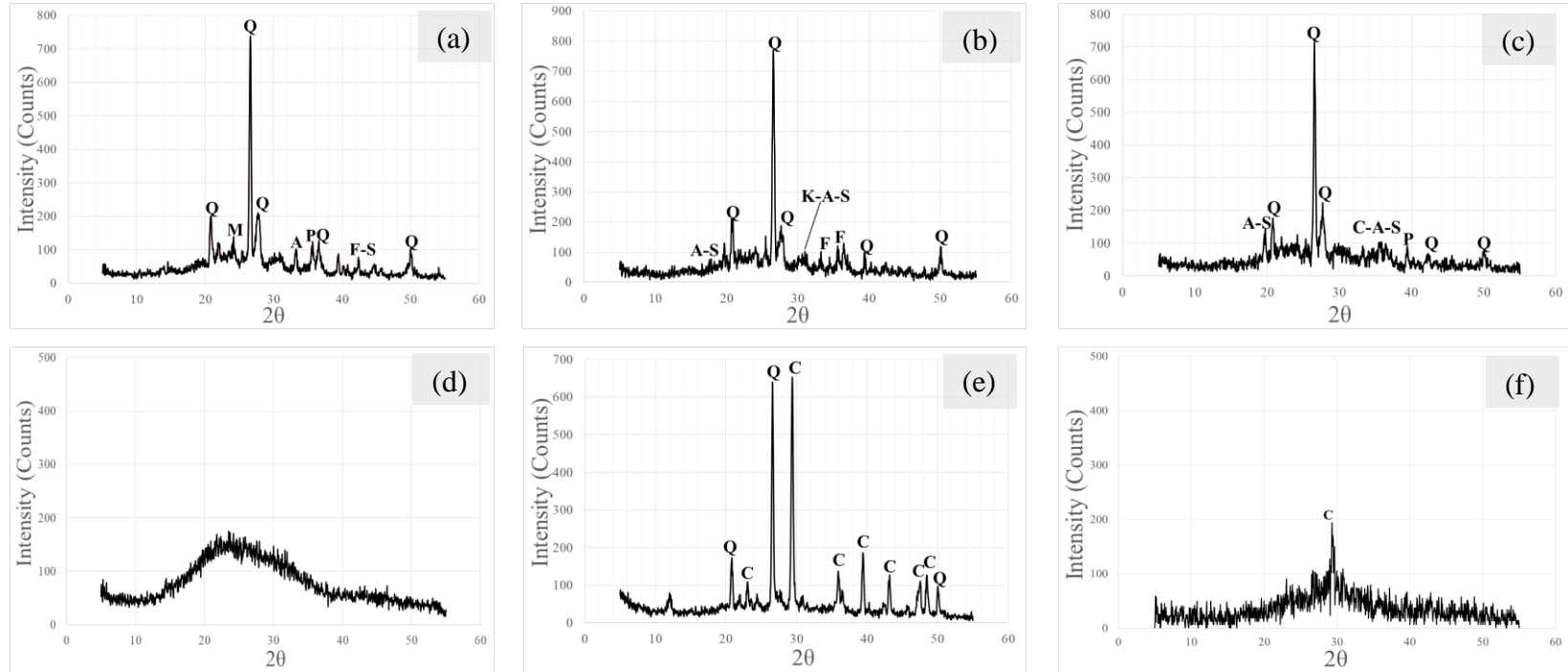


Figure 3.3. Crystallographic structures of red clay brick waste (a), hollow brick waste (b), roof tile waste (c), glass waste (d), concrete waste (e) and slag (f)

#### **3.1.1.4 Morphological properties of precursors**

Scanning electron microscopy (SEM) analyses were performed to observe the morphological properties of precursors. Figure 3.4 and Figure 3.5 present the SEM images taken from the ground CDW-based materials and slag. Images on the left side have a magnification of 1000× and ones on the right side have a magnification of 5000×. Also, images on the right side are taken from the center area of the image on the left side.

Figure 3.4 shows that clayey waste materials, which are relatively softer, have rounded and fractured particles. Accordingly, geopolymers with clayey material content do not suffer from workability. As particle size distribution analyses indicated, roof tile has smaller particles than red clay brick and hollow brick. Red clay brick is observed with its larger particle sizes comparing with roof tile and hollow brick. It is seen that all clayey materials have particles of different sizes, which promotes homogenous particle size distribution seen from particle size analyses.

Figure 3.5 demonstrates how glass waste and ground granulated blast furnace slag were harder than clayey materials. Images with the magnification of 5000× clearly show that glass waste and slag have very angular particles because of their hardness values. Also, smooth surfaces of slag and glass waste draw attention. Angular shapes of glass and slag are supposed to decrease the workability. However, better adherence and interfacial transition zone characteristics may also be expected.

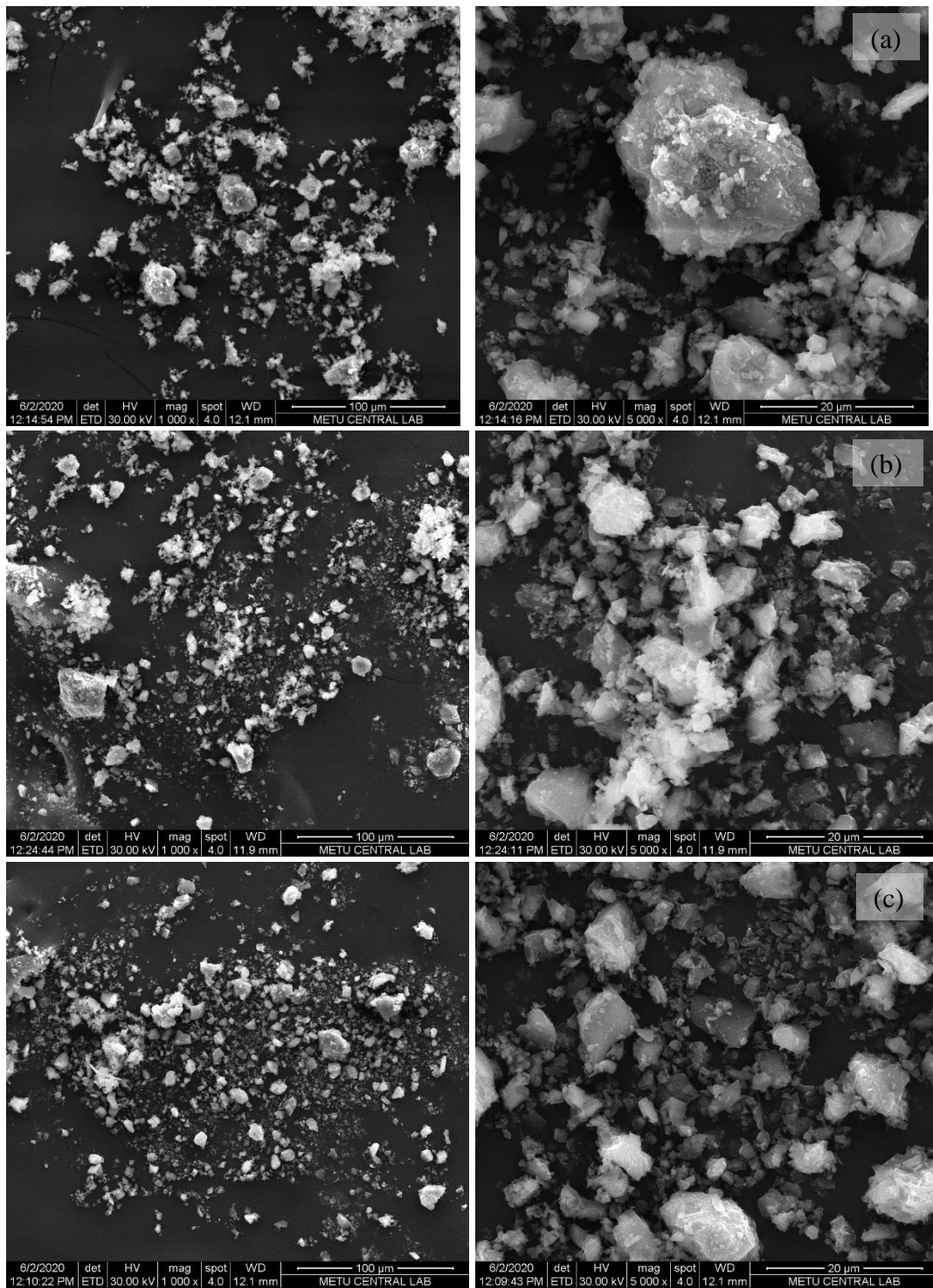


Figure 3.4. Scanning electron microscopy images of red clay brick waste (a), hollow brick waste (b) and roof tile waste (c), (images on left and right side have magnifications of 1000× and 5000× respectively)



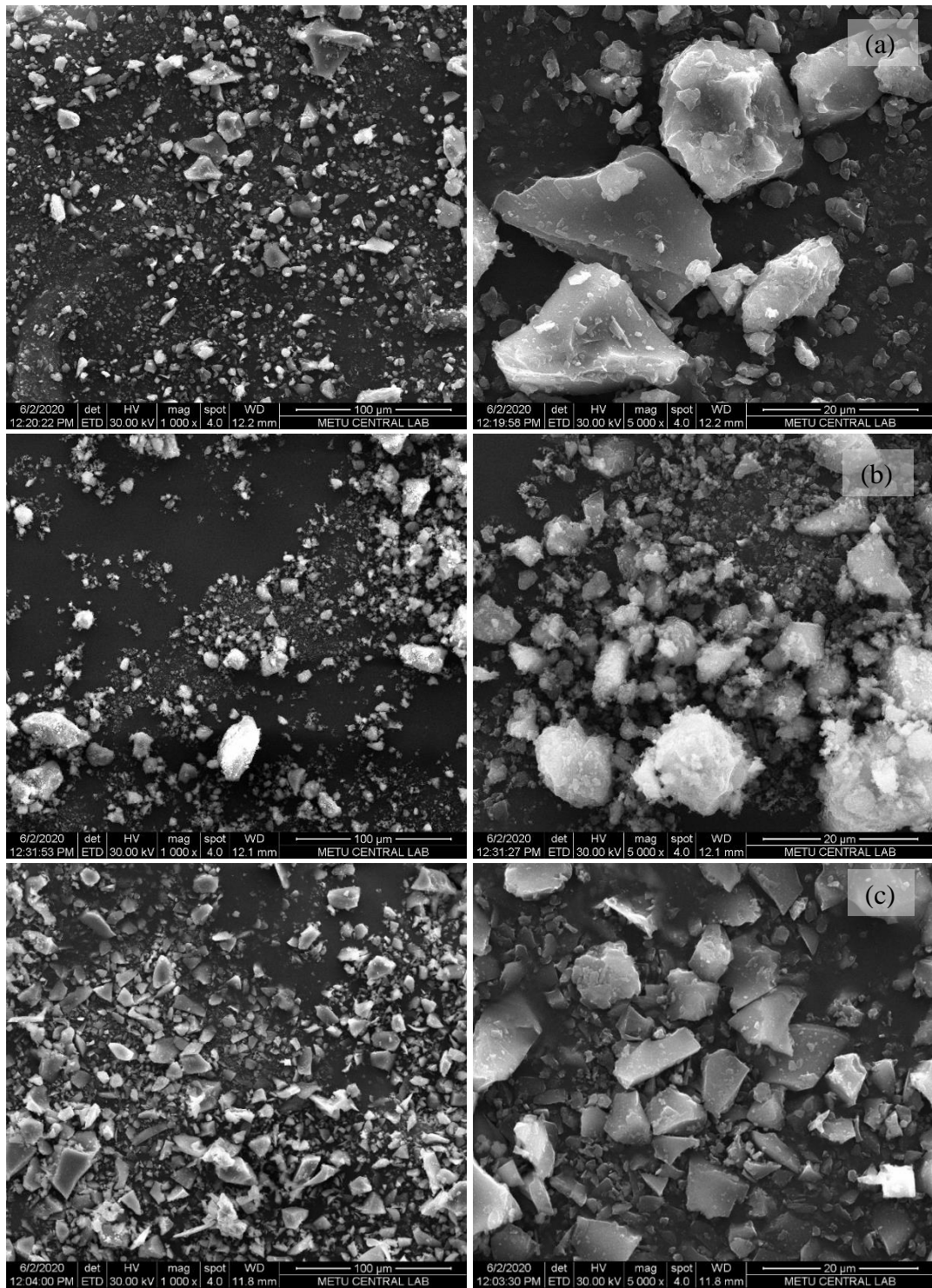


Figure 3.5. Scanning electron microscopy images of glass waste (a), concrete waste (b) and slag (c), (images on left and right side have magnifications of 1000× and 5000× respectively)

If concrete waste is investigated, it is seen that concrete waste has rounded particles like clayey materials. However, less amount of angular particles is also seen. The fact that concrete contains both angular and round particles is due to the concrete having different components. In this way, in addition to tobermorite and portlandite crystals,  $\text{CaCO}_3$ , which is a relatively soft component, emerges as a result of carbonation. Therefore it can be said that concrete has relatively higher amount of impurities.

### 3.1.2 Sand

Since concrete waste constitutes a significant part of construction and demolition wastes, recycled concrete aggregate was used to produce EGC in this study, paralleling recycling and sustainability purposes. Thus, as seen in the preliminary studies, concrete waste, which is not suitable for use at high rates for geopolymer production, has been evaluated in mortar production as fine sand. Since the micro-mechanical design of EGC requires the use of fine aggregate, aggregate with a particle size less than 2 mm was used in the study. Figure 3.6 display the particle size distributions of fine recycled concrete aggregate, reference (rilem) sand and higher and upper limits for reference sand. It is seen that recycled concrete aggregate has finer particles than the lower limit of the reference sand.

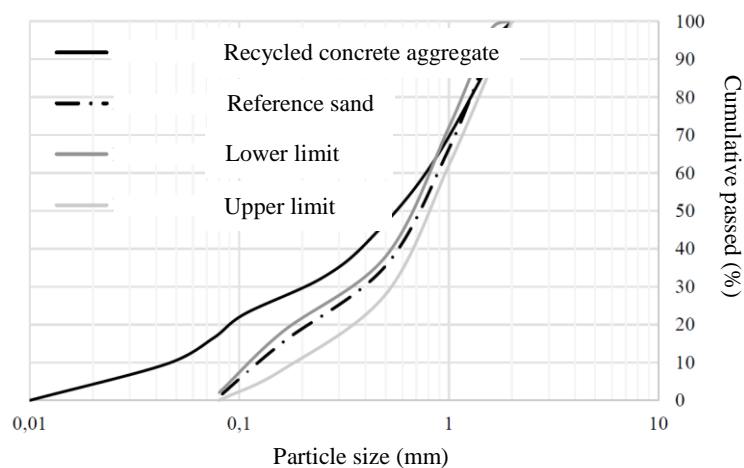


Figure 3.6. Particle size distribution of recycled fine aggregate utilized in EGC

Physical properties of recycled concrete aggregate and reference sand are seen in Table 3.4. The most remarkable physical properties of recycled concrete aggregate are porosity and water absorption rate results. The porosity and water absorption amount of recycled concrete aggregate are approximately seven times the porosity and water absorption rate of reference sand because of the presence of finer particles smaller than 100  $\mu\text{m}$  in recycled concrete aggregate.

Table 3.4 Physical properties of recycled concrete aggregate

	Recycled concrete aggregate	Reference sand
Loose unit weight ( $\text{kg}/\text{m}^3$ )	1353	1681
Dense unit weight ( $\text{kg}/\text{m}^3$ )	1273	1626
Oven-dried specific weight	1.95	2.55
Saturated dry-surface specific gravity	2.17	2.63
Apparent specific gravity	2.50	2.68
Water absorption amount (%)	11.1	1.6
Porosity (%)	21.7	3.7

### 3.1.3 Alkaline activators

Three types of alkaline activators were used in this thesis study. While sodium hydroxide [NaOH] was used as the main activator, sodium silicate [ $\text{Na}_2\text{SiO}_3$ ] and calcium hydroxide [ $\text{Ca}(\text{OH})_2$ ] were included in some EGC designs. Alkaline activators used in this thesis study can be seen in Figure 3.7.

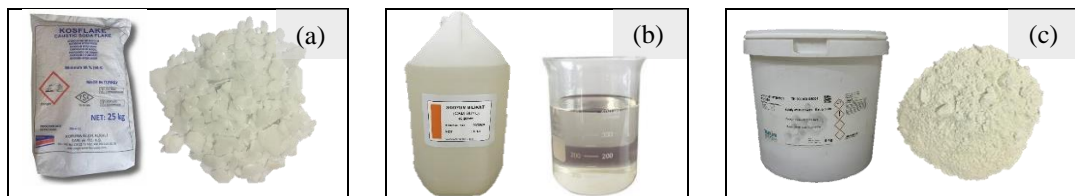


Figure 3.7. Alkaline activators (a) NaOH, (b)  $\text{Na}_2\text{SiO}_3$  and (c)  $\text{Ca}(\text{OH})_2$

### 3.1.3.1 Sodium hydroxide (NaOH)

A commercial NaOH in pellet form with high purity was used by dissolving in water. It was seen in preliminary studies that NaOH can be used directly in the mixture right after dissolving in water. However, high heat generated while dissolving makes it difficult to work in some mixtures, so prepared NaOH mixture was used after it was waited for one day and reached room temperature. Table 3.5 exhibits the chemical content of NaOH used in this thesis study.

Table 3.5 Chemical content of NaOH in pellet form

Content	Limit	Amount
Sodium hydroxide (%)	Min. 98.0	98.27
Sodium carbonate (%)	Max. 0.40	0.35
Sodium chloride (%)	Max. 0.10	0.020
Ferrite (ppm)	Max. 15.0	13.17

While the amount of NaOH was calculated according to the molarity in the first part of the study, since it is difficult to obtain the constant water to binder ratio in this method, the calculation was made according to the Na amount in the remaining of the study. Necessary information regarding mixture calculations will be given in the relevant sections.

### 3.1.3.2 Calcium hydroxide

It is seen that satisfactory strength development could be obtained without calcium hydroxide addition. However, to see the effect of calcium hydroxide as a calcium-rich activator in autogenous self-healing performance, it was included in some EGC designs. A commercially available calcium hydroxide with the following specifications (Table 3.6) was used.

Table 3.6 Specifications of calcium hydroxide

Content or specification	Amount
Molarity (g/mol)	74.09
Density (g/cm <sup>3</sup> )	2.24
Melting point (°C)	550
Purity (%)	Min. 87
MgO (%)	Max. 1
Insoluble matter in acid (%)	Max. 1
Loss on ignition (%)	Max. 3
Particle size [90 μm] (%)	Min. 90
Solubility in water (g/l)	1.7

### 3.1.3.3 Sodium silicate

A commercial sodium silicate is used in aqueous form. Chemical content and some specifications are presented in Table 3.7. Although sodium silicate indicates the  $\text{Na}_2\text{SiO}_3$ , sodium silicate solution contains water molecules as expected. The silica modulus, which is the molar  $\text{SiO}_2/\text{Na}_2\text{O}$  ratio of sodium silicate solution, is 1.9, which is appropriate for alkali-activation. Sodium silicate was not used in all geopolymer paste and mortars in the thesis study. The viscosity of sodium silicate solution is higher than that of sodium hydroxide and using sodium silicate solution as an activator may decrease the workability of alkali-activated system. Also, preliminary studies show that sodium silicate solution reduces the setting time. Therefore using sodium silicate solution is not easy in the context of workability. However, a combination of sodium silicate solution and sodium hydroxide generally provides better strength development characteristics rather than single sodium hydroxide. The amount of sodium hydroxide solution is determined as a mass ratio of sodium hydroxide.

Table 3.7 Chemical content and specifications of sodium silicate solution

Content or specification	Amount
SiO <sub>2</sub> (%)	24
Na <sub>2</sub> O (%)	11
H <sub>2</sub> O (%)	65
Silica modulus [SiO <sub>2</sub> /Na <sub>2</sub> O]	1.9
Baume scale	40
Density (gr/cm <sup>3</sup> )	1.35

### 3.1.4 Fiber

As it is known, higher ductility, toughness and multiple crack formation by fiber bridging can be obtained using relatively short fibers. In this thesis study, although different fibers (polyethylene, nylon-mono, polyvinyl-alcohol, polypropylene, carbon) were tried during EGC development, it has been determined that a combination of polyethylene (PE) and nylon-mono (NM) fibers have a good performance. Different fibers tried in the context of the thesis work can be seen in Figure 3.8

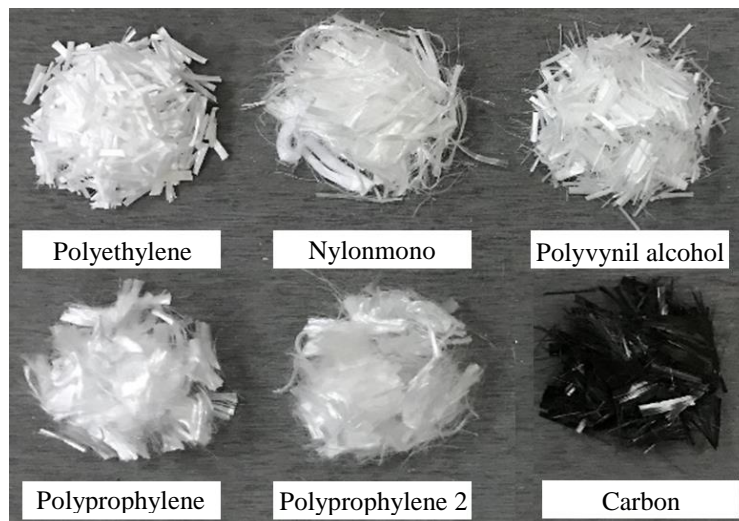


Figure 3.8. Fibers tested in the thesis work

The optimum amount and combination of fiber to be used in mixtures was determined with a series of preliminary tests, including flexural performance measurements of mixtures with different types of utilization rates (2.0 PE – 0.0 NM, 1.75 PE – 0.25 NM, 1.50 PE – 0.50 NM, 1.25 PE – 0.75 NM, 1.00 PE – 1.00 NM). Preliminary test results showed that increased PE fiber content resulted in higher mid-span beam deflection results which can be regarded as the indicator of overall ductility of mixtures. However, increasing PE fiber content above 1.25% does not make a significant difference in terms of flexural performance. Given the lower cost of NM fibers compared to PE fibers and the similar beneficial effects of using NM fibers as obtained in the flexural strength measurements, the amount of PE fibers can be used with percentages of 1.25% when used with NM with percentages of 0.75% without substantially sacrificing flexural performance. Thus optimum fiber content was determined as a combination of 1.25% PE and 0.75% NM by volume. Properties of PE and NM fibers are shown in Table 3.8.

Table 3.8 Specifications of fibers

Fiber	Length (mm)	Radius ( $\mu\text{m}$ )	Strength (MPa)	Modulus of elasticity (GPa)	Specific weight ( $\text{kg/m}^3$ )
Polyethylene	9	12	3500	123	970
Nylon-mono	19	26	966	25	1140

### 3.2 Method

Three types of specimens were produced in this thesis work. Firstly geopolymer pastes were developed to observe the reactivity of materials and the feasibility of utilizing them in alkali-activation. Also, geopolymerization reaction products were determined by microstructural investigations. Then mortars with different aggregate sizes were developed. Mechanical performance of different aggregate sizes was observed and the effect of different aggregate sizes was studied through scanning

electron microscopy (SEM) analyses. Finally, engineered geopolymer composites (EGC) were produced. Detailed information will be presented in related sections.

### 3.2.1 Determination of Si, Al and Ca ions availability

All CDW-based materials were analyzed with inductively coupled plasma optical emission spectroscopy (ICP-OES) to observe Si, Al and Ca ions availability. CDW-based materials were dissolved in NaOH solution (1 M). Solid to liquid ratios were 1:100 (Figure 3.9). Suspensions were sieved (75  $\mu\text{m}$ ) and diluted with 5% HCl solution. After that, ICP-OES analyses were conducted on prepared solutions. Table 3.9 presents the dissolution rates of CDW-based materials according to ICP-OES results.



Figure 3.9. Preparing ICP-OES specimens

Table 3.9 Dissolution rate of CDW-based materials

Precursor	ICP-OES Results (mg/L)		
	Al	Si	Ca
RCB	363	424	0*
RT	230	647	0*
HB	293	576	0*
G	27	937	0*
C	5252	150	6

\* Results below a certain value reported to be as zero



### **3.2.2 Geopolymer paste preparation with single CDW and testing**

Early studies conducted in the context of this thesis work are concentrated on developing geopolymers with single CDW-based materials. Firstly developed geopolymer pastes were activated with only sodium hydroxide and specimens were cured at higher temperatures. Geopolymer pastes were produced firstly by NaOH pellets which were dissolved in drinkable water. NaOH solutions were prepared with three different molar ratios of Na as 10%, 12% and 15%, then left in laboratory conditions to cool down to room temperature. Water to binder ratios of all specimens were 0.35, alkaline activator to binder ratios were 0.48, 0.51 or 0.55 and mix designs are summarized in Table 3.10. No chemical admixtures were used to avoid interaction between chemical admixtures and alkaline activator. Concrete waste was not used in the first generated geopolymer paste samples, as concrete waste reduces workability.

CDW-based precursor was placed in a mortar mixer and was mixed for 60 s, and then the solution was poured into the mixer and stirred for 210 s. After a 15 s of waiting period, paste was mixed for an additional 60 s and then placed in 50 mm sized cubic molds. Immediately after molding, the specimens were placed in the oven for curing until the testing age of 24, 48 or 72 h, as can be seen in Figure 3.10. For each specimen group, different specimens were cured at 50, 65, 75, 85, 95, 105 and 115 °C for 24, 48 and 72 h.

Compressive strength of specimens was determined by a testing machine right after the curing process. Additionally, some of the selected specimens were examined by scanning electron microscopy (SEM) and energy-dispersive x-ray spectroscopy (EDX), x-ray diffraction (XRD) and thermogravimetric analysis / differential thermal analysis (TGA/DTA) to observe chemical, mineralogical, microstructural and morphological characterization. The results obtained from these studies guided the further studies of the thesis. For the sake of simplicity, geopolymer pastes with single precursor will be called single paste.

Table 3.10 Geopolymer paste compositions with single precursor

Precursor (450 g)	NaOH solution			W/B ratio	AA/B ratio
	Na	NaOH	Water		
	%	(g)	(g)		
Red clay brick (RCB)	10	78.3	139.9	0.35	0.48
	12	93.9	136.4	0.35	0.51
	15	117.4	131.1	0.35	0.55
Roof tile (RT)	10	78.3	139.9	0.35	0.48
	12	93.9	136.4	0.35	0.51
	15	117.4	131.1	0.35	0.55
Hollow brick (HB)	10	78.3	139.9	0.35	0.48
	12	93.9	136.4	0.35	0.51
	15	117.4	131.1	0.35	0.55
Glass (G)	10	78.3	139.9	0.35	0.48
	12	93.9	136.4	0.35	0.51
	15	117.4	131.1	0.35	0.55



Figure 3.10. Cubic geopolymer paste specimens

### 3.2.3 Geopolymer paste preparation with multi CDW and testing

Based on the results of the first geopolymer pastes produced with a single CDW-based precursor, new pastes were developed with the binary combinations of clayey precursors (red clay brick, hollow brick and roof tile) since clayey materials had better strength development. Despite the fact that the preparation of geopolymer pastes with binary CDW-based material is completely the same as the preparation of pastes with single CDW-based material. However, the amount of NaOH was set up according to the molarity of NaOH, not the Na amount, since it is thought that obtaining constant water to binder ratio is complicated due to the water release caused by NaOH dissolution. Glass, on the other hand, was not included in these mixtures as it could not provide sufficient strength on its own.

Table 3.11 Geopolymer paste compositions with binary precursor

Precursor (g)			NaOH solution			W/B ratio	AA/B ratio
RCB	HB	RT	Molarity (M)	NaOH (g)	Water (g)		
750	-	250	10	128.0	320	0.32	0.45
500	-	500	15	192.0	320	0.32	0.51
250	-	750	19	243.2	320	0.32	0.56
750	250	-	10	128.0	320	0.32	0.45
500	500	-	15	192.0	320	0.32	0.51
250	750	-	19	243.2	320	0.32	0.56
-	250	750	10	128.0	320	0.32	0.45
-	500	500	15	192.0	320	0.32	0.51
-	750	250	19	243.2	320	0.32	0.56

Because of the satisfactory results obtained from the first studies with geopolymer with single clayey material content, performance of geopolymer with binary clayey materials with relatively low NaOH molarity was wanted to investigate. Since some single geopolymer pastes were cracked, the water to binder ratio was decreased from

0.35 to 0.32 in these mixtures. Geopolymer pastes with binary precursor designs are seen in Table 3.11. Since the results of geopolymer pastes with single precursors showed that low curing temperatures (65, 75 and 85 °C) had lower strength results, curing temperatures in geopolymer pastes with binary precursors were revised to be 95, 105, 115 and 125 degrees, while curing periods did not change. For the sake of simplicity, geopolymer pastes with binary precursors will be called binary paste.

Tests conducted on binary pastes were the same as those conducted on single pastes. Detailed explanations about the tests and experiments will be given in the relevant sections.

### **3.2.4 Geopolymer mortar preparation and testing**

According to the results obtained from the geopolymer pastes, geopolymer mortars containing different sizes of sand have been developed. Recycled concrete aggregate was used as sand with three different particle sizes of 4.00 - 2.00 mm, 2.00 - 0.85 mm and 0.85 - 0.10 mm. NaOH concentrations were 10 M, 15 M and 19 M as in the binary geopolymer pastes. Since almost all binary geopolymer paste samples' strength increased parallel to the temperature increment from 95 to 105 °C, the curing temperatures of the mortars were set as 105, 115, and 125 °C. Geopolymer mortar designs are illustrated in Table 3.12. Since recycled concrete aggregate dilutes the geopolymer paste, the curing time was kept 72 hours to achieve a better interfacial transition zone between the aggregate and the paste.

The effect of fine recycled concrete aggregate (FRCA) with the different surface areas on interfacial transition zone was investigated by changing the sand sizes used in the production of mortars. SEM analyses were also conducted for interfacial transition zone examination. Additionally, the effect of FRCA amount on properties of mortar was investigated with different FRCA to binder ratios.

Table 3.12 Geopolymer mortar compositions

Binder (g)	FRCA Size	Molarity (M)	NaOH (g)	Water (g)	FRCA (g)	FRCA/ Binder
550	4.75-2.00	10	76.5	192.5	198.0	0.36
550	4.75-2.00	15	114.8	192.5	198.0	0.36
550	4.75-2.00	19	143.5	192.5	198.0	0.36
550	4.75-2.00	10	76.5	192.5	247.5	0.45
550	4.75-2.00	15	114.8	192.5	247.5	0.45
550	4.75-2.00	19	143.5	192.5	247.5	0.45
550	4.75-2.00	10	76.5	192.5	302.5	0.55
550	4.75-2.00	15	114.8	192.5	302.5	0.55
550	4.75-2.00	19	143.5	192.5	302.5	0.55
550	2.00-0.85	10	76.5	192.5	198.0	0.36
550	2.00-0.85	15	114.8	192.5	198.0	0.36
550	2.00-0.85	19	143.5	192.5	198.0	0.36
550	2.00-0.85	10	76.5	192.5	247.5	0.45
550	2.00-0.85	15	114.8	192.5	247.5	0.45
550	2.00-0.85	19	143.5	192.5	247.5	0.45
550	2.00-0.85	10	76.5	192.5	302.5	0.55
550	2.00-0.85	15	114.8	192.5	302.5	0.55
550	2.00-0.85	19	143.5	192.5	302.5	0.55
550	0.85-0.10	10	76.5	192.5	198.0	0.36
550	0.85-0.10	15	114.8	192.5	198.0	0.36
550	0.85-0.10	19	143.5	192.5	198.0	0.36
550	0.85-0.10	10	76.5	192.5	247.5	0.45
550	0.85-0.10	15	114.8	192.5	247.5	0.45
550	0.85-0.10	19	143.5	192.5	247.5	0.45
550	0.85-0.10	10	76.5	192.5	302.5	0.55
550	0.85-0.10	15	114.8	192.5	302.5	0.55
550	0.85-0.10	19	143.5	192.5	302.5	0.55

### **3.2.5 Engineered geopolymer composite preparation and testing**

#### **3.2.5.1 Selection of materials for EGC design**

Although clayey materials have better strength development in geopolymer pastes and mortars, concrete waste and glass are also included in the EGC production. While very high strength can be obtained from alkali-activation of clayey materials in pastes and mortars, EGC does not need high strength. On the contrary, when the specimens are cracked with preloading, a less mature matrix is preferred instead of very high toughness in order to create multiple micro-cracks. Also, ground granulated blast furnace slag (S) was included in some mixtures to investigate the effect of slag as a potential calcium source.

All geopolymer pastes and mortars were produced by only NaOH.  $\text{Na}_2\text{SiO}_3$  was later included in the design of EGCs to further evaluate the self-healing process of EGCs. The first reason for this is that self-healing is more complex phenomenon than strength development. In the literature, there are many studies that have concentrated on alkali-activation of conventional precursors (i.e., fly-ash, metakaolin, ground granulated blast furnace slag, etc.). However, the feasibility of CDW-based materials still had to be studied. When self-healing capability is considered, different parameters which may affect self-healing should have been investigated. Accordingly,  $\text{Na}_2\text{SiO}_3$  and  $\text{Ca}(\text{OH})_2$  were included in some EGC designs, just as slag was added.

The optimum amount of CDW-based precursors with/without slag to be used in the geopolymer mixtures was determined based on a series of preliminary tests, including workability, compressive strength and flexural strength measurements performed at ambient temperature with compositions having different CDW-based precursors and slag utilization rates. After the preliminary investigations, the mixture including the combination of 25% RT, 15% RCB, 20% HB, 10% G, 10% C and 20% S, by the total weight of all CDW-based precursors, was determined to be the

optimum and starting mixture design (S1) in terms of workability and compressive strength. The starting mixture design (S1) was then diversified in terms of the alkaline activator types and concentrations to obtain S3 and S5 mixtures. S1, S3 and S5 mixtures were finally produced without slag to have S2, S4 and S6 mixtures, respectively. Thus, in total, six geopolymers mixture designs were set (Table 3.13)

Sodium hydroxide quantity was determined based on Na to binder ratio. Sodium hydroxide solutions contain 6 or 10wt% Na according to the whole binder weight. After that, the water amount is defined to keep a water/binder ratio, 0.35. Because sodium hydroxide is determined according to the sodium amount, sodium hydroxide molarity values do not exist in Table 3.13.

Contingent on the EGC design, sodium hydroxide was utilized in combinations with calcium hydroxide or sodium silicate solution. While S3 and S4 have 2% of additional calcium hydroxide, S5 and S6 contain 6% to procure more hydroxyl ions because of these ions' siloxo and silicate breaking capability (Reig *et al.*, 2014). It is reported that elevated pH resulted from hydroxide type of activator decreases the dissolvability of calcium hydroxide because of the OH<sup>-</sup> saturation (Provis and Bernal, 2014).

A combination of lime and Na<sub>2</sub>SiO<sub>3</sub> promotes early reactions of alkali-activation (Wang, Scrivener and Pratt, 1994). Also, activating slag with Na<sub>2</sub>SiO<sub>3</sub> solution is suitable for early reactions (Qing-hua, Tagnit-hamou and Sarkar, 1991). Thus, calcium hydroxide was utilized with sodium silicate solution (S3 and S4) to observe the effect of early strength development on self-healing behavior. Additionally, S5 and S6 have 6% calcium hydroxide with no sodium silicate solution to investigate silica releasability of tile and bricks, which are rich in silica, when the activator does not provide SiO<sub>4</sub> tetrahedrals to the system. Considering the lack of silica because of the exclusion of silicate species from activator in S5 and S6, sodium hydroxide and calcium hydroxide amounts were increased to dissolve more silica tetrahedrals in the precursor. Recycled concrete aggregate with a maximum aggregate size of 2 mm is utilized as sand in all EGCs. Sand/binder ratio was 0.35 for all EGCs.

Table 3.13 EGC Mixture Designs

Amount, by weight	EGC ID					
	S1	S2	S3	S4	S5	S6
RT (%)	25	30	25	30	25	30
RCB (%)	15	17	15	17	15	17
HB (%)	20	23	20	23	20	23
G (%)	10	10	10	10	10	10
C (%)	10	20	10	20	10	20
S (%)	20	-	20	-	20	-
Sand / binder	0.35	0.35	0.35	0.35	0.35	0.35
Water / binder	0.35	0.35	0.35	0.35	0.35	0.35
Alkaline activators						
Na	6%	6%	6%	6%	10%	10%
NaOH (g)	106.8	106.8	106.8	106.8	178.0	178.0
Na <sub>2</sub> SiO <sub>3</sub>	2×NaOH	2×NaOH	2×NaOH	2×NaOH	-	-
Ca(OH) <sub>2</sub>	-	-	2%	2%	6%	6%
Fibers, by the total volume of mixtures (%)						
NM	0.75	0.75	0.75	0.75	0.75	0.75
PE	1.25	1.25	1.25	1.25	1.25	1.25

Conducted preliminary tests showed that PE and NM have higher resistance to elevated pH environments. It is also found that using polyethylene (PE) and nylon (NM) fibers with percentages of 1.25% and 0.75% by volume together produces enhanced deflection hardening behavior with multiple crack formation and low crack spacing. PE fiber content of more than 1.25% does not make much difference in the context of ductility increment or multiple crack formation; however, it increases the cost.



### 3.2.5.2 Production of EGCs

All EGCs were mixed in a laboratory-type mixer with a capacity of 12 liters. Precursors were mixed for 60 s at 100 rpm and then sodium hydroxide (cooled in laboratory conditions for 24 h) solution was added to the mixer and mixed for 120 s at the same speed. If EGC has sodium silicate or calcium hydroxide, they were added and mixed for 120 s. Fibers were incorporated into the mixture and mixed for 180 s at a speed of 300 rpm.

From each mixture,  $240 \times 80 \times 15 \text{ mm}^3$  prismatic specimens were produced to directly investigate the self-healing capability from optical observation through an optical microscope at  $125\times$  magnification. Cylindrical specimens ( $\text{Ø}100 \times 200 \text{ mm}^2$ ) were also prepared for cutting disc specimens with dimensions of  $\text{Ø}100 \times 50 \text{ mm}^2$  to investigate the changes in transportation properties. Fifty-mm cubic specimens were also produced to determine the compressive strength at different ages. Calcium hydroxide, especially sodium silicate, which was included in the system to see its effect on the healing mechanism, provided strength without high-temperature curing. Therefore, these samples were cured at room conditions. All specimens were demolded at the age of 24 h and cured under laboratory conditions ( $23 \pm 2 \text{ °C}$ ,  $50\% \pm 5\%$  relative humidity) for 7 days. The specimens were then preloaded and exposed to wetting-drying cycles.

### 3.2.5.3 Artificial crack formation by preloading and self-healing process

Prismatic specimens were preloaded, which can be seen in Figure 3.11a, under 70% of the ultimate flexural deformation capacity. Disc specimens were preloaded (Figure 3.11b) with splitting tensile loading under a load of 70% splitting tensile strength. After preloading, an accelerated self-healing period was applied on all sound and preloaded specimens to heal multiple microcracks formed after preloading (Figure 3.11c). This period contains a cycle of wetting in a water tank at a temperature of  $23 \pm 2 \text{ °C}$  for 24 h and then drying in an environment with a relative

humidity of 50% for 24 h. Crack widths were measured with an optical microscope before the accelerated self-healing period and then at 7, 28, 56, and 90 days after the starting day of self-healing.



Figure 3.11. Preloading of (a) prismatic- and (b) disc specimens, and (c) cracks formed after preloading

The measured cracks were repictured to determine the amount of self-healing. The same procedure was applied to the transportation properties of disc specimens. In

order to observe the transportation properties in more detail over time, electrical impedance and water absorption measurements were taken on the 14<sup>th</sup> day. Water absorption tests were conducted according to ASTM C 1585–11 (2013). Electrical impedance measurements were carried out using a concrete resistivity meter with uniaxial configuration. For this test,  $\text{Ø}100 \times 50 \text{ mm}^2$  cylindrical specimens were used in such a way that the sawed surfaces measuring 100 mm were inserted directly perpendicular to the set of plate electrodes, with cylindrical water-saturated sponges included to provide sufficient electrical contact between the electrodes and specimens. All tests were conducted on three separate specimens for each mixture design.

#### **3.2.5.4 Self-healing evaluation by transportation properties, water absorption and microstructural investigation**

Changes in the transportation properties were used to assess the self-healing. Electrical impedance (EI) and water absorption (WA) rate (sorptivity) measurements were made right before and after the preloading process. Then, measurements were made at 7<sup>th</sup>, 21<sup>st</sup>, 56<sup>th</sup> and 90<sup>th</sup> days. A resistance measurement device for cementitious materials working with an alternative current was used for electrical impedance recordings. Disc shaped ( $\text{Ø}100 \text{ mm} \times 50 \text{ mm}$ ) EGCs were cut from cylindrical ones ( $\text{Ø}100 \text{ mm} \times 200 \text{ mm}$ ) to EI and WA investigations. Three different identical disc specimens were used for each EGC group. A line was drawn on each disc being used as a reference for current direction. Wet foam rubbers were placed electrodes to ease electron transportation between EGC specimens and electrodes. Resistance measurement device have a wide range of frequency range between 1 Hz and 30.000 Hz, and being able to determine phase angle from  $0^\circ$  to  $180^\circ$ . 1000 Hz was defined as working frequency with the purpose of avoiding polarization (Hou, 2008). Since all EI results were below 10 degrees ( $\cos 10 \cong 0.99$ ) and measured areas were same for all specimens, EI values were recognized as resistance values. EI recording equipment is shown in Figure 3.12.



Figure 3.12. Electrical impedance testing device

Determination of water absorption (WA) rates (sorptivity) were made in compliance with ASTM C1585-11 (2011). Dimensions and numbers of WA specimens were the same as those of EI. Weighted oven-dried specimens and sides were insulated with silicon to make water contact on only bottom of specimen which was immersed in water. Specimens were weighted at certain times of 1, 2, 3, 4, 6, 8, 12, 16, 20, 25, 36, 49, 64, 81, 120 and 360 minutes (Figure 3.13). Slope of the curve of  $l$  [mm] to time ( $\text{sec}^{1/2}$ ) was recognized as WA rate.  $l$  refers to ratio of mass change to cross-section area of disc and water density. Further information can be found in ASTM C1585-11 (2011).

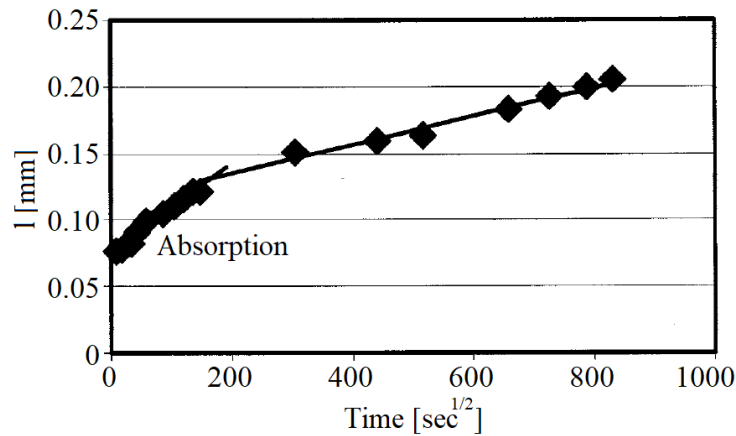


Figure 3.13. l – time curve (ASTM C1585-11, 2011)

Crystalline formations and if exist amorphous portions of EGC matrix and healed cracks were investigated by X-ray diffraction analyses (XRD). Also, surface of EGCs were analyzed to compare surface and healed crack. XRD analyses were conducted on powder samples of about 20 mg. Additionally, scanning electron microscopy (SEM) analyses were conducted to see what type of formations heal the existing cracks. Chemical content was determined by energy-dispersive X-ray spectroscopy (EDX) and line mapping analysis was performed to compare crack and surface in the context of chemical content. Cubic-shaped specimens with dimensions of 1 cm and obtained from EGCs completed healing period of 90 days were used SEM and EDX analyses.

### 3.2.5.5 Self-healing evaluation through mechanical recovery

Effects of self-healing on the mechanical properties were also determined. Determination of the self-healing had to be made not only by transportation properties, optical observation and microstructural analyses but also by the effect on mechanical properties. Accordingly, self-healing was also evaluated by mechanical recovery. Preloaded and sound prismatic specimens were exposed to the same wetting-drying cycles. At the end of the healing period, both preloaded and sound prismatic specimens were loaded under flexural loading. As can be seen in Figure

3.14, the midpoint displacements of prismatic specimens were recorded through a deflectometer. Flexural load and midpoint displacement for each EGC were drawn. Graphics of reloaded EGCs were placed right after the preloaded EGCs. In this context, mechanical recoveries were assessed both deflection hardening behavior and ductility of reloaded EGCs at the end of the healing period.



Figure 3.14. Midpoint displacement recording with deflectometer

## CHAPTER 4

### RESULTS AND DISCUSSION

#### 4.1 Geopolymer pastes with single CDW-based material

##### 4.1.1 Compressive strength

Table 4.1 presents the uniaxial compressive strength results of all CDW-based geopolymer pastes with a single precursor content. All results were reported as the average of three specimens for each mixture design. Strength results of geopolymers cured at 50 °C could not be obtained as they could be crumbled in hand.

As can be seen, curing temperature below 100 °C and curing period of 24 h could not reach up to 20 MPa for roof tile (RT); however, curing longer than 24 h needs less curing temperature to gain a desirable amount of strength. There is no need to curing 72 h due to the small difference between 48 h and 72 h. However, maximum strength values of RT were achieved at 115 °C, which are 35.5, 42.3 and 31.4 MPa for 10%, 12% and 15% of Na content, respectively. These values are significantly different from strength values for 105 °C and 115 °C. In general, 48 h of curing is required at lower temperatures than 100 °C, but when it is switched to higher temperatures, it's sufficient to achieve desirable results for 24 h of curing.

The maximum compressive strength result of red clay brick (RCB) is 45 MPa, at which 12% of sodium, 72 h of curing at 105 °C. In addition to this, 10% and 15% molarity of sodium have compressive strength results higher than 40 MPa by 48 h of curing for 95 °C and 115 °C, respectively. Maximum strength result of RCB at median temperatures belongs to specimen activated by 10% Na and this is attributed to relatively coarser particles of RCB. Coarser particles require less water and

consequently, paste becomes more workable and can be compacted easily. Thus a very dense hardened paste structure is obtained. Also, curing at median temperatures prevents the formation of cracking. This dense structure will be seen in further sections as supported by the scanning electron microscopy results.

Maximum compressive strength results of hollow brick (HB) for all three sodium molarities were achieved for 24 h curing and 115 °C and higher temperatures of curing, just like in RT. However, it's possible that desirable strength results can be obtained by lower temperatures than 115 °C cured for 48 h.

Considering Na concentration, maximum strength results were achieved for RT, RCB and HB at 12% Na concentration. This situation promotes that increasing sodium content ease dissolution of aluminosilicate sources (Singh *et al.*, 2016). However, increasing sodium content and low mobility of alkali ions introduce an optimum sodium content. In the case of upper values of this optimum Na content, diffusion of alkali ions and consequently polymerization becomes harder (Alonso and Palomo, 2001).

Glass waste (G) results indicate that getting high strength results requires high molarity of sodium and low curing periods or 72 h of curing period and temperatures between 75 °C and 105 °C. G activated with 10% Na activator and cured for 72h specimens have compressive strength results of 35.8, 34.2, 36.1 and 33.5 MPa for 75, 85, 95 and 105 °C of curing temperatures, respectively. G suffers from a lack of Al<sub>2</sub>O<sub>3</sub> and compressive strength development behavior according to curing temperature, period and Na concentration differs from waste bricks. Compressive strength results of G are lower than brick and tile wastes generally. There are some studies to provide additional aluminum to waste glass activated systems (Pascual, Tognonvi and Tagnit-hamou, 2014), and it's reported that increasing additional aluminum content provides stabilization to the system.



Table 4.1 Compressive strength results of geopolymer pastes (28 days) with single CDW-based precursor content

CDW Type	Curing Period (h)	Compressive Strength (MPa)																				
		10% (Na)							12% (Na)							15% (Na)						
		65	75	85	95	105	115	125	65	75	85	95	105	115	125	65	75	85	95	105	115	125
RT	24	4.5	6.2	10.2	18.1	29.6	35.5	28.7	5.6	8.0	9.6	20.6	30.3	42.3	32.5	4.2	5.3	7.4	20.3	21.5	31.4	25.8
	48	6.5	14.5	22.9	23.7	23.4	31.1	23.8	5.7	8.7	24.3	24.7	31.8	32.6	27.5	4.7	6.6	17.2	23.7	21.6	29.8	27.6
	72	6.9	15.5	23.2	23.9	23.5	31.5	24.6	7.4	9.7	30.5	23.6	31.5	35.7	30.5	5.1	7.7	21.6	21.2	24.2	30.5	28.9
RCB	24	4.2	5.4	9.7	17.4	30.6	19.8	23.5	4.3	4.7	6.7	8.0	21.6	34.8	13.6	4.4	5.1	5.7	6.5	9.6	27.3	20.1
	48	6.2	11.2	22.5	41.8	23.4	22.4	19.9	5.5	6.3	13.1	19.1	19.5	33.9	18.3	5.5	5.6	7.2	10.8	27.3	42.5	23.4
	72	7.1	12.4	35.3	40.2	23.5	21.6	21.1	6.6	7.1	14.2	33.9	45.0	33.5	17.1	5.7	6.8	9.7	16.0	39.0	38.0	27.0
HB	24	4.2	4.1	7.8	26.1	18.6	19.8	43.7	5.3	6.6	5.1	9.4	12.6	45.7	45.8	7.2	8.6	4.2	8.6	12.2	38.9	26.7
	48	4.3	15.3	26.6	27.9	19.7	22.4	38.3	4.1	7.6	10.4	22.7	20.9	40.0	37.1	9.0	8.8	6.2	30.1	32.5	33.4	25.3
	72	5.1	17.1	30.8	25.7	19.5	21.6	35.5	6.1	8.1	30.9	18.4	20.1	37.7	39.3	9.5	11.2	10.8	18.5	28.2	33.3	24.9
G	24	4.6	8.1	9.2	15.9	18.6	20.7	15.0	5.5	5.3	6.9	17.8	20.3	25.1	16.5	3.1	5.1	5.9	15.5	26.5	30.3	22.7
	48	5.9	17.2	19.5	19.0	19.7	19.2	19.0	5.6	6.3	7.0	18.1	20.9	27.4	18.3	4.1	4.2	5.5	15.6	26.3	26.4	25.6
	72	5.9	35.8	34.2	36.1	33.5	19.2	15.9	6.8	25.6	25.3	26.8	28.0	24.7	18.1	4.0	18.2	17.9	20.2	24.7	25.2	21.0

\*65, 75, 85, 95, 105, 115 and 125 refers to curing temperatures in °C

Except for RT almost all specimens have a trend to give higher strength results as curing temperature increases. However, there are optimum curing temperatures for every specimen and strength decreases after this temperature. This trend indicates that high temperature may harm specimens. According to Ken et al. (2015), prolonged curing at higher temperatures could destroy the granular structure of geopolymer. These optimum curing temperatures can be seen in Table 4.2. Some of the optimum temperatures of HB are 125 °C means that the optimum curing temperature of HB may be higher than 125 °C. HB has the highest Si/Al ratio of all bricks wastes, which is 2.9.

Table 4.2 Optimum curing temperatures according to maximum compressive strength results

CDW-based precursor	Na (%)	Optimum curing temperatures (°C)		
		24	48	72
RB	10	115	115	115
	12	115	115	115
	15	115	115	115
RCB	10	105	95	95
	12	115	115	105
	15	115	115	105
HB	10	125	125	125
	12	125	115	125
	15	115	115	115
G	10	115	105	95
	12	115	115	105
	15	115	115	115

Curing in high temperatures requires energy consumption. So the feasibility of the curing process taking more than 24 h should be investigated. As it can be seen, long-time curing for G has a significant effect at lower temperatures relatively. The rate of strength development of RCB is more significant in high temperatures, especially

for 72 h than HB and RT. It's attributed that RCB is coarser than the other waste bricks and its adsorbed water is less than the others. Besides, dissolution of solid particles is at the surface (Duxson, Fernandez-Jimenez, *et al.*, 2007) and according to Shi et al. (2005) rate of chemical reaction is doubled with every temperature increase of 10 °C.

All bricks and RT trend to give higher strength development after 24 h as curing temperature and Na concentration increase. Raising Na content provides more dissolution and dissolved aluminate and silicate species introduce more condensation as requirements of chemical reactions are fulfilled.

In order to statistically justify the abovementioned observations, Pearson correlation studies were conducted to observe the relationship between compressive strength and design parameters (sodium concentration, curing period and temperature) and the results are shown in Table 4.3. While a '+1' of the correlation coefficient indicates the perfect positive relation, '-1' refers to a perfect negative relation and '0' means there is no relation between strength and design parameters. All calculations were made between compressive strength and design parameters. Correlation coefficients exhibit that curing temperature is the most important parameter for strength development. Temperature correlations coefficients of RT and HB, which are 0.864 and 0.801, respectively, clearly demonstrate that curing temperature increment raises strength. RCB and G, which have correlation values of 0.635 and 0.574, have noticeable correlations, although not as much as RT and HB.

For all precursors, the correlation between the curing period and strength is rather weak, but still positive. G has the maximum correlation between strength and curing period, which is 0.364. It is clearly seen that while clayey materials have positive higher correlations between temperature and strength, their correlations between curing period and strength are quite low, such that RCB, HB and RT have correlation coefficients of 0.295, 0.143 and 0.114, respectively.

All correlations between strength and activator concentration are negative, however rather closest to zero. Accordingly, it can be said that although the increase in sodium

concentration has a slightly negative effect on the strength, it does not have a significant effect.

Table 4.3 Single geopolymer paste strength's Pearson correlations with curing period, temperature and concentration

Precursor		Curing period	Temperature	Concentration
G	Pearson Correlation	0.364	0.574	-0.091
	Sig. (2-tailed)	0.003	0.000	0.479
	N	63	63	63
HB	Pearson Correlation	0.143	0.801	-0.077
	Sig. (2-tailed)	0.263	0.000	0.551
	N	63	63	63
RCB	Pearson Correlation	0.295	0.635	-0.122
	Sig. (2-tailed)	0.019	0.000	0.341
	N	63	63	63
RT	Pearson Correlation	0.114	0.864	-0.096
	Sig. (2-tailed)	0.373	0.000	0.455
	N	63	63	63

## 4.1.2 Microstructural analyses of single geopolymers pastes

### 4.1.2.1 X-Ray diffraction (XRD) analyses

Since HB with 12% Na, cured for 24 h at 115 °C has the highest strength (45.8 MPa), three of HB specimens' (12% Na, cured for 24 h at 75 °C, 115 °C and 125 °C) microstructures were investigated with X-ray diffraction analyses. Diffraction patterns of these specimens can be seen in Figure 4.1. Numerical values are not presented on the y-axis as all the graphs are presented on top of each other. CDW-based materials used at the starting of the thesis study were different according to the crystallographic structures. Thus XRD graphs of raw materials (indicated with rm) presented in this section differ slightly from other sections. Minerals exist in XRD graphics and their powder diffraction file (pdf) numbers are: A=albite (pdf:96-900-

0705), An=anorthite (pdf:96-900-0363), C=cancrinite (pdf:96-900-4053), D=diopside (pdf:96-900-5183), M=melilite (pdf: 96-900-7367) Mu=mullite (pdf:96-900-1568), Q=quartz (pdf:96-900-9667), S=sodalite (pdf:96-900-5742), H=hematite (pdf:96-900-2591).

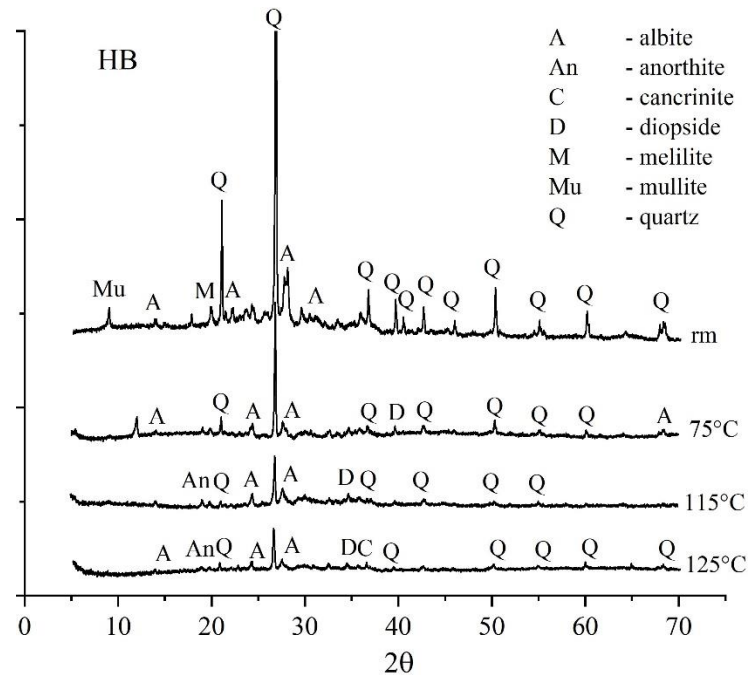


Figure 4.1. XRD patterns of HB raw material (rm) and alkali-activated HB for 12% Na and 24 h of curing at different temperatures

It's indicated that the main geopolymerization product of HB is albite. As Provis and van Deventer (2009) mentioned, albite (NAS6) is an aluminosilicate product of sodium-activated feldspar containing clay. Although the solubility of crystalline phases is quite low, the amount and intensities of quartz minerals are reduced after geopolymerization. Increasing curing temperature initiates the formation of cancrinite, which is a secondary phase of NaOH-activated fly ash according to Provis and Bernal (2014) and anorthite formation, which is a mineral of plagioclase. The amount of albite, which is another plagioclase, is more than anorthite. This situation is due to the low calcium content of brick wastes. Anorthite exists in specimens cured at 115 °C and 125 °C temperatures, with compressive strength results of 45.7 MPa and 45.8 MPa, respectively. However, specimens cured at 75 °C do not contain

anorthite mineral, which has a 6.6 MPa compressive strength result. Even so, it should not be considered that low strength result is just dependent on mineral structure.

In Figure 4.2, XRD peaks of raw material and alkali-activated RCB geopolymers pastes cured at 105 °C and 115 °C for 24 h and 72 h can be seen. Sodalite is one of the two dominant minerals together with cancrinite and it is a secondary phase of NaOH-activated fly ash binders, just like cancrinite (Provis and Bernal, 2014). Besides, sodalite is a product of NaOH-activated kaolinite (Davidovits, 1994). Common sides of geopolymers contain cancrinite or sodalite are having a higher Si/Al ratio and being rich in Al content (Oh *et al.*, 2010; Provis *et al.*, 2014). As it can be seen, conversion of cancrinite to sodalite or reverse could be possible for different curing conditions. It's stated before that hematite is reactive at not ordinary temperatures, alkali-activated RCB pastes do not contain hematite mineral, so it can be said that 100 °C is enough for its reactivity.

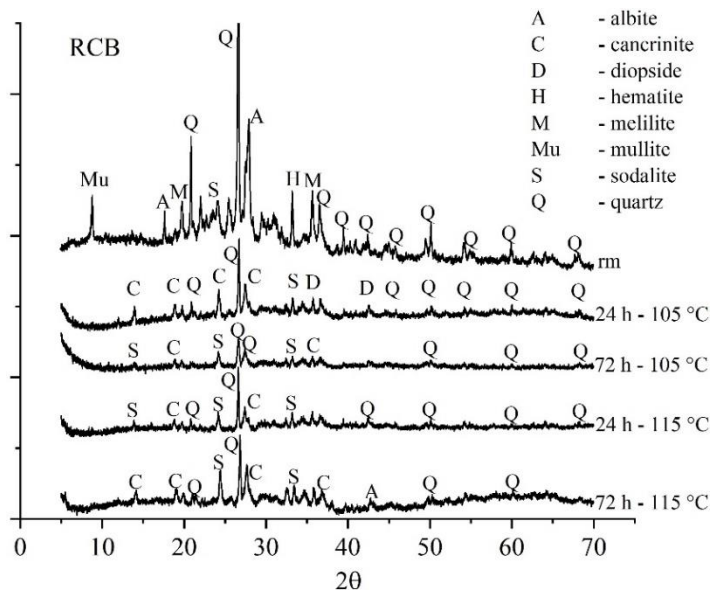


Figure 4.2. XRD patterns of RCB raw material (rm) and alkali-activated RCB with 12% Na for different curing conditions

As can be seen in Figure 4.1 and Figure 4.2, while HB and RCB have similar mineral contents, their reaction products have entirely different crystallographic structures

despite the same curing conditions. This is attributed to the particle size distributions, shape and morphology. According to Provis et al. (2009), while fly ash particles react with an alkaline solution, the primary reaction product consolidates on particle surfaces and some particles of fly ash may be covered with reaction products; thus, these particles react very slowly. This situation may cause a variety of dissolution, gelation, reorganization and polymerization mechanisms. Especially for gelation, reorganization, and polymerization mechanism, while one of them takes place, another one may have occurred.

#### **4.1.2.2 Scanning electron microscopy (SEM) analyses**

In order to observe the microstructure of single geopolymer pastes, appropriate pieces of specimens were subjected to SEM analysis. Besides, energy dispersive X-ray analyses (EDX) were performed to observe chemical formations of geopolymerizations. Unreacted/undissolved particles can be seen in Figure 4.3a,b and these particles are due to a partial dissolution of waste materials (Bernal *et al.*, 2012; Moungam *et al.*, 2017). Agglomeration of these particles makes their behavior as coarse aggregate and consequently, viscosity increases and the porous structure is formed. However, the activator that contains 12% Na, facilitates the dissolution of HB and provides Si and Al availability to the system. Thus, the volume of reaction products, especially N-A-S-H, increases, as can be seen in Figure 4.3c and d. Compressive strength results promote this situation which are 7.8, 19.8, 45.7 and 45.8 MPa for HB cured for 24 h, temperatures and Na content of 85°C-10%, 115°C-12% and 125°C-12% respectively.

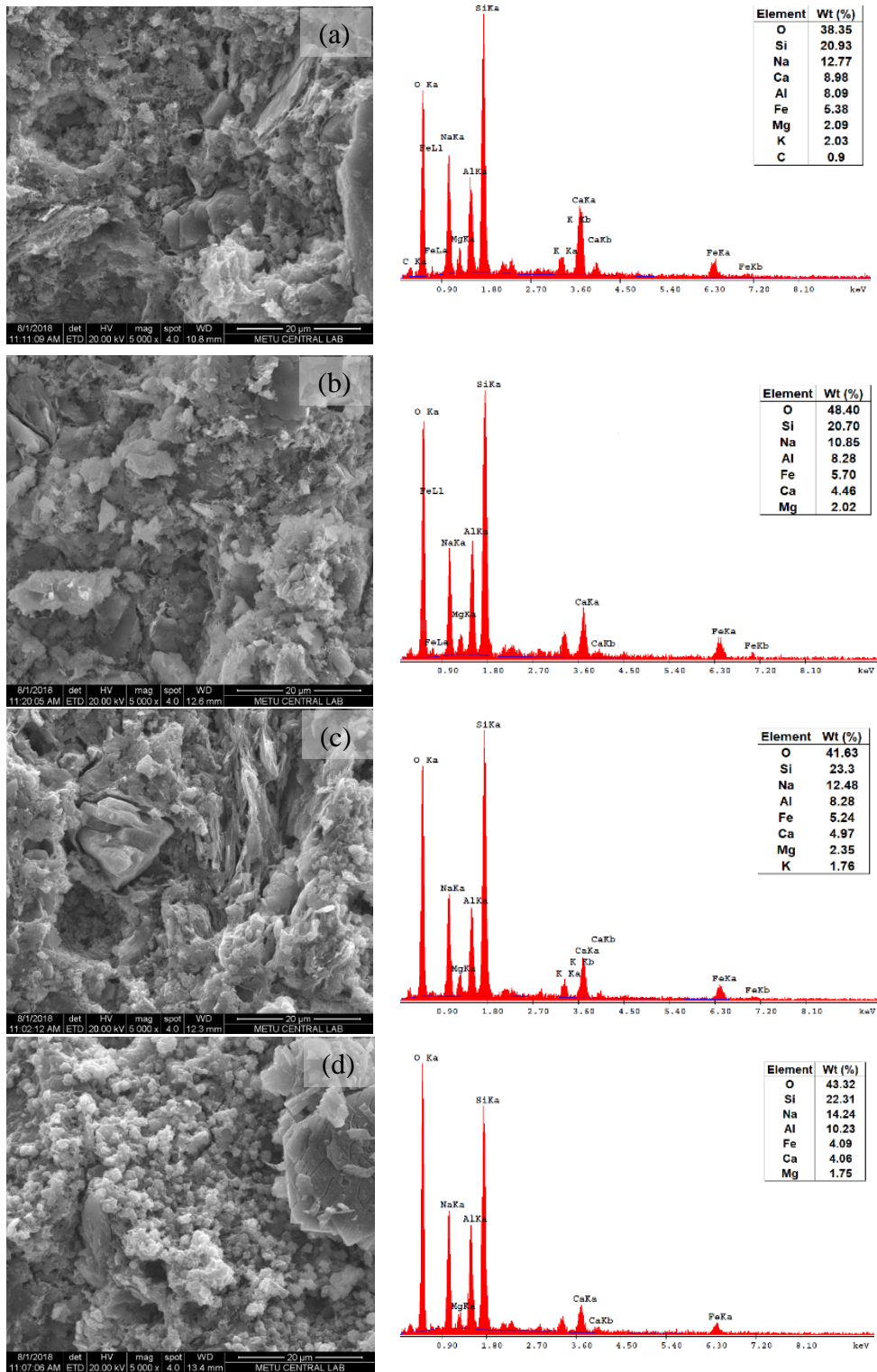


Figure 4.3. SEM images and EDX results of alkali-activated HB cured for 24 h, temperatures and Na ratio of (a) 85 °C and 10% (b) 115 °C and 10% (c) 115 °C and 12% (d) 125 °C and 12%



As shown in Figure 4.4, increasing curing time makes the structure of HB paste denser and results in more N-A-S-H products. However, cracks which can be seen in Figure 4.4b (red bordered), are caused by long-term curing at high temperatures. These cracks are attributed to that low Na concentration causes high water content for constant water to binder ratio and consequently provokes high cracking potential of paste. Thus there is not much difference in compressive strength between curing time for 24 h and 72 h, for low molarity of Na containing specimens above 105 °C.

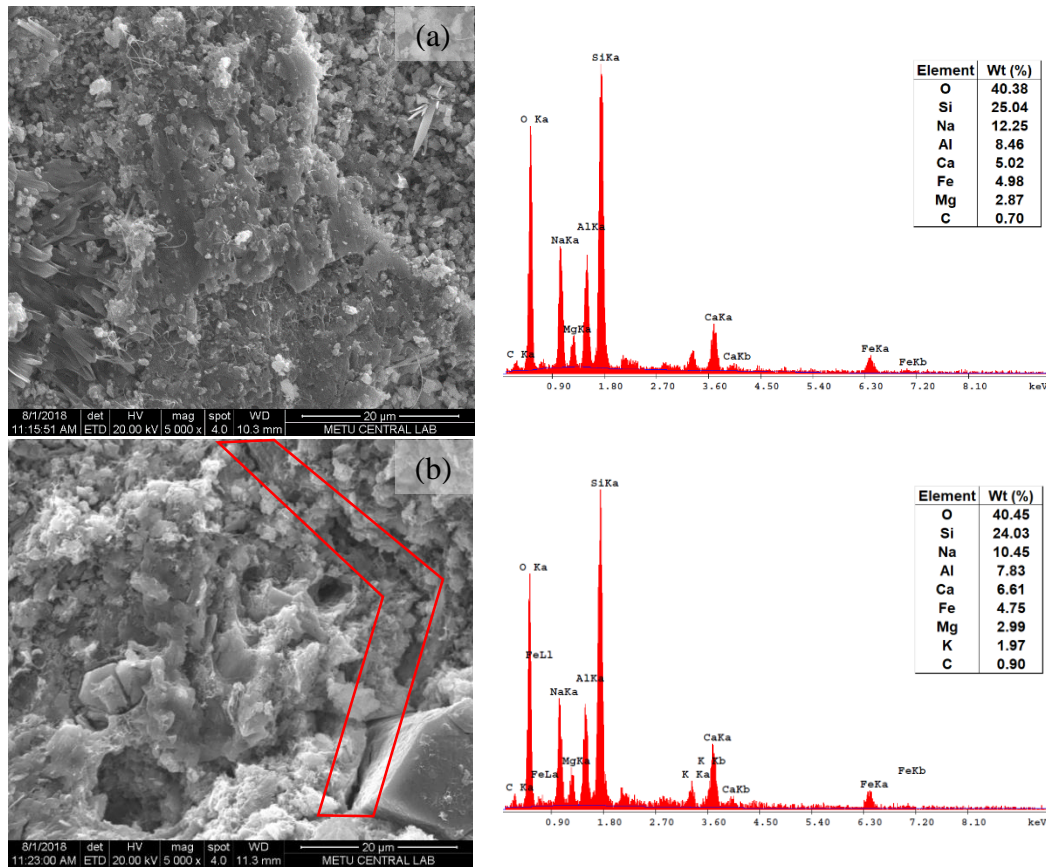


Figure 4.4. SEM images and EDX results of alkali-activated HB cured for 72 h, temperatures and Na ratio of (a) 85 °C and 10% (b) 115 °C and 10%

Figure 4.5 presents the SEM images and EDX results of RCB activated with 12% Na and cured at 105 and 115 and for 24 h and 48 h. Paste in Figure 4.5a has a porous structure according to b,c, and d. Cracks can be seen in all images; however, a,c and d have linked cracks. Even though pastes in Figure 4.5c and d have very dense structures, their cracks reduce strength results of these specimens.

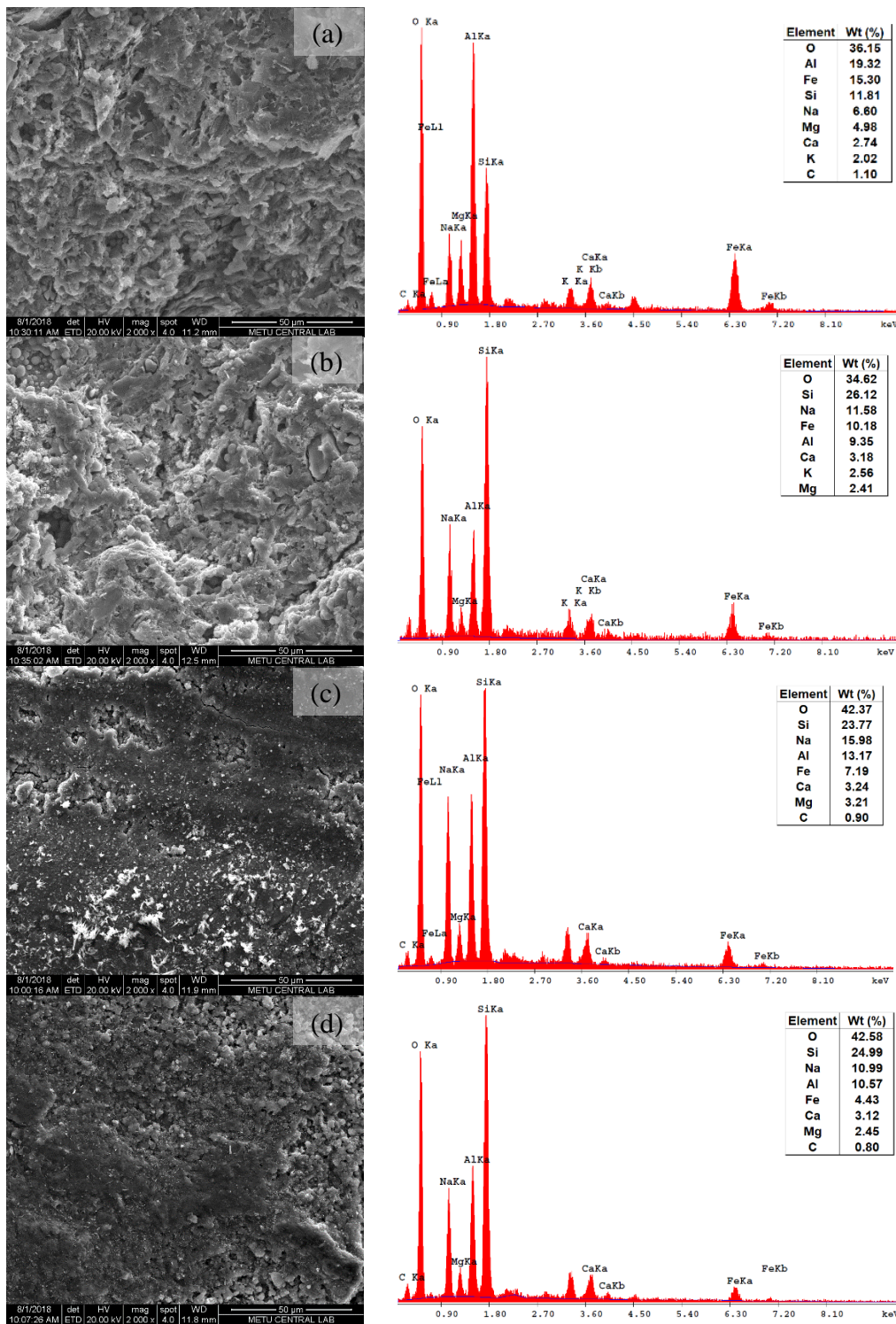


Figure 4.5. SEM images and EDX results of alkali-activated RCB activated with 12% Na and cured at temperatures and curing period of (a) 105 °C and 24 h (b) 105 °C and 72 h (c) 115 °C 24 h (d) 115 °C 72 h

#### 4.1.2.3 Thermogravimetric (TGA) and differential thermal analyses (DTA)

TGA and DTA graphics can be seen in Figure 4.6. According to Kucharczyk et al. (2018), mass changes are mainly due to dehydration and dehydroxylation below 550 °C, and decarbonation above 550 °C. It can be seen in Figure 4.6, G has the highest free water loss among them. Considering the same grinding effort for all wastes, it is expected that G remained coarser than other CDW-based materials and has the highest free water content for the same w/b ratio. Weight loss above 300 °C is mainly due to loss of chemically bound water. Loss of chemically bound water are 3.5%, 3.7%, 3.6% and 5.5% for HB, RT, RCB and G, respectively. However amount of chemically bound water of G is higher than other CDW-based materials. Also, its chemically bound water is the highest. Water first acts as a medium for dissolution and then participates in geopolymerization reactions (Hajimohammadi, Ngo and Kashani, 2018) and after the geopolymerization, it is released back to the system (Provis and van Deventer, 2009).

The main reaction product of geopolymerization is N-A-S-(H) which contains not structurally bound water and the reaction product of alkali-activated high-calcium systems is C-A-S-H which has a similar structure of C-S-H. So, the presence of chemically bound water indicates the formation of C-S-H similar structures. Additionally, as shown in Figure 4.6a, the fineness of wastes and the amount of releasing free water are inversely proportional. Another point is increasing Si/Al raises water loss according to Figure 4.6a and it is attributed to that low Si/Al geopolymers have water that is more tightly bound within gel (Duxson, Lukey and Van Deventer, 2007). Besides, RCB has the lowest water loss in Figure 4.6a; it's because that RCB is finer than other waste materials and requires more water to be precisely compacted in moulds.

In Figure 4.6b, HB cured for 72 h has less free water content than HB cured for 24 h. It is attributed to that HB cured for 24 h has not completed geopolymerization reactions yet, as it can be seen from compressive strength results of HB cured at 85 °C, for 24 h and 72 h are 7.8 and 30.8 MPa. However, RCB specimens cured for 24

h and 72 h at 115 °C have approximately the same TGA graphs. The reason for this similarity is due to almost complete geopolymerization reactions of RCB for 24 h. This situation can be seen from the compressive strength results of RCB specimens cured for 24 h and 72 h, 34.8 MPa, and 33.5 MPa, respectively.

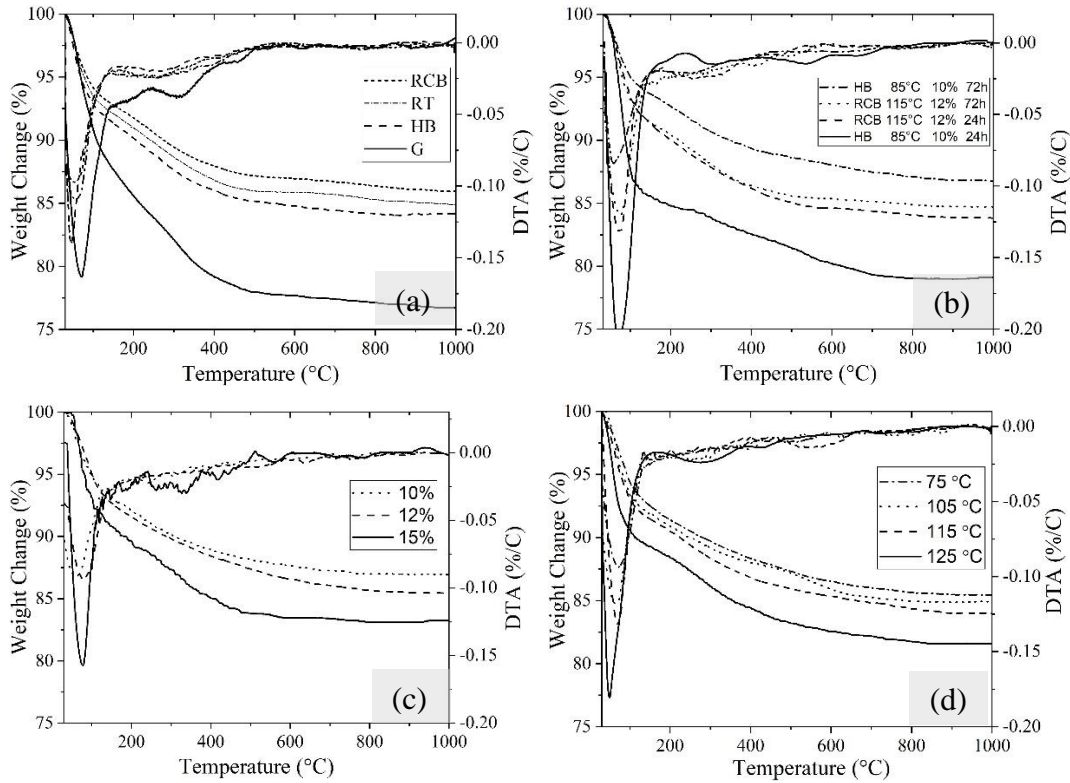


Figure 4.6. TGA & DTA graphics of single geopolymer pastes

TGA and DTA graphs of G pastes cured for 24 h at 115 °C with different Na concentrations can be seen in Figure 4.6c. According to Tashima et al. (2012), NaOH-activated glass fiber waste systems have a Na concentration gradient between partially reacted precursor particle surfaces and matrix, differently from KOH-activated systems. Weight losses of G pastes in Figure 4.6c have a trend to result in higher weight loss as increasing Na concentration in agreement with Tashima et al. (2012). According to Mustafa Al Bakria et al. (2011), geopolymer pastes with insufficient water content can not reach desirable strength results. HB pastes with Na ratio of 12% and cured for 24 h at 75, 105, 115 and 125 °C, which have 6.6, 12.6,

45.7 and 45.8 MPa compressive strength respectively and their weight loss can be seen in Figure 4.6d. In accordance with Bakria et al. (2011), free water content increases as compressive strength increases.

## **4.2 Geopolymer pastes with binary CDW-based material**

### **4.2.1 Compressive strength**

#### **4.2.1.1 Effect of curing temperature**

Uniaxial compressive strength results obtained from geopolymers with clayey precursors as combinations of RCB-RT, RCB-HB and RT-HB can be seen in Table 4.4. All results are presented as the average of three specimens. Although the lowest results were obtained at 95 °C, the increasing curing time raised strength values up to 80 MPa. For most of the binary geopolymer specimens, curing temperature increment raised strength; however, this strength increment ended after an optimum temperature. Accordingly, for high strength, instead of increasing the curing temperature as much as possible, it is necessary to find the optimum curing temperature for the precursor used. Temperatures above this optimum curing temperature lead to shrinkage which was also observed by Mo et al. (2014). Shrinkage may result in cracking and therefore strength of the specimen may decrease. In addition, the relatively low compressive strength at high temperatures is attributed to the deterioration of the geopolymerization products at temperatures higher than the optimum curing temperature. If geopolymer strength development rate is considered, it is known that geopolymerization products fill the pores; however, when the strength development rate is very high, precursors may be trapped in rapidly grown geopolymerization products. Thus ungeopolymerized precursors may hinder strength development. In addition to the ungeopolymerized precursor particles, the rapid growth of reaction products at early times of geopolymerization may cause voids in some parts.

Table 4.4 Compressive strength results of geopolymer pastes (28 days) with binary CDW-based precursor content

Binary Paste	Molarity	10 M				15 M				19 M			
	Curing T. (°C)	95	105	115	125	95	105	115	125	95	105	115	125
75RCB -25RT	24 h	19.3	21.9	23.0	23.4	20.6	27.5	27.8	30.7	15.1	16.0	18.2	39.6
	48 h	20.3	24.4	25.1	26.1	24.8	38.8	33.5	30.2	24.6	28.2	34.8	43.2
	72 h	22.4	23.4	24.2	23.6	26.9	39.1	34.5	27.5	35.5	46.2	48.7	46.1
50RCB -50RT	24 h	19.8	23.6	24.8	20.8	20.1	27.6	36.8	23.5	16.5	23.1	28.2	19.6
	48 h	26.7	29.9	32.7	27.6	21.6	34.1	32.7	28.9	32.4	35.2	44.9	27.6
	72 h	24.2	30.3	32.1	24.9	25.1	30.7	34.3	26.0	31.3	35.4	48.6	27.1
25RCB -75RT	24 h	21.0	24.5	25.1	22.6	19.5	25.2	22.0	21.2	10.2	17.7	24.2	31.3
	48 h	27.1	30.6	33.9	28.0	23.9	28.2	27.2	23.7	33.2	44.1	57.1	42.3
	72 h	25.3	31.2	33.1	25.1	26.2	31.0	34.5	26.8	29.6	36.3	44.9	34.8
75RCB -25HB	24 h	21.6	26.6	33.5	31.9	12.3	19.6	38.2	38.5	10.9	14.4	20.2	25.1
	48 h	28.5	29.4	28.1	28.3	26.8	43.3	45.0	42.9	16.3	45.5	62.9	65.1
	72 h	26.6	27.1	27.4	25.9	50.7	45.7	55.3	48.1	23.8	54.3	50.0	46.3
50RCB -50HB	24 h	26.2	27.9	35.3	37.1	12.0	16.5	22.8	45.8	11.2	14.3	22.1	29.6
	48 h	36.4	26.8	31.4	36.4	21.0	45.4	60.4	45.1	25.9	27.5	44.5	38.1
	72 h	35.9	37.9	34.4	38.7	29.4	54.5	64.2	44.4	33.7	35.2	39.9	35.0
25RCB -75HB	24 h	26.6	27.3	37.6	35.2	13.7	16.6	28.1	30.3	11.3	12.0	21.0	25.9
	48 h	30.4	31.4	42.1	37.3	24.2	33.9	79.6	69.6	13.7	30.4	48.9	47.5
	72 h	34.5	32.8	37.9	36.8	35.7	57.0	80.0	73.7	29.5	40.2	46.5	45.1
75RT -25HB	24 h	22.6	30.0	33.2	35.2	18.2	21.3	42.2	42.3	19.5	23.3	35.5	36.8
	48 h	24.7	33.9	40.1	30.3	29.5	43.4	45.0	54.9	23.1	35.7	35.5	36.6
	72 h	23.9	33.3	36.0	31.2	33.3	46.3	58.2	44.2	26.6	34.1	30.4	28.1
50RT -50HB	24 h	18.2	20.2	31.2	33.2	13.9	22.6	23.4	53.8	12.0	16.7	23.6	43.7
	48 h	24.3	32.4	38.3	40.6	15.5	36.2	48.3	55.1	16.4	20.8	39.7	46.5
	72 h	23.6	29.4	36.9	41.1	35.0	40.2	60.8	70.2	28.1	45.5	40.1	48.0
25RT -75HB	24 h	15.3	29.5	28.0	28.2	17.3	23.6	28.8	51.4	11.2	15.0	23.5	42.7
	48 h	20.6	30.5	26.8	36.9	30.2	38.3	63.3	55.5	19.3	30.1	31.7	43.2
	72 h	23.2	28.9	33.8	29.1	38.2	58.2	51.4	53.1	30.6	41.6	26.9	46.1

#### **4.2.1.2 Effect of curing period**

When the relationship between curing period and compressive strength of binary geopolymers are examined, it is seen that increment in curing period raises the strength generally. This relation is more apparent for curing periods of 24 h and 48 h. However, when the curing period extended to 72 h for geopolymers cured at 125 °C, strength reductions take place because of the harmful effects of higher temperatures on geopolymeric structures. Since geopolymerization occurs sufficiently at certain temperatures, continued curing at the same temperature harms the geopolymer structure rather than adding a benefit. Therefore, it seems that curing at high temperatures for an extended curing period is not always beneficial (Memon *et al.*, 2011). Possible causes of these degradations have been attributed to the deterioration of the geopolymer gel structure and associated gel shrinkage and dehydration. However, not all of the samples cured at high temperatures (125 °C) for a long time (72 h) experienced a reduction of compressive strength (for example, 75RCB -25RT with 19 M of NaOH, 25RCB-75RT and 75RCB-25HB with 15 M of NaOH). This is related to the amorphous portions of the geopolymerization products. The abundance of amorphous structure in geopolymerization products prevents the deterioration below-mentioned more difficult (van Jaarsveld, van Deventer and Lukey, 2002).

#### **4.2.1.3 Effect of NaOH concentration**

Considering the NaOH molarity, there is a general increasing trend in strength due to the NaOH molarity increment. Nevertheless, the effect of NaOH molarity on strength is a function dependent on parameters such as precursor combination, curing time and temperature. For geopolymerization reactions consisting of dissolution, condensation and crystallization phases (Xu and Van Deventer, 2000), the most important factor affecting the reaction mechanism and strength development ratio is the higher pH of the environment that triggers all processes. The dissolution phase

has a direct effect on the release of silica and alumina species from the precursor. Therefore, the high NaOH concentration provides the high pH and hydroxyl species required for the dissolution of CDW-based raw materials. However, the amount of NaOH exceeding the optimum molarity may lead to SiO<sub>4</sub> tetrahedrals coagulation (Rattanasak and Chindaprasirt, 2009) and rapid set behavior (Palomo, Grutzeck and Blanco, 1999).

#### **4.2.1.4 Effect of precursors combination**

Since RCB and RT have similar chemical content (Table 3.1), their combinations have similar compressive strengths. For the combination of RCB and RT, it is observed that the low molarity of NaOH does not need extended curing, and a curing period of 24 h is enough for geopolymerization. However, when NaOH molarity increased to 19 M, higher pH introduces more SiO<sub>4</sub> and AlO<sub>4</sub> tetrahedrals into the system. Therefore, geopolymers with a NaOH molarity of 19 M need an extended curing period to complete all dissolved species from precursors. In addition, temperature increment for this RCB-RT binary geopolymers does not affect the strength with low NaOH molarity (10 M), while the increasing curing temperature raises the strength with the molarity increment. In fact, the strength of the 25RCB-75RT sample, which is activated with 10 M NaOH and cured for 24 h at 95 °C, is 20 MPa, while the same geopolymer is cured at 115 °C for 48 h, the strength value increases to 35 MPa. However, when the NaOH molarity increases to 19 M, the same sample cured at 95 °C for 24 h gives 10 MPa of strength. This is because alumina and silica ions, which exist in high amounts but cannot react sufficiently in 24 h, decrease the strength. However, when the same geopolymer is cured for 48 h, the ions that complete the geopolymerization reactions increase the strength to 34 MPa thanks to sufficient curing. The same geopolymer gives its highest strength value at 115 °C with 48 h of cure. For this sample, the geopolymerization is not completed within 48 h for 15 M NaOH, which can be seen from strength increment after 48 h.



However, strength values that decrease at the end of 72 h in the case of using 19 M NaOH show that 48 hours curing is sufficient.

The compressive strengths of geopolymers with combinations of RCB-HB are seen in Table 4.4. Although the relationship between activator molarity and curing period of RCB-HB geopolymers is similar to RCB-RT specimens, the effect of higher molarity is more remarkable than RCB-RT. Such that, RCB-HG geopolymers with 10 M NaOH have close strength results for identical specimens with different curing periods and temperatures. However, geopolymers with 15 and 19 M NaOH require extended curing period to reach complete geopolymerization. As before mentioned, higher (OH)<sup>-</sup> ion concentration dissolves precursor and introduces more SiO<sub>4</sub> and AlO<sub>4</sub> tetrahedrals into the system. Therefore, while 24 h of curing is sufficient for complete geopolymerization of the less amount of alumina and silica species resulting from low molarity, longer curing time is required to obtain a complete geopolymerization for geopolymers with higher (15 M and higher) NaOH concentration.

Similar to RCB-HB geopolymers, the increased molarity in these specimens gives satisfactory results with an extended period of curing. The importance of long-term curing at high curing temperature for RT-HB samples activated with 15 and 19 M NaOH is seen from the strength results. Such that, while the 50RT-50HB sample, activated with 15 M NaOH, was cured at 95 °C for 24 h, it gives strength of 16 MPa, when the curing time increased to 72 hours, this value increased to 37 MPa. In addition, while the same sample gives 56 MPa strength at the end of 24 h at 125 °C temperature, this value increases to 69 MPa with 72 h of curing.

RCB-RT, RCB-HB and RT-HB binary geopolymers have close strength results when their activator molarity is 10 M. Maximum compressive strength is 42 MPa, obtained from 25RCB-75HB binary geopolymer activated with 10 M NaOH and cured at 115 °C for 48 h. When NaOH molarity becomes 15 M, the strength value of this geopolymer increased to 80 MPa. However, an excessive amount of NaOH (19 M) results in a high amount of strength loss. Such that, 49 MPa is obtained from the

same specimen cured at same conditions when its NaOH molarity increased to 19 M.

Pearson coefficients between strength and design parameters (molarity, curing period and temperature) were calculated (Table 4.5) to observe the relationship between compressive strength and design parameters. When compared with single geopolymer pastes, the first thing to notice is that the Pearson coefficients between temperature and strength are relatively lower. The reason is attributed to the fact that the curing temperature range is limited between 95 °C and 125 °C, where higher strength results are obtained for single geopolymer pastes. Differently from single geopolymer pastes, almost all binary pastes (All RCB-RT and RCB-HB combinations) have higher correlations between strength and curing period rather than curing temperature. This situation indicates that the extended curing period becomes more important when higher curing temperatures (95 ~ 125 °C) are applied.

Another different point of binary pastes from single geopolymer pastes is that many specimens have positive correlations between strength and molarity. For example, 75RCB-25RT has a correlation coefficient of 0.477. Both higher positive correlations coefficients of strength between curing period and molarity showed that extended curing period and molarity increase makes sense when higher curing temperatures (95 ~ 125 °C) are applied.

Table 4.5 Binary geopolymers paste strength's Pearson correlations with curing period, temperature and molarity

Precursor		Curing period	Temperature	Molarity
75RCB- 25RT	Pearson Correlation	0.454	0.356	0.477
	Sig. (2-tailed)	0.005	0.033	0.003
	N	36	36	36
50RCB- 50RT	Pearson Correlation	0.436	0.130	0.266
	Sig. (2-tailed)	0.008	0.448	0.117
	N	36	36	36
25RCB- 75RT	Pearson Correlation	0.457	0.223	0.295
	Sig. (2-tailed)	0.005	0.191	0.080
	N	36	36	36
75RCB- 25HB	Pearson Correlation	0.459	0.408	0.258
	Sig. (2-tailed)	0.005	0.014	0.129
	N	36	36	36
50RCB- 50HB	Pearson Correlation	0.516	0.439	-0.117
	Sig. (2-tailed)	0.001	0.007	0.497
	N	36	36	36
25RCB- 75HB	Pearson Correlation	0.519	0.492	-0.052
	Sig. (2-tailed)	0.001	0.002	0.762
	N	36	36	36
75RT- 25HB	Pearson Correlation	0.243	0.555	-0.004
	Sig. (2-tailed)	0.153	0.000	0.981
	N	36	36	36
50RT- 50HB	Pearson Correlation	0.456	0.727	0.047
	Sig. (2-tailed)	0.005	0.000	0.787
	N	36	36	36
25RT- 75HB	Pearson Correlation	0.392	0.546	0.115
	Sig. (2-tailed)	0.018	0.001	0.504
	N	36	36	36

### **4.3 Geopolymer mortars with single CDW-based material and recycled concrete aggregate**

Table 4.6 represents the compressive strengths of all geopolymers mortars with CDW-based precursors and recycled concrete aggregate as sand. All geopolymers were cured for 72 h to obtain maximum geopolymerization, especially for higher NaOH molarities (15 and 19 M). HB, RT or RCB utilized as precursor was used separately, using aggregate-binder ratios of 0.36, 0.45 and 0.55. Three different sizes of aggregate (recycled concrete aggregate) were used as indicated in Table 4.6, as 4.75, 2.00 and 0.85, which indicate the aggregate sizes between 4.75 - 2.00 mm, 2.00 - 0.85 mm and 0.85-0.10 mm, respectively. If NaOH concentration is considered, almost all geopolymer mortars give the maximum strength values in those activated with 15 M NaOH. As mentioned for geopolymer mortars, relatively high NaOH molarities (15 or 19 M) require an extended period of curing time. However, excessively higher molarities lead to strength reductions because of the silica coagulation (Atiş *et al.*, 2015) resulted from a tremendous amount of ion existence. Similar to the results obtained from geopolymers pastes, 15 M as an optimum NaOH molarity is also obtained for mortar development. The factor that enables the transition from paste to mortar and affects the binding properties to a great extent is aggregate. Strength results clearly indicate that decreasing aggregate size raises the strength. This is attributed to better interfacial transition zone properties. As it is known, when the cracks formed in the concrete under load coincide with the aggregate, then it continues to a path around aggregate on the interfacial transition zone (Sahmaran *et al.*, 2012). Also, decreasing aggregate size raises the specific surface area of the aggregate and increases the interfacial transition zone. The filler effect of smaller particles is another effect increasing strength results. Increasing density and reducing the void ratio of matrix result in higher strength results.

Table 4.6 Compressive strength results of geopolymer mortars (28 days) with CDW-based precursors and recycled concrete aggregate

Curing Temperature (°C)		105°C			115°C			125°C			
Aggregate Size (mm)		4.75	2.00	0.85	4.75	2.00	0.85	4.75	2.00	0.85	
HB	0.36	10 M	32.1	37.6	38.5	30.8	39.5	39.9	29.8	37.2	37.9
		15 M	43.5	51.7	53.6	40.0	49.0	56.7	35.3	45.2	48.8
		19 M	36.8	44.5	48.5	32.2	38.9	49.1	30.7	37.7	42.5
	0.45	10 M	33.3	37.2	41.3	31.6	37.8	42.0	31.0	34.2	37.1
		15 M	41.2	49.0	51.2	38.4	45.8	49.8	34.9	42.3	41.8
		19 M	34.1	42.9	49.5	32.0	37.9	52.8	32.6	37.8	34.2
	0.55	10 M	32.6	33.7	39.7	32.6	35.3	43.4	30.8	28.7	45.6
		15 M	38.3	48.8	53.5	36.8	44.7	55.9	31.2	41.0	58.7
		19 M	34.6	40.7	44.3	34.2	37.7	58.5	29.8	36.8	58.3
RT	0.36	10 M	31.5	37.3	38.4	28.5	36.2	36.9	29.3	30.8	35.5
		15 M	38.9	50.5	60.7	37.6	46.4	64.1	38.1	44.9	61.9
		19 M	34.7	39.7	42.6	33.6	38.8	51.6	31.7	33.2	49.9
	0.45	10 M	27.9	44.2	45.5	25.8	41.7	45.6	26.5	33.4	41.1
		15 M	35.0	51.8	66.2	33.5	47.5	65.8	33.8	46.0	63.8
		19 M	47.6	51.6	61.9	40.1	49.9	56.0	38.5	41.6	52.3
	0.55	10 M	34.4	36.3	46.3	29.9	33.2	46.5	31.8	33.0	48.8
		15 M	38.6	49.1	49.7	36.8	44.4	52.5	38.1	43.0	54.7
		19 M	41.7	42.3	55.0	39.4	40.2	48.1	38.9	39.5	47.5
RCB	0.36	10 M	29.5	30.2	38.3	26.6	27.1	34.4	24.0	27.5	33.5
		15 M	38.7	41.3	61.7	36.6	39.4	46.3	33.1	37.8	45.6
		19 M	43.3	44.4	50.2	39.8	41.5	50.4	37.1	39.0	51.1
	0.45	10 M	29.3	30.1	34.4	24.1	26.6	31.7	23.1	26.9	30.2
		15 M	40.6	50.1	60.1	40.2	43.6	51.4	33.3	39.1	50.7
		19 M	37.4	39.6	42.4	32.6	34.2	40.2	30.3	32.4	41.7
	0.55	10 M	30.0	32.1	39.6	26.4	29.0	40.6	23.6	30.6	42.6
		15 M	41.5	47.7	61.0	34.8	41.7	61.7	33.2	38.8	59.1
		19 M	35.9	43.4	51.6	31.6	39.6	50.0	26.0	35.0	48.9

0.36, 0.45 and 0.55 are sand to binder ratios

10M, 15 M and 19 M are NaOH molarities

Table 4.7 shows mortar strength's correlation coefficients between aggregate size, curing temperature, molarity and water to binder ratio. Correlation coefficients of strength and aggregate sizes, which are -0.679, -0.555 and -0.676 for HB, RCB and RT, respectively, proved that smaller aggregates enhance strength development. Although the increase in molarity does not mean much for HB (correlation coefficient of 0.261), it is more important for RCB in terms of strength increase (correlation coefficient of 0.462). Water to binder ratio does not have a significant effect according to the correlation coefficients.

Table 4.7 Geopolymer mortar strength's Pearson correlations with aggregate size, curing temperature, molarity and water to binder ratio

Precursor		Aggregate size	Temperature	Molarity	Water/binder
HB	Pearson Correlation	-0.679	-0.198	0.261	-0.001
	Sig. (2-tailed)	0.000	0.076	0.019	0.991
	N	81	81	81	81
RCB	Pearson Correlation	-0.555	-0.243	0.462	0.048
	Sig. (2-tailed)	0.000	0.029	0.000	0.669
	N	81	81	81	81
RT	Pearson Correlation	-0.676	-0.144	0.357	0.052
	Sig. (2-tailed)	0.000	0.198	0.001	0.644
	N	81	81	81	81

Line mapping analyses through scanning electron micrographs were made to observe both adherence between recycled concrete aggregate and geopolymer paste and interfacial transition zone properties. Figure 4.7a presents an SEM image of aggregate paste connection with a magnification of 100×. In that figure (1) represents aggregate, (2) represents geopolymer paste. Figure 4.7b presents closer view of the area shown with a square in Figure 4.7a. As it is known, the interfacial transition zone (ITZ) of conventional concrete, which is approximately 50 μm, is the weakest link of the chain (Mehta and Monteiro, 2006). Even aggregate and paste have higher

strengths because of the weak ITZ binder may be easily broken down. Hereby ITZ is investigated by SEM observations and line mapping analysis. Figure 4.8 represents the ITZ (Figure 4.8a) and line mapping analysis (Figure 4.8b). Since all the elements are shown on top of the same graphic, numerical values are not given on the y-axis of line mapping analysis.

As it is expected, recycled concrete aggregate (marked with 1 on Figure 4.8b) contains a high amount of calcium and a low amount of silicon compared to the geopolymer paste (marked with 2 on Figure 4.8b). Geopolymer paste is rich in silicon, aluminum, sodium and oxygen with almost no calcium content, indicating the formation of N-A-S-H as a geopolymeric binder. The most striking point in the line mapping analysis is that the calcium intensity did not suddenly decrease in the area where the aggregate ends and the interfacial transition zone begins (marked with 3 on Figure 4.8b). Instead, the calcium density dropped gradually. In addition, the rapidly increasing silicon density in this region and sodium, oxygen and aluminum, which have densities increasing at slower rates than silicon, show that a structure of C-N-A-S-H has been formed in this region.

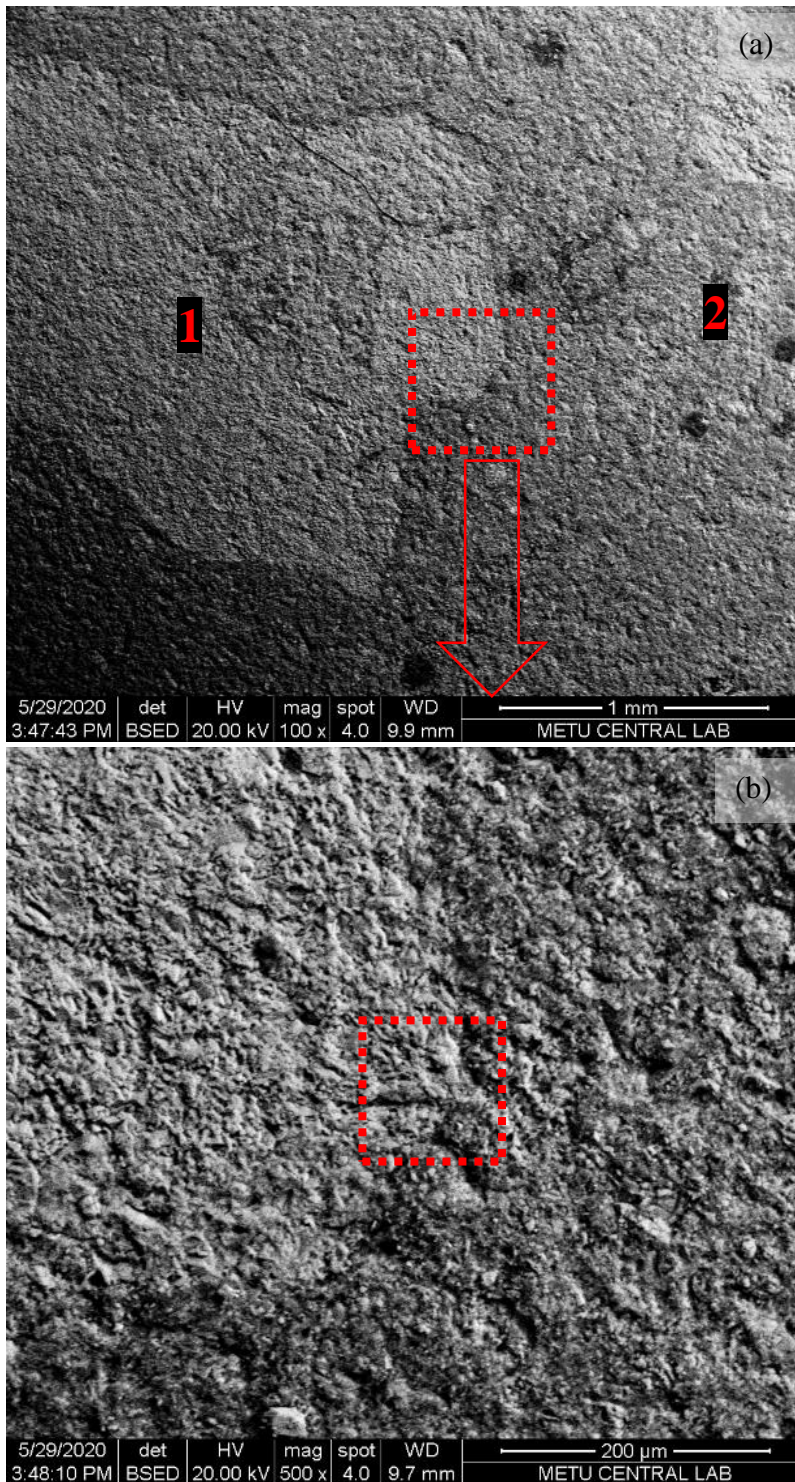
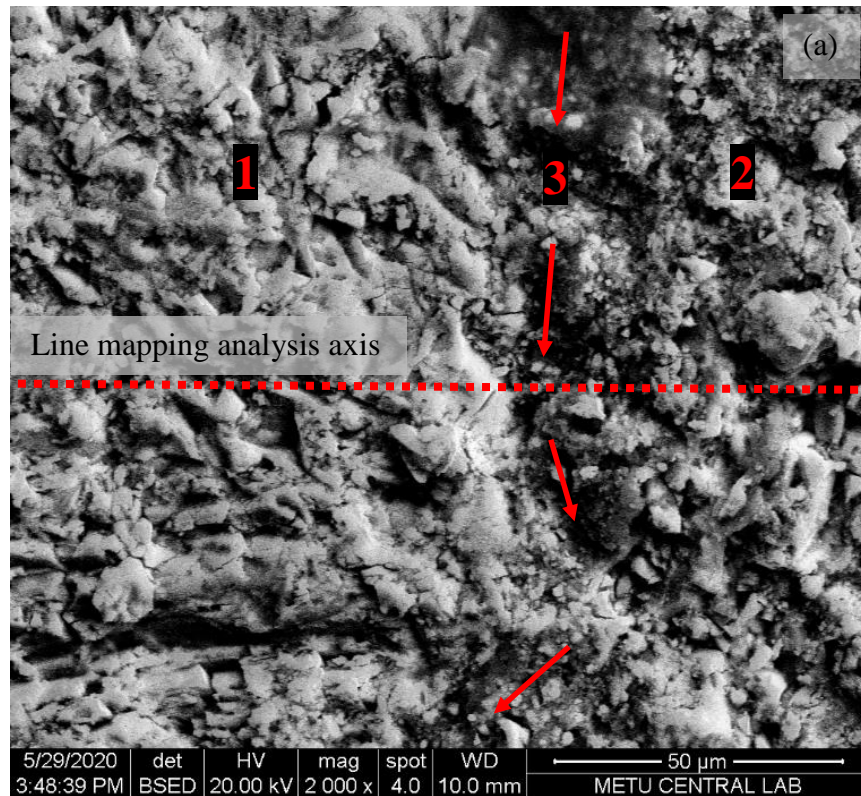
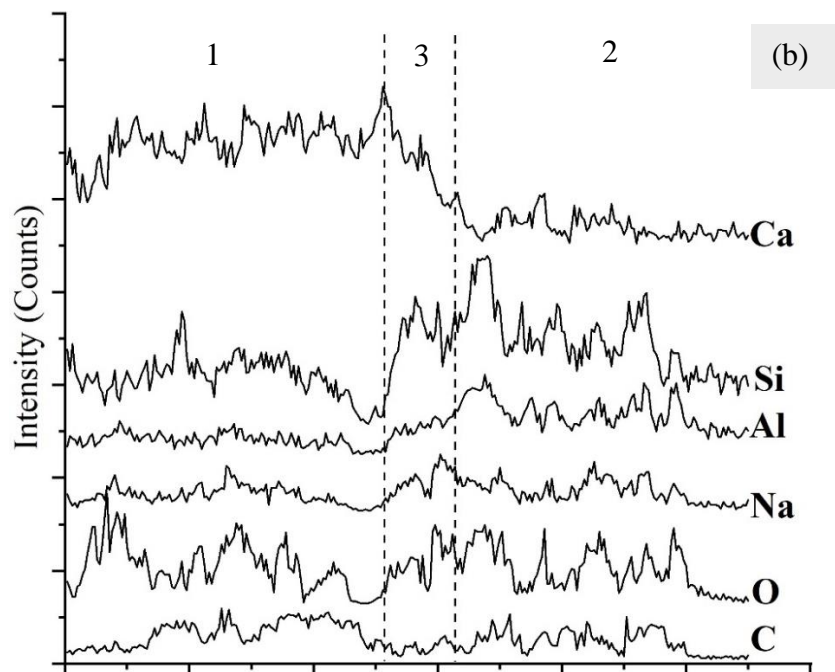


Figure 4.7. SEM images of aggregate paste connection  
 (a) an area [100×] contain both aggregate (1) and geopolymer paste (2), red dotted frame points zoomed area in (b) [500×] red dotted frame points zoomed area in the following figure





\*Arrows point interfacial transition zone



\*1, 2 and 3 represent recycled concrete aggregate, geopolymer paste and ITZ

Figure 4.8. (a) Zoomed area of previous figure [2000×] (b) mapping analysis of line through both aggregate, interfacial transition zone and paste

## 4.4 Mechanical properties and self-healing capability of EGCs

As mentioned in Section 3.2.5.1, all CDW-based materials were utilized in the EGC development in the last part of the study, and sodium hydroxide, sodium silicate and calcium hydroxide were used in optimum proportions as activators. In addition, the EGCs were cured in room conditions, not at high temperatures. Mixture designs of EGCs can be seen in Table 3.13.

### 4.4.1 Compressive strength

Compressive strength results of all EGC mixtures, which were obtained from three separate specimens for a given age and averaged, are listed in Table 4.8. The results show that all EGCs continue to gain strength by time due to the progression of reactions, similar to cementitious systems. It is known that slag addition accelerates geopolymerization by generating a more amorphous structure (Li and Liu, 2007). In line with this, all specimens with slag have higher compressive strength results than specimens under the same conditions (curing period and activator) except S5 and S6 cured for 28 days. For example, at the end of 7, 28, and 90 days, S1 has compressive strengths of 24.2, 37.5, and 40.3 MPa; however, S2 has 18.4, 26.0, and 30.7 MPa, respectively. This is attributed to the self-cementing capability of slag and the development of a denser matrix microstructure with the use of slag (Sitarz, Urban and Hager, 2020). However, the presence of 6%  $\text{Ca(OH)}_2$  and slag in S5 seems to lead to a solution supersaturated with the calcium species; therefore, geopolymerization reactions may have been inhibited. S3 and S4 have maximum compressive strengths compared to other mixtures on the 7<sup>th</sup>, 28<sup>th</sup>, and 90<sup>th</sup> days. This result comes from the use of  $\text{Na}_2\text{SiO}_3$  with  $\text{Ca(OH)}_2$ , which together helps geopolymerization reactions by silicate, calcium, and sodium species. While the combined use of  $\text{Na}_2\text{SiO}_3$  and  $\text{Ca(OH)}_2$  increases strength, it is observed that this combination lowers the setting time and makes workability worse because alkali silicates have a higher viscosity than alkali hydroxides (Provis and Bernal, 2014).

When  $\text{Na}_2\text{SiO}_3$  was removed from the activator, the strength results decreased significantly. For example, S5 has compressive strengths lower than S3 and S1, and S6 has compressive strengths lower than S4 and S2 under the same conditions and age. This shows that although  $\text{Ca}(\text{OH})_2$  and  $\text{NaOH}$  concentrations increased, they did not contribute to geopolymerization in the absence of  $\text{Na}_2\text{SiO}_3$ . Therefore, the strength results were 18.9 and 13.6 MPa on the 7<sup>th</sup> day for the specimens with and without slag (S5 and S6 mixtures). These values increased to 25.2 and 25.6 MPa on the 28<sup>th</sup> day for the S5 and S6 mixtures, respectively.

Table 4.8 Compressive strength results of EGCs

Curing Day	Compressive strength (MPa)					
	S1	S2	S3	S4	S5	S6
7	24.2	18.4	28.2	20.4	18.9	13.6
28	37.5	26.0	42.1	28.7	25.2	25.6
90	40.3	30.7	53.5	32.8	30.7	27.8

#### 4.4.2 Transportation properties

##### 4.4.2.1 Electrical impedance

The electrical impedance (EI) results are shown in Table 4.9. The results are not presented as average values of three specimens to show the variation in themselves. While the EI of cementitious systems has been affected by porosity, pore solution, and pore connectivity (Spragg *et al.*, 2013), factors affecting the EI of alkali-activated materials are much more complex. The electrical properties of geopolymers are highly affected by the concentration of free alkali metal ions (i.e.,  $\text{Na}^+$ ,  $\text{Ca}^{+2}$ ,  $\text{K}^+$ ) (Zeng and Wang, 2016). Additionally, hydroxyl ions and water increase the electrical conductivity (Hanjitsuwan *et al.*, 2014) and consequently decrease the electrical impedance of the geopolymer. According to Adamson (1973) while  $\text{Na}^+$  and  $\text{Ca}^{+2}$  cations have equivalent conductivities of 50.1 and 59.5  $\text{cm}^2 \text{equiv}^{-1} \Omega^{-1}$ , respectively,  $\text{OH}^-$  anion has equivalent conductivity of 198  $\text{cm}^2 \text{equiv}^{-1}$

$\Omega^{-1}$ . A magic angle spinning nuclear magnetic resonance (MAS NMR) study conducted by Duxson et al. (2005) showed that geopolymers cured for two months have  $\text{Na}^+$  cations in their pore solution. Therefore, it can be said that the hydroxyl concentration has an influence on EI owing to the higher electrical conductivity and sodium ions with its later availability.

Factors that detract the geopolymer pore solution from neutrality will affect the electrical properties of the matrix.  $\text{Al}(\text{OH})^-$ , which comes from the dissolution of the precursor, can be balanced by alkali metal cations sourced from an alkaline activator (Somna *et al.*, 2011). Additionally, silica tetrahedral is an anion-like alumina tetrahedral and should be charge-balanced with alkali cations. Therefore, the amount of alumina and silica tetrahedral changes with geopolymerization affects the electrical properties by binding to other alkali metal cations. Therefore, at a specific time, the electrical properties of a geopolymer can be affected by many parameters that are not designed for electrical properties. Maturity and matrix development affect cementitious systems and geopolymers differently in terms of electrical properties. Continuing hydration is expected to increase the EI results of cementitious systems paralleling the increasing volume of hydration products such as tobermorite, portlandite, ettringite, decreasing volume of pores, and consuming water with hydration. However, geopolymerization reactions differ from cement hydration. A grid nanoindentation study (Zhang *et al.*, 2017), which covers over 270 indents per specimen, exhibits that geopolymer with a Si/Al ratio of 1.6 has porous phases of 6.2% and 20.6% at the end of 7 and 28 days of curing, while their volume of geopolymer gel increased from 46.6% to 55.7%. Additionally, water participating geopolymerization may be released free back to the system later (Provis and van Deventer, 2009). Accordingly, a decrement in the EI of alkali-activated systems may be expected over time.

### ***Electrical Impedance of Sound Specimens***

In order to explain the variations in the electrical impedance results better, the graphical representation of the EI results is presented in Figure 4.9. All sound

specimens showed increments after the 7<sup>th</sup> day; however, while S1 and S5 showed a trend of reverse exponential increase in EI results up to 90 days, S2 S3 and S6 decreased after the 28<sup>th</sup> day and rose again before the 90<sup>th</sup> day. Different from these specimens, S4 had a decrement after the 56<sup>th</sup> day. After 28 days, the EI results of S2, S3, and S6 and after 56 days, the EI results of S4 decreased with increasing pore volume, in agreement with Zhang et al. (2017), who mentioned that the geopolymer pore volume may increase in time. However, S2, S3, and S6 have very sharp EI increases at 14 and 28 days. For example, sound S2 specimens have EI results of 1.7, 0.7, and 1.0 k $\Omega$  on the 7<sup>th</sup> day. These results increased to 5.5, 8.3, and 7.8 k $\Omega$  on the 14<sup>th</sup> day. One of the reasons for these rapid increments in the EI results of S2, S3, and S6 is the early efflorescence with the formation of Na<sub>2</sub>CO<sub>3</sub> filling cracks and pores in the geopolymer matrix. Efflorescence is a phenomenon caused by free alkali metal carbonation, generally existing in the early ages, with CO<sub>2</sub> from the atmosphere (Djobo *et al.*, 2017).

Table 4.9 Electrical impedance results

		Electrical impedance (k $\Omega$ )														
		7			14			28			56			90		
S1	S	1.9	2.4	2.3	5.9	6.2	6.5	8.7	7.6	9.1	10.4	9.2	10.9	12.6	11.0	12.4
	P	4.7	5.7	6.8	5.8	7.4	8.9	8.1	9.0	10.5	11.6	9.5	11.3	12.3	9.7	12.4
S2	S	1.7	0.7	1.0	5.5	8.3	7.8	8.4	10.4	11.9	4.5	4.2	4.0	7.4	8.7	7.1
	P	1.5	4.0	1.2	7.9	11.7	9.3	12.8	11.8	13.8	5.7	8.5	6.1	6.7	10.2	7.4
S3	S	15.4	14.8	11.4	22.4	20.5	24.6	21.5	27.5	26.3	13.3	16.6	14.0	6.2	6.5	6.0
	P	12.7	19.6	20.6	23.5	31.1	29.5	30.2	35.1	32.9	18.9	25.0	19.9	19.1	23.7	20.4
S4	S	3.9	2.8	4.6	37.3	44.0	39.9	61.5	58.6	67.8	69.5	71.0	75.1	34.6	38.9	37.2
	P	16.8	16.2	15.8	31.3	42.0	32.9	42.0	49.2	47.5	41.5	50.0	49.5	27.3	38.0	34.6
S5	S	1.6	1.6	1.7	3.1	4.3	7.2	41.4	42.5	47.1	88.9	64.4	89.8	128.0	84.4	100.0
	P	4.4	4.4	4.4	7.6	12.6	14.9	72.6	63.5	69.1	77.3	77.0	78.0	103.0	129.0	148.0
S6	S	7.5	5.2	5.0	21.2	18.0	23.2	31.8	24.0	33.6	27.4	25.4	33.1	27.7	22.9	29.5
	P	9.2	9.2	12.4	21.6	19.8	31.2	29.8	28.0	34.0	26.0	23.1	26.3	25.2	23.1	34.7

S-sound, P-preloaded

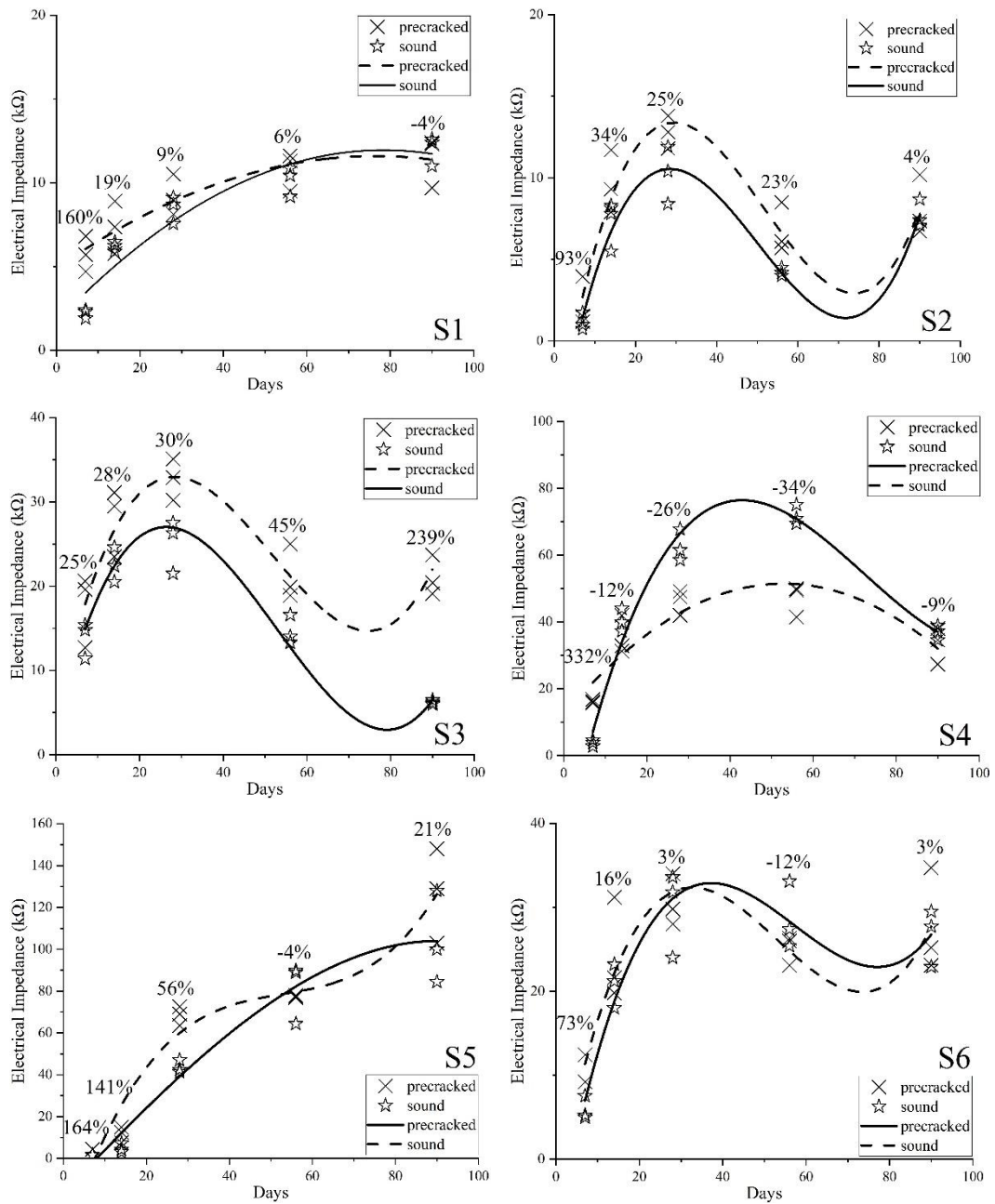


Figure 4.9. Graphical representation of electrical impedance results

As Kan et al. (2019) mentioned, wet–dry cycles facilitate efflorescence by the formation of  $\text{Na}_2\text{CO}_3$ . However, it has been recognized that significant efflorescence occurred on the surfaces of S2, S3, S4, and S6, leading to a misleading early self-healing capability according to the EI results. Sodium ions in the matrix react with  $\text{CO}_2$  in the atmosphere and form natrite ( $\text{Na}_2\text{CO}_3$ ) minerals, which can be easily

dissolved in water (Figure 4.10). Although natrite provides a temporary crack sealing, the EI results are affected by this phenomenon. Higher increments in the EI results of S2, S3, S4, and S6 are therefore attributed to this early misleading efflorescence, which can be clearly seen in the optical microscopic images (Figure 4.12 and Figure 4.13). Additionally, the formation of  $\text{Na}_2\text{CO}_3$  consumes free  $\text{Na}^+$  ions in the pore solution rapidly; thus, the EI results increase owing to ion consumption. However, white-colored, crack- and pore-filling material of  $\text{Na}_2\text{CO}_3$  formed as a result of carbonation is a material that can dissolve in water in which the specimen is wetted. While the specimens were exposed to wetting and drying cycles, the progressive wetting period dissolved some amount of white  $\text{Na}_2\text{CO}_3$  crystals. At the same time, the concentration of alkali cations in the pore solution is reduced through carbonation and geopolymerization reactions. Later,  $\text{Ca}^{+2}$  ions reacted with  $\text{CO}_2$  to form calcite minerals ( $\text{CaCO}_3$ ). Then, at the end of the cycling curing, many cracks were filled with  $\text{CaCO}_3$ , as proven by XRD analyses. Both filled pores with  $\text{CaCO}_3$ , and a decrease in the amount of alkali cations in the pore solution increased the falling EI results. However, on the 90<sup>th</sup> day, sound S3 had an average EI value of 6.2 k $\Omega$ , which is smaller than the EI value on the 7<sup>th</sup> day (13.9 k $\Omega$ ). This is attributed to the role of water in the geopolymerization reactions. During the early stages of geopolymerization, water acts as a medium for the dissolution of precursors. Later, water participates in geopolymerization reactions. Unlike cement hydration, further geopolymerization does not entirely consume water. According to Provis and van Deventer (2009), water is released back to the nanopores after the geopolymerization reactions. Accordingly, in cases where geopolymerization reactions take place very intensely and close to completion, it can be expected that a high amount of water is present, which is released after the substantially completed reactions. The lower EI values of S3 on the 90<sup>th</sup> day are attributed to the higher geopolymerization of this mixture with evidence of a compressive strength of 53.5 MPa at the age of 90<sup>th</sup> days, which is the maximum result among the studied mixtures.



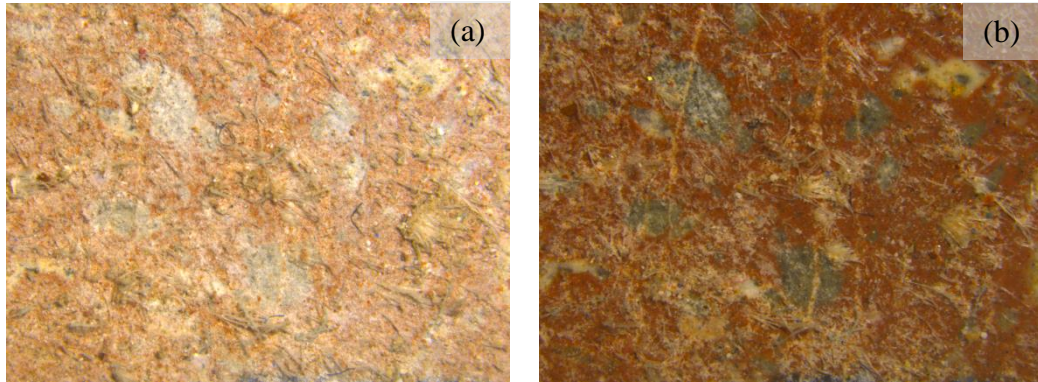


Figure 4.10. Typical misleading efflorescence on specimen (a) before and (b) after sprinkling water

EI results indicate that while S2 and S6 have early efflorescence, S1 and S5 do not (Figure 4.12 and Figure 4.13). This is attributed to the early reactions of slag resulting in C-N-A-S type gel formation. According to Yang et al. (2012), sodium silicate activated fly ash-slag blend results in sodium-calcium aluminosilicate (C-N-A-S) hydrate formation and early C-N-A-S formation bound free  $\text{Na}^+$  cations in the system; therefore, a lower amount of efflorescence formed in S1 and S5. These results are in agreement with Zhang et al. (2013), who reported that 20% slag addition reduces the initial efflorescence. However, this effect is not valid for S3, which has a sharp increment in EI results after the 7<sup>th</sup> day. This is attributed to the presence of NaOH,  $\text{Na}_2\text{SiO}_3$ , and  $\text{Ca}(\text{OH})_2$  activators. Since  $\text{Ca}^{+2}$  is more reactive than  $\text{Na}^+$  (Zhao, Liu, Zuo, *et al.*, 2019) the addition of  $\text{Ca}(\text{OH})_2$  increases  $\text{OH}^-$  ion concentration and obstructs the dissolution of NaOH. At the same time, dissolved  $\text{Na}_2\text{SiO}_3$ , reacts with  $\text{Ca}^{+2}$  ions sourced from  $\text{Ca}(\text{OH})_2$ , resulting in mainly C-S-H similar structures containing a minor amount of C-N-A-S in favor of  $\text{Na}^+$  cations coming from dissolution of  $\text{Na}_2\text{SiO}_3$ . Lower sodium content, which is only sourced from  $\text{Na}_2\text{SiO}_3$ , is not sufficient to form a dominant C-N-A-S structure. Thus, reactive calcium species came from slag consumed by participating in the C-S-H structure and lower amount of C-N-A-S before the formation of higher amounts of C-N-A-S. These formations are in accordance with Yip et al. (2005), who stated that geopolymers with metakaolin and slag content have C-S-H content rather than

geopolymer gel in the case of relatively low activator concentrations at the early stages of geopolymerization. Subsequently, the decreased  $\text{OH}^-$  ion concentration owing to the previously formed C-S-H structure and C-N-A-S, make NaOH dissolution easy, and dissolved NaOH provides  $\text{Na}^+$  cations to the system and leads to the lowering of the EI results.

### ***Electrical Impedance of Preloaded Specimens***

Numerical values in Figure 4.9 show the percentage of increments in average EI values after preloading. After preloading at the end of 7 days of curing, increases in the EI values of S1 and S5, which are 160% and 164%, respectively, were attributed to the higher fracture toughness and fiber-to-matrix chemical bonding caused by early reactions of the slag resulting in the formation of C-N-A-S and less efflorescence, as mentioned above. C-N-A-S formation rather than efflorescence provides a denser structure and adherence between fiber and matrix. Cracking in the matrix with these conditions leads to the formation of wider cracks that up to  $97\ \mu\text{m}$  obstruct electron transportation. Consequently, EI values increased in accordance with Yıldırım et al. (2015), who reported similar results for cementitious systems. However, the EI values of sound and preloaded S3 specimens on the 7<sup>th</sup> day are very close to each other, while the EI of sound S3 is already higher than that of sound S1 and sound S5. This is attributed to the addition of  $\text{Ca}(\text{OH})_2$ , which directly provides  $\text{Ca}^{+2}$  ions to the system. Thus, S3 has a very dense structure than S1 and S5 on the 7<sup>th</sup> day, which can be seen from the compressive strengths on the 7<sup>th</sup> day of S1, S3, and S5 were 24.2, 28.2, and 18.8 MPa, respectively.

The EI difference in sound and preloaded S1 samples decreased during the healing period (further wetting-drying cycles), and the average of the EI results of sound samples exceeded that of the preloaded samples on the 90<sup>th</sup> day. Almost all specimens showed the same trend except for S3. The EI results of preloaded S3 were higher than those of sound ones during the entire testing period. This is attributed to the higher early geopolymerization rate of S3 samples, which have 28.2 a

compressive strength of on the 7<sup>th</sup> day; therefore, continuing geopolymerization was not as effective as other mixtures.

Similar to the sound ones, preloaded S2, S3, and S6 have sharp EI increases at 14 and 28 days. For example, three specimens of S2 have EI results of 1.5, 4.0, and 1.2 k $\Omega$  on the 7<sup>th</sup> day. These results increased to 7.9, 11.7, and 9.3 k $\Omega$  on the 14<sup>th</sup> day. The EI increment of preloaded S2 is slightly sharper than that of sound S2, which is attributed to the easy penetration of CO<sub>2</sub> from the atmosphere into the cracks and matrix during the drying process. Further, the penetrated CO<sub>2</sub> reacts with sodium ions in the matrix and rapidly forms Na<sub>2</sub>CO<sub>3</sub>. Thus, misleading early self-healing occurred with higher intensity and EI increased. The EI increase of preloaded S4 on the 14<sup>th</sup> and 28<sup>th</sup> days is not as sharper as that of preloaded S2, which is attributed to the fact that adding Ca(OH)<sub>2</sub> to the system delays NaOH dissolution; therefore, a lower Na concentration results in less Na<sub>2</sub>CO<sub>3</sub> formation. Thus, the increase in EI of preloaded S4 is not as sharp as that of S2. However, this is not valid for the S6 mixture containing both NaOH and Ca(OH)<sub>2</sub> because of the increase in NaOH concentration up to 10%.

#### **4.4.2.2 Water Absorption**

The water absorption (WA) rate results are shown in Figure 4.11 as the absorption rate. Unlike electrical impedance results, water absorption results are affected by fewer parameters (pore size distribution, volume of pores, and their connectivity). After preloading, cracked and sound specimens have similar WA changes in time; therefore, the results are discussed under the same title. As can be seen from Figure 4.11, all specimens have a maximum point in which their water absorption value is the highest and then declines at different ages. While S3 peaks on the 14<sup>th</sup> day, others have peaks on the 28<sup>th</sup> day. According to Zhang et al. (2017), the geopolymer percentage of the porous phase may increase over time. Jang & Lee (2016) reported that geopolymers containing three different fly ashes have porosities of 30.5%, 29.8%, and 29.1% on the 3<sup>rd</sup> day and 29.4%, 33.3%, and 31.4% on the 90<sup>th</sup> day for

the same specimens. Additionally, all three specimens in the mentioned study had larger median pore diameters on the 90<sup>th</sup> day than on the 3<sup>rd</sup> day. According to these results, there is no direct relationship between the pore structure and strength development of geopolymers, as in conventional cementitious systems. Ma et al. (2013) mentioned that the development of the pore structure of geopolymers over time is slower than that of cementitious systems, and extending the curing time may be beneficial for the enhancement of pore structure. In this study, WA results at later ages (56<sup>th</sup> and 90<sup>th</sup> days) clearly show that wetting-drying cycles enhance the geopolymer pore structure by decreasing pore connectivity and then reducing the absorption rates. Parallel to sound specimens, preloaded ones have similar WA changes over time.

Although the WA results (which are affected by the porous structure) and the EI results (which are affected by many more parameters) do not have to be compatible, the WA and EI results of S1 appear quite similar. However, all specimens have a trend of having a maximum WA result, and then a decrement is observed. If the S2 mixture is evaluated, it is seen that WA results of sound and preloaded specimens approach each other on the 14<sup>th</sup> and 28<sup>th</sup> days. Then, higher WA results of the preloaded S2 specimens than those on the 56<sup>th</sup> and 90<sup>th</sup> days are observed again. This situation depicts the misleading early self-healing (Figure 4.10) in accordance with the EI results owing to the carbonation of free sodium content, which results in the formation of Na<sub>2</sub>CO<sub>3</sub>. Although this trend is not as apparent as for S2, it is also seen in S3 and S4. WA results of preloaded S5 and S6 specimens could not reach the WA results of sound ones. This case is attributed to the fact that although higher NaOH molarity and Ca(OH)<sub>2</sub> content, geopolymerization reactions suffer from a lack of Na<sub>2</sub>SiO<sub>3</sub>. The lack of Si cations at early ages leads to more unreacted free alkali cations (Na<sup>+</sup> and Ca<sup>+2</sup>), and some of these cations leach to water during the wetting period. As mentioned below, the parameters that affect EI and WA are not in complete harmony. Geopolymerization and increasing gel volume have a direct effect on decreasing (healing) the WA results. However, S5 and S6, with lower compressive strength than S1, S2, S3, and S4, have less geopolymerization;

therefore, the WA results of sound S5 and S6 are much better than those of preloaded S5 and S6.

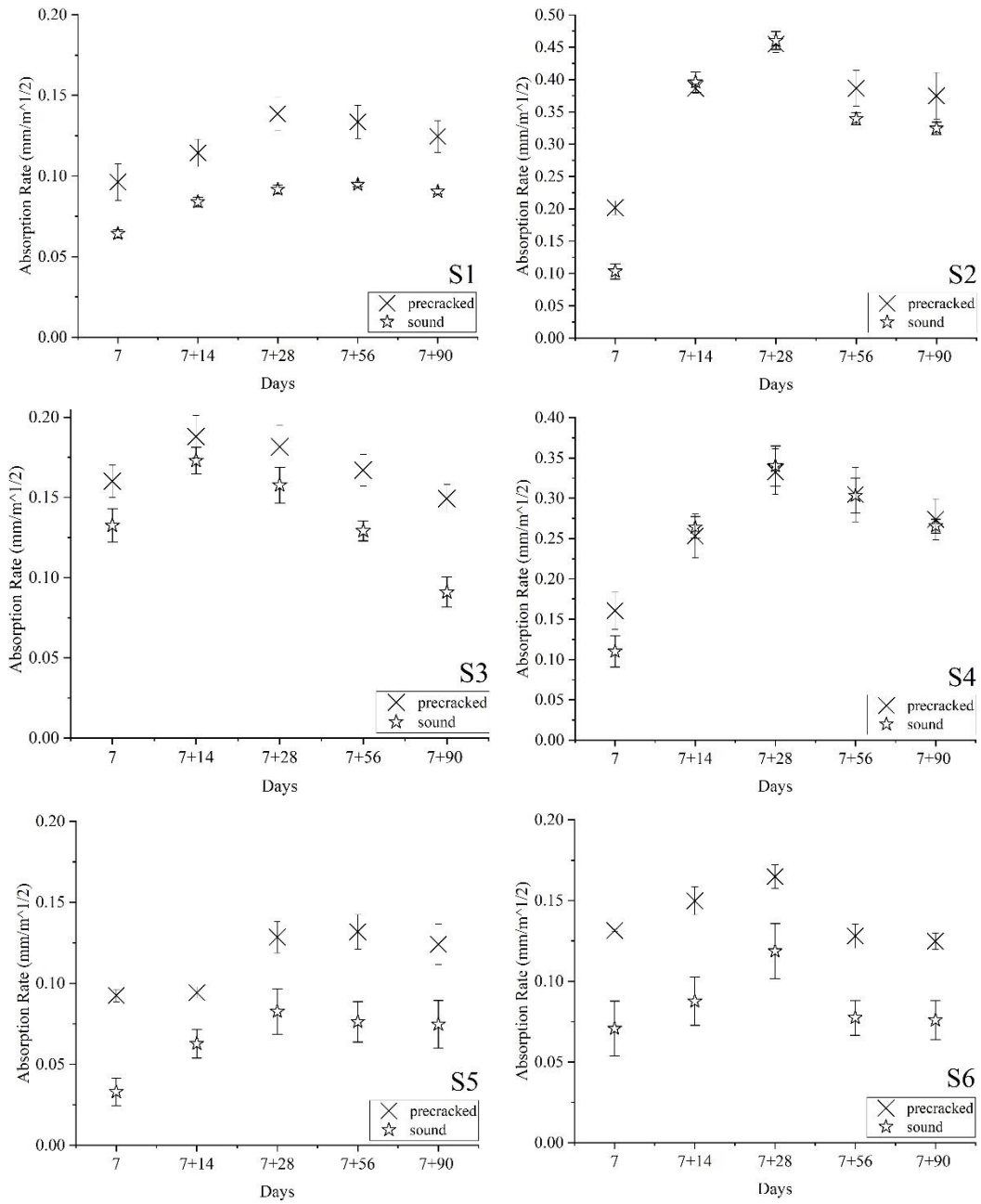


Figure 4.11. Absorption results of EGCs

Mixtures including slag (S1, S3, and S5) had the highest absorption rate values of 0.15, 0.20, and 0.14 mm/m<sup>0.5</sup>, respectively, while mixtures without slag (S2, S4, and S6) had the highest absorption rate values of 0.45, 0.35, and 0.17 mm/m<sup>0.5</sup>, respectively. These results clearly show that slag incorporation leads to a denser structure with less porosity in accordance with mercury intrusion porosimetry results of slag-incorporated fly ash-based geopolymer (Li and Liu, 2007).

#### 4.4.3 Optical investigation

Figure 4.12 and Figure 4.13 display the optical images of the cracked specimens exposed to wetting-drying cycles on the 7<sup>th</sup>, 28<sup>th</sup>, 56<sup>th</sup> and 90<sup>th</sup> days. Images taken on the 7<sup>th</sup> day were photographed immediately after preloading. S1 has cracks with widths of 33, 49, and 50 μm that have healed entirely according to its crack pattern. While the color of the material filling the cracks of S1 was initially white, it approached the color of the matrix on the 90<sup>th</sup> day (Figure 4.12-S1-90). This is attributed to the self-healing not only caused by the carbonation of Na<sup>+</sup> or Ca<sup>+2</sup> ions but also by continuing geopolymerization to fill the cracks. XRD diffractograms of the powders scratched from cracks that will be discussed in the next section support this case. S2 has a huge amount of efflorescence with Na<sup>+</sup> carbonation on the 28<sup>th</sup> day (Figure 4.12-S2-28), which is called a misleading early self-healing phenomenon. While traces of these carbonation products are seen in Figure 4.12-S2-56, more stable calcium carbonate products and additional continuing geopolymerization products formed on the 90<sup>th</sup> day (Figure 4.12-S2-90). As explained in the EI results, S3 has higher maturity on the 7<sup>th</sup> day. Its free Ca<sup>+2</sup> cations are highly consumed owing to the formation of C-S-H similar structures, and other ions participating in geopolymerization were consumed. Therefore, insufficient self-healing is expected according to the formation of CaCO<sub>3</sub>. Paralleling this, cracks in S3 healed more slowly than other EGCs, as can be seen from Figure 4.12-S3-28,56.

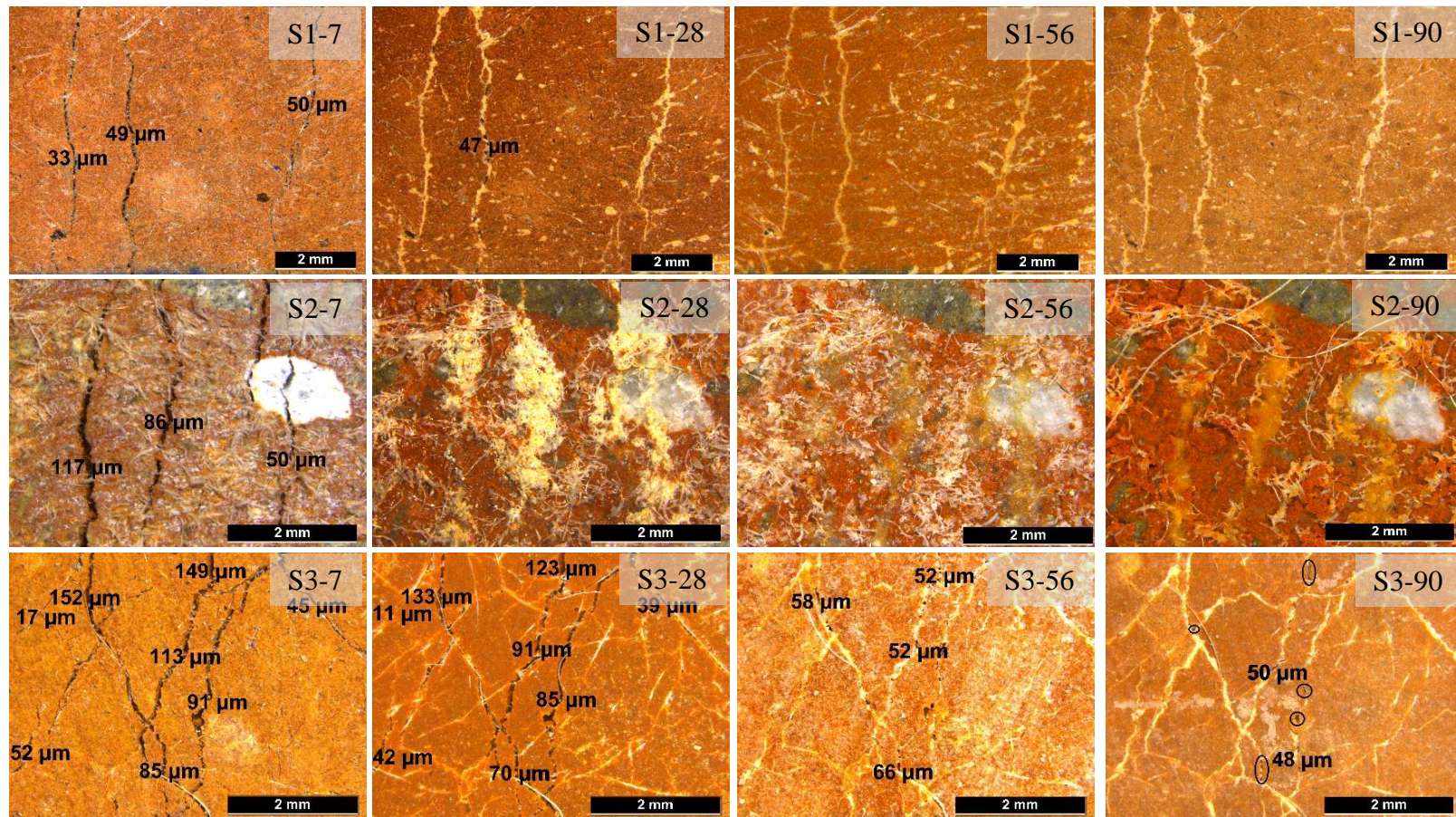


Figure 4.12. Optical images of specimens (S1, S2 and S3) on the 7<sup>th</sup>, 28<sup>th</sup>, 56<sup>th</sup>, and 90<sup>th</sup> days

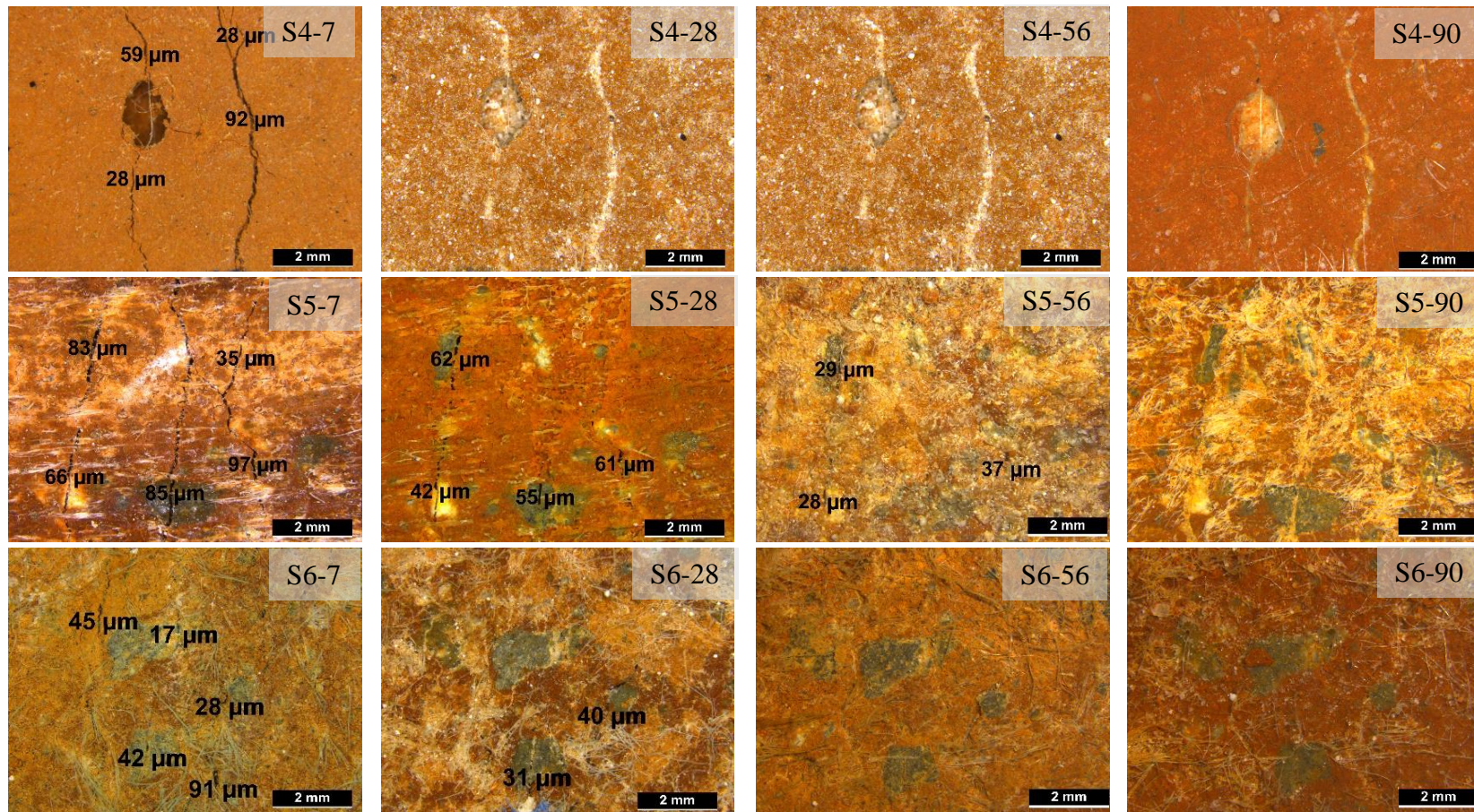


Figure 4.13. Optical images of specimens (S4, S5 and S6) on the 7<sup>th</sup>, 28<sup>th</sup>, 56<sup>th</sup>, and 90<sup>th</sup> days



Although cracks of S3 seem to have healed substantially on the 90<sup>th</sup> day, there are very small dot-shaped gaps in some places. As in S3, the EI results of S4 did not increase much on the 90<sup>th</sup> day, and this is seen from cracks that do not heal completely. On the 28<sup>th</sup> day, Na<sub>2</sub>CO<sub>3</sub> formations, which lead to misleading self-healing owing to the temporary EI increment, can be seen as white spots in Figure 4.13-S4-28. The cracks in S5 healed distinctly from the 7<sup>th</sup> day to the 90<sup>th</sup> day, which was promoted by the EI results. There was no efflorescence on the 28<sup>th</sup> day (Figure 4.13-S5-28), indicating that the EI increment of S5 at this time is not owing to efflorescence formation but rather from continuing geopolymerization. The absence of a decrease in EI results after the 28<sup>th</sup> day also supports this situation. S6 has several white spots indicating efflorescence on the 28<sup>th</sup> day (Figure 4.13-S6-28). However, on the 56<sup>th</sup> day and 90<sup>th</sup> day, cracks completely healed, which can also be seen from the increment in EI results of S6.

#### **4.4.4 Mechanical properties after self-healing**

Figure 4.14 exhibits the mechanical recovery of all EGCs. In mechanical recovery graphics, 1 represents the load-midpoint displacement graphic of pre-cracked specimens while preloading performed. 2 defines the load-midpoint displacement graphic of reloading of the cracked specimen after the healing period was completed. 3 represents the load-midpoint displacement graphic of sound (reference) specimen after 90 days. Because preloaded specimens' displacement remains constant after the healing period, reloading graph (2) is started on the point where preloading graph (1) is ended on the x-axis.

It is seen from all mechanical recovery graphics; all EGCs have deflection hardening behavior after the healing period. Although some healed specimens do not show as high ductility as reference specimens, high initial slopes of reloading graphics of healed specimens show that they can still perform multiple micro-cracks.

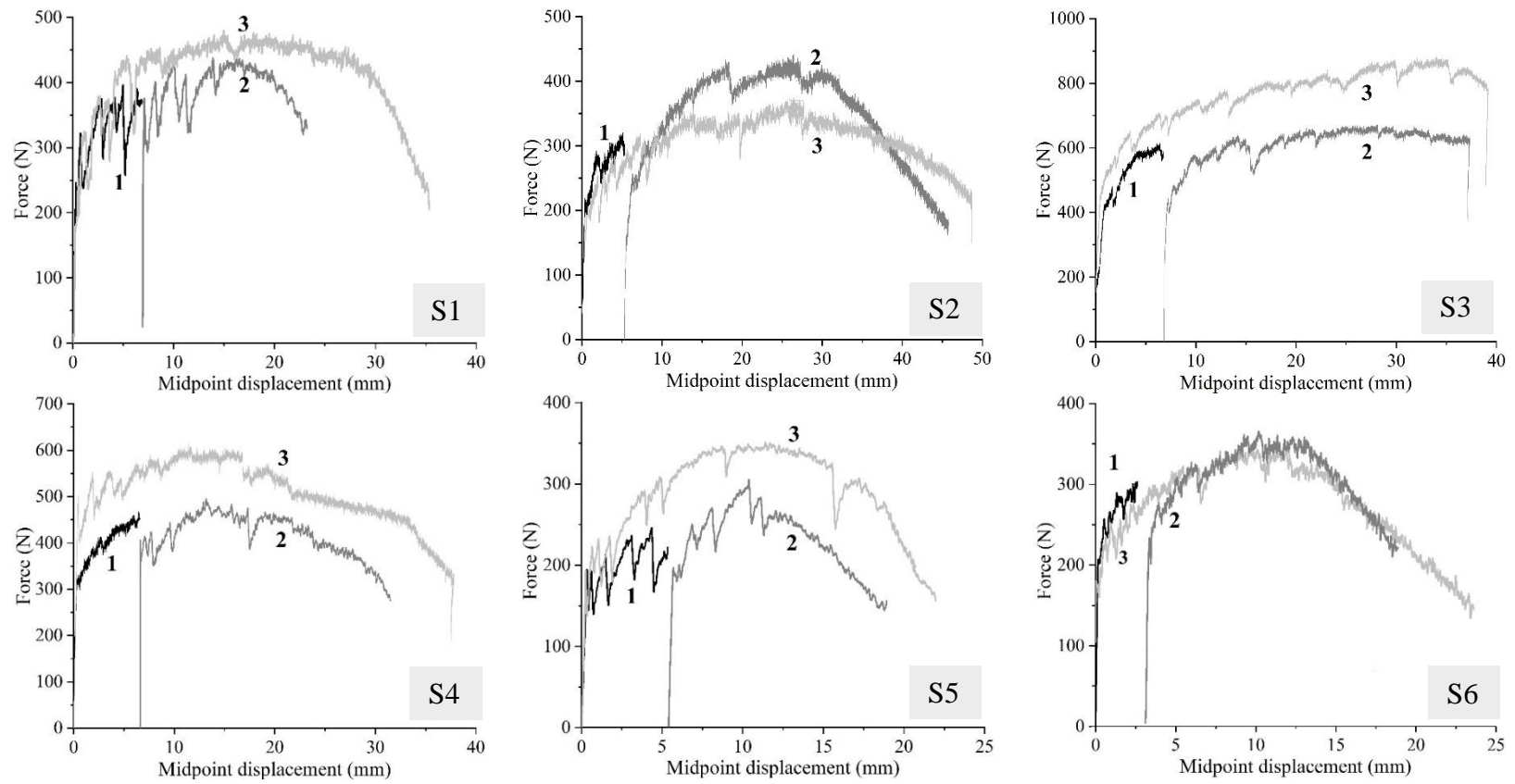


Figure 4.14. Mechanical recovery of EGCs (1 – preloading, 2 – reloading, 3 – reference)

The indented structure of S1's preloading graphic illustrates the precise multiple microcrack formation. Similar to this, the indented graphic of the reloading process prove that self-healing does not only fill cracks but also provide the adherence between fiber and matrix filling in healed crack. The reloading graphic of S1 could not reach the ductility of the reference specimen of S1. This is attributed to the higher toughness of S1 coming from slag content (Li and Liu, 2007). A high rate of early geopolymerization reactions raise the toughness of the matrix and crack widths are slightly wider than EGCs without slag. While reference S1 has a midpoint displacement up to 30 mm, reloaded one has a deflection of approximately 25 mm. In this context, S1 could not get a complete mechanical recovery.

Unlike other EGCs, reloaded S2 can bear a higher flexural load than reference S2. As can be seen from Figure 4.12, cracks of S2 have entirely healed after 90 days. This situation indicates an apparent adherence between the material filling the crack and both fibers and the internal surface of the crack. Also, it is considered that the density of material filling narrow cracks is slightly higher than the density of ones filling wider cracks. An increment in crack width could make a complete recovery difficult as the species which are supposed to react for healing are found on the crack surface, and it is difficult for these species to reach deeper of crack opening. Therefore the increasing crack opening may result in a decrement in both the density of healing material and adherence between the material filling crack and the internal surface of the crack.

Reloaded S3 has a displacement-force graphic parallel to the reference S3. However, reloaded S3 has not been able to reach reference one. As mentioned in section 4.4.2.1, the presence of NaOH, Na<sub>2</sub>SiO<sub>3</sub>, and Ca(OH)<sub>2</sub> together as activator introduces more Ca<sup>+2</sup> existence rather than Na<sup>+</sup> (Zhao, Liu, Zuo, *et al.*, 2019). Consequently, C-S-H similar structures are formed rather than alkali aluminosilicate hydrates after early reactions. Therefore decrement in the amount of calcium species leads to less CaCO<sub>3</sub> formation, which is essential for self-healing. Partially healed cracks which can be seen in Figure 4.12, support this situation.

S4 has a similar mechanical recovery performance to S3. Although S4 has multiple microcrack formation, midpoint displacement curve declines earlier than S3. According to this, S3 has higher toughness and this is attributed to the presence of slag. S5 and S6 have lower flexural strength and less midpoint displacement capacities than other EGCs. The compressive strength results have already shown that removing  $\text{Na}_2\text{SiO}_3$  from the activator combination reduces the mechanical properties. Parallel to this, EGCs without  $\text{Na}_2\text{SiO}_3$  suffer from lack of flexural properties. However, by means of lower mechanical properties and less toughness, a clear deflection hardening behavior, which can be seen from humps of curves, exist. While reloaded S5 could not reach reference S5, S6 has a complete mechanical recovery with its reloading curve reaching reference one.

#### **4.4.5 Microstructural investigations**

##### **4.4.5.1 X-ray diffraction analyses**

To compare the healing products and matrix at the end of the 90-day complete healing period, powder samples were scratched from the healed cracks and matrix. The matrix was intentionally scratched from the surface to observe the differences in the crack and on the surface. Figure 4.15 presents the XRD diffractograms of powders obtained from healed cracks (gray lines) and the surface of the matrix (black lines). Minerals existing in the diffractograms are quartz (Q,  $\text{SiO}_2$ , PDF: 96-153-2513), calcite (C,  $\text{CaCO}_3$ , PDF:96-900-9668), natrite (N,  $\text{Na}_2\text{CO}_3$ , PDF: 96-901-1305), diopside (D,  $\text{CaMgO}_6\text{Si}_2$ , PDF: 96-900-0334), muscovite (M,  $\text{Al}_3\text{H}_2\text{KO}_{12}\text{Si}_3$ , PDF: 96-101-1050), calcium sodium aluminosilicate (C-N-A-S,  $\text{CaNa}_2\text{AlO}_4\text{Si}$ , PDF: 96-101-0112), carnegieite (Cr,  $\text{AlNaO}_4\text{Si}$ , PDF: 96-101-0954), lisetite (L,  $\text{Al}_4\text{CaNa}_2\text{O}_{16}\text{Si}_4$ , PDF: 96-900-1030), andradite (A,  $\text{Al}_{0.5}\text{Ca}_3\text{Fe}_{1.5}\text{O}_{12}\text{Si}_{4.7}$ , PDF: 96-900-1230), nepheline (Ne,  $\text{AlNaO}_4\text{Si}$ , PDF: 96-901-0481), lime (Li,  $\text{CaO}$ , PDF: 96-101-1096), and calcium aluminosilicate hydrate (C-A-S-H,  $\text{Al}_{1.6}\text{Ca}_3\text{Fe}_{0.4}\text{O}_{12}\text{Si}_3$ , PDF: 96-810-4277). Although they may differ given their minerals, different

aluminosilicate hydrate-based mineral formations in all EGCs can be observed from diffractograms. The most striking difference in the XRD analyses of the healed cracks and surface of the matrixes for all EGCs is the more visible  $\text{CaCO}_3$  peaks of the healed cracks. Although  $\text{CaCO}_3$  is seen as the main healing product, lower  $\text{Na}_2\text{CO}_3$  also exists. While S1 and S5 with slag content have direct C-N-A-S peaks at  $2\theta$  of  $20.85^\circ$ , S3 has muscovite and lisetite minerals as aluminosilicate-based formations. However, the amorphous structure, which is seen from the broad halo between  $2\theta$  of  $18^\circ$  and  $28^\circ$  for S1 shifted to the right and placed between  $2\theta$  of  $20^\circ$  and  $40^\circ$  for S3, indicating the formation of amorphous sodium aluminosilicate hydrate (N-A-S-H) (Bødønoiu, Abood Al-Saadi and Voicu, 2015).

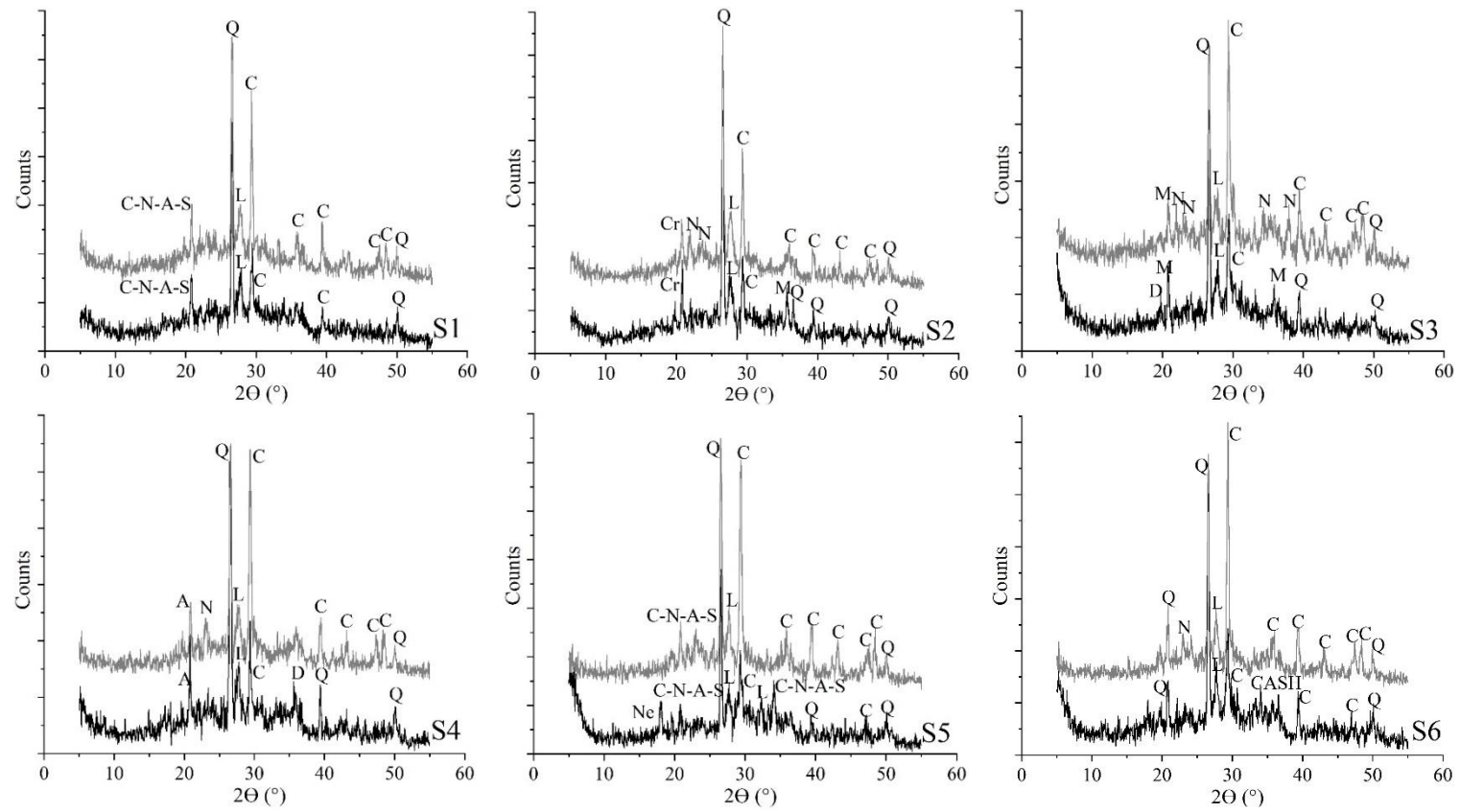


Figure 4.15. XRD diffractograms of matrix (black) and healed cracks (gray)

S3 has diopside, which is a calcium silicate mineral with magnesium, unlike S1 and S5. In addition, S5 has a nepheline mineral indicating the formation of a sodium aluminosilicate structure. S2, S4, and S6 have similar amorphous structures, indicating N-A-S-H type amorphous gel formation. S2 has a carnegieite pointing out for sodium aluminosilicate formation, and S4 has andradite, which is a calcium aluminosilicate structure. XRD diffractograms of all specimens have higher calcite crystal peaks at  $2\theta$  of  $29.35^\circ$ , indicating that one of the ultimate healing products is  $\text{CaCO}_3$ . S1 and S3 specimens with slag having higher calcite peaks than S2 and S4 without slag indicate that slag has a positive effect on the autogenous self-healing capability of EGCs. According to Kan et al. (2019), self-healing products of metakaolin and fly ash (both Class-F and C) geopolymers do not contain calcite crystals. As reported here and can also be seen from the literature studies, calcite formation is highly dependent on the calcium content of raw materials. Additional calcite peaks formed and intensities of some calcite peaks increased in the XRD diffractograms of healed cracks. In addition, the XRD patterns of healed cracks have natrite ( $\text{Na}_2\text{CO}_3$ ) peaks with relatively lower intensities as also reported by Reig et al. (2014). According to the XRD analysis, natrite is the secondary self-healing product after calcite. In addition, self-healing is also promoted by the ongoing geopolymerization reactions. The XRD diffractogram of S1 mixture implies that S1 has the maximum rate of ongoing geopolymerization due to the alkaline activator combination of NaOH and  $\text{Na}_2\text{SiO}_3$ .  $\text{Ca}(\text{OH})_2$  addition accelerated early reactions and reduced ongoing geopolymerization at later ages.

#### **4.4.5.2 Scanning electron microscopy and energy dispersive X-ray spectroscopy analyses**

Since all specimens' crack healing patterns were similar, completely healed cracks were chosen for SEM analyses from randomly selected mixtures can be seen from Figure 4.16 and Figure 4.17. Figure 4.16a shows a fully self-healed crack of S2 specimen after 90 days of healing period beyond the initial 7-day curing. To

determine the elemental structure of the healed crack, a line-scan analysis was performed on the line marked with a yellow dashed line, which can be seen in Figure 4.16a and b. The line-analysis graph shows the amount of elements on the entire yellow line. In Figure 4.16b, while the area between bold vertical lines at point 35 and 136 represents the healed crack, outside of these lines represent the matrix around the healed crack. The coexistence of C and Ca and the increase of C and Ca together at some points (i.e., points 99, 122, 128, and 132) are attributed to the formation of  $\text{CaCO}_3$ . Figure 4.16c and d show the area marked with the red dashed rectangle in Figure 4.16a and c, respectively. According to EDX analysis shown in Figure 4.16e and with C, O, and Ca amounts of 19.99%, 38.62%, and 9.26%, respectively, the healing products contain  $\text{CaCO}_3$  as reported from the line-scan analysis and XRD results. Healing products also contain Si, Na, and Al, which points out for the ongoing geopolymerization. However, it is difficult to determine the type of geopolymerization product formed.

A selected area from the matrix surface of the 97-day-old specimen of S2 mixture is shown in Figure 4.17. Figure 4.17a shows the presence of  $\text{Na}_2\text{CO}_3$  (natrite) mineral, which forms as a result of the reactions between  $\text{Na}^+$  ions dissolved in the matrix and the  $\text{CO}_2$  in the air (Komnitsas and Zaharaki, 2007). It is seen that while carbonation products fill inside the cracks, they are also available on the matrix surface. Another product shown in Figure 4.17b is calcite ( $\text{CaCO}_3$ ). Although calcite already exists in the raw material, higher intensities of  $\text{Ca}^{+2}$  ions as observed in both EDX analysis here and in XRD analysis in the previous section imply for the formation of additional calcite crystals on the matrix surface as a result of the reaction of  $\text{Ca}^{+2}$  ions in the pore water and atmospheric carbon dioxide. According to the EDX analysis (Figure 4.17c) of another area where calcite is formed, the existence of sodium with calcite shows that natrite formation also occurs together with calcite, which explains the calcite and natrite minerals that appear at the close  $2\theta$  angle in the XRD analysis.



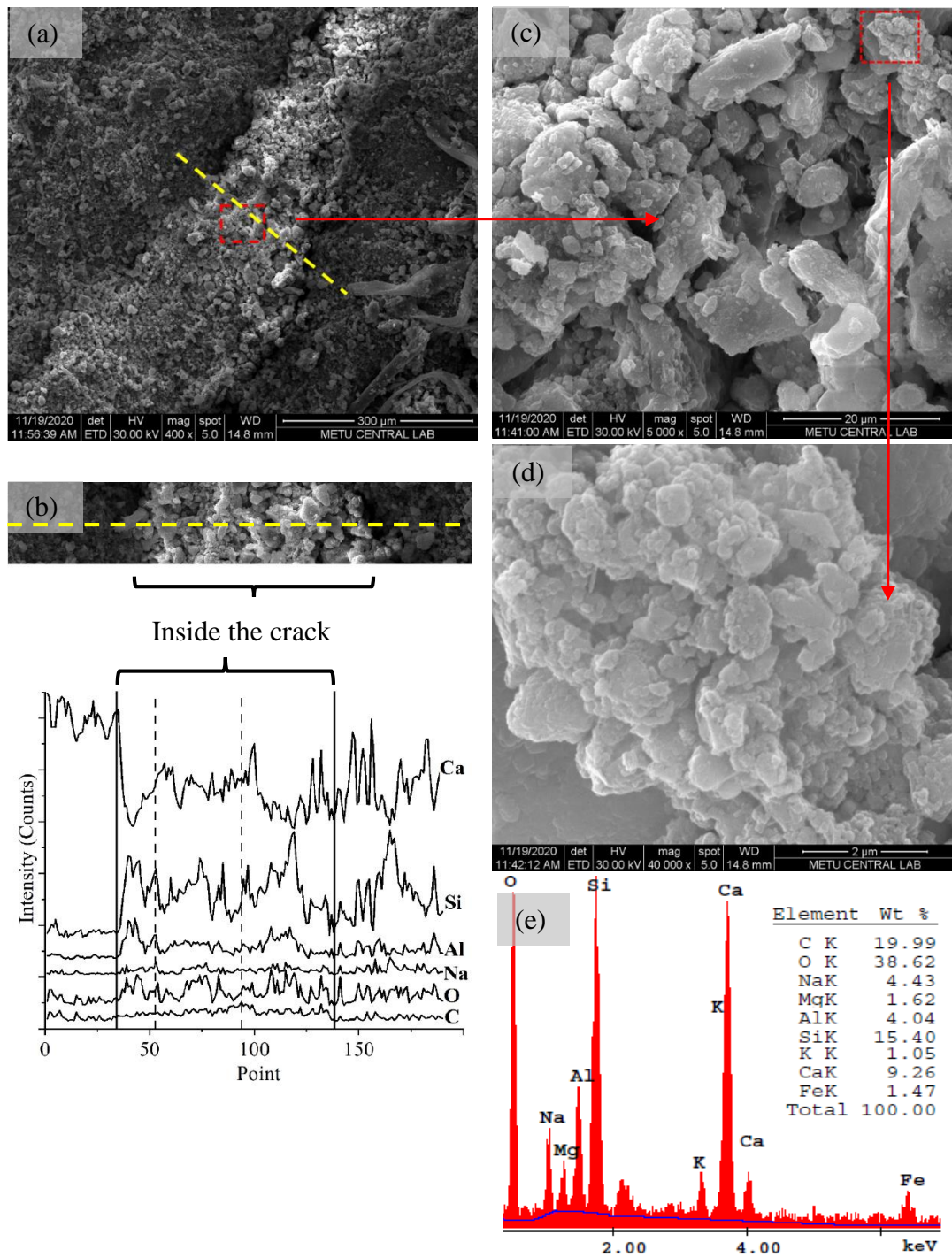
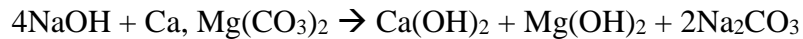
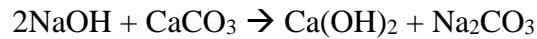


Figure 4.16. (a) SEM image of healed crack, (b) line-scan analysis images with (c) 5000× and (d) 40000× magnification of red dashed marked area, and (e) EDX analysis

According to Abdel-Gawwad et al. (2019), NaOH activation of raw materials containing calcite causes calcium hydroxide and sodium carbonate formation, as described below. This situation explains the coexistence of natrite and calcite formation.



In Figure 4.17d, a plate-shaped particle originating from brick waste, which was not completely dissolved, is seen. The reaction products observed around this particle indicate that geopolymerization takes place on this particle. These types of unreacted particles that do not participate in geopolymerization may contribute to the nucleation effect. Although some of the raw materials that do not participate in the geopolymerization reactions do not contribute to the development of the matrix directly, their contribution through the nucleation effect may support the mechanical properties, similar to cementitious systems (Siad *et al.*, 2018). Hajimohammadi et al. (2011) stated that nucleation may take place close to the silica particles, which can be a similar case for Si-containing clayey particles here.

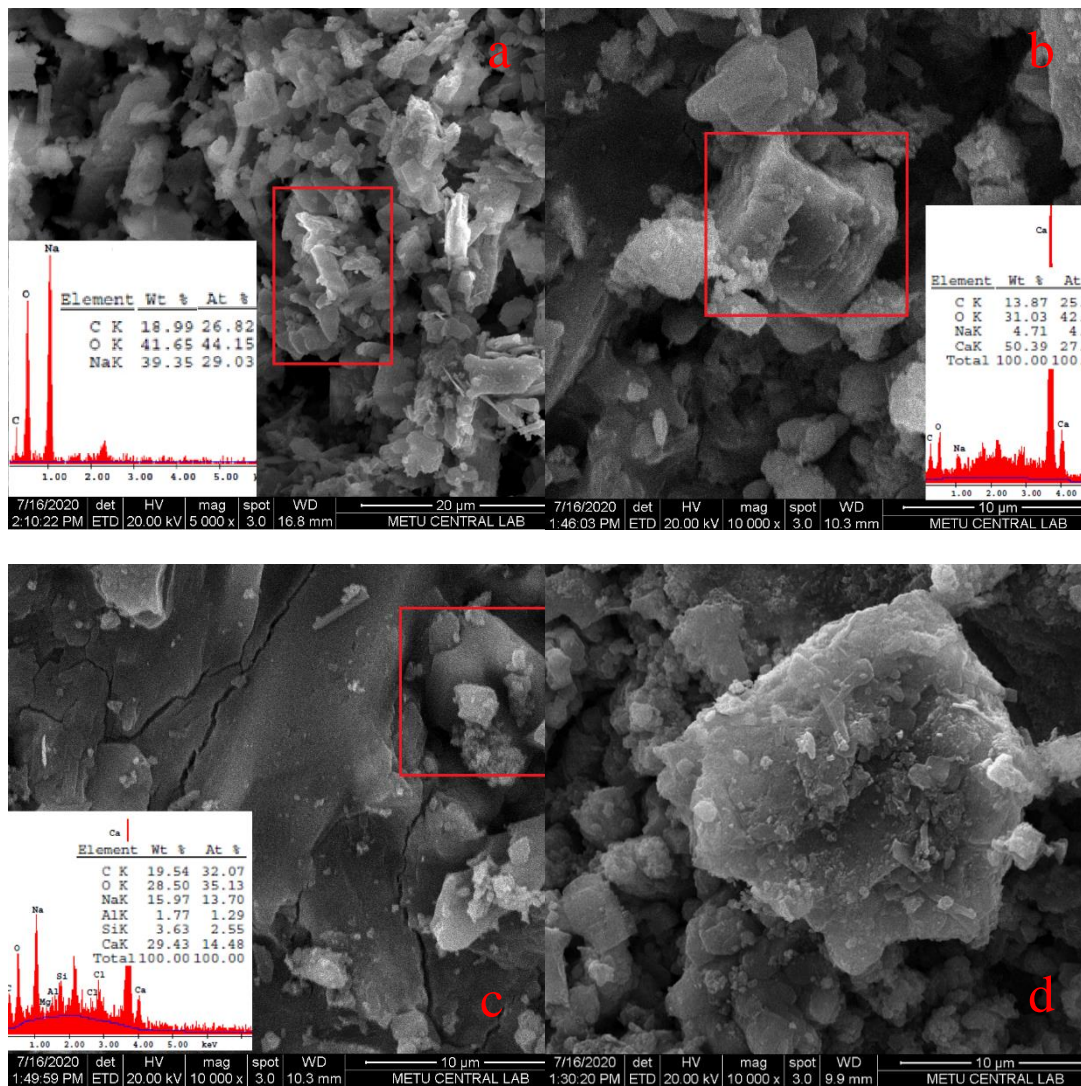


Figure 4.17. SEM images of S2 specimen showing formations of (a) sodium carbonate, (b) calcium carbonate, (c) sodium carbonate and calcium carbonate together, and (d) unreacted brick particle



## CHAPTER 5

### SUMMARY, CONCLUSIONS AND RECOMMENDATIONS

Alkali-activated materials and geopolymers are materials that have the ability to be used as a binding material in many respects. While it was considered as a fire-resistant material when it was first developed, later it was considered to be an alternative binding material to cement. Geopolymers can match the mechanical performance of cementitious systems to a great extent. Although its durability performance may be satisfactory, its crack formation tendency is a drawback of developing large structural members with alkali-activation. In this context, providing self-healing ability to geopolymers would be a solution that will overcome this drawback by sealing cracks. However, healing a crack cannot be justified by observing if the crack is sealed only at the surface. In addition, the depth of the crack should be filled so that there is no loss in mechanical properties. The experimental studies conducted within the scope of this doctoral dissertation focused on the design requirements of the geopolymer material with self-healing capability. Additionally, construction and demolition waste-based materials were utilized as precursor for alkali-activation. This study, which fundamentally comprises of three stages, consists of the production of geopolymer paste and mortar from waste materials, the development of EGC that has the ability to create multiple micro-cracks from these mortars, and the self-healing ability of these EGCs.

This work refers optimum design for alkali-activation of construction and demolition waste-based materials, in the context of both material proportions, activator type and concentration, curing condition and temperature. Although five different construction and demolition waste-based materials can be used for geopolymer production, clayey materials (tiles and bricks) containing high amounts of aluminosilicate minerals make them more advantageous for alkali-activation.

The dissertation study, then, describes the requirements for developing mortar by utilizing geopolymer paste and recycled concrete aggregate with different maximum aggregate sizes. As expected, recycled concrete aggregates have a high amount of calcium carbonate and are susceptible to lack of adherence because of their brittle and crumbly behavior comparing the conventional concrete aggregate. Microstructural investigations were made to observe the adherence between recycled concrete aggregate and geopolymer paste in mortar. Finally, engineered geopolymer composites with the ability of multiple microcracking formation were developed. Some of the EGCs were comprising of complete construction and demolition waste-based precursors, and others have ground granulated blast furnace slag addition. Although sodium hydroxide was enough for alkali-activation of CDW-based precursors, sodium silicate solution and calcium hydroxide were also utilized as an alkaline activator to see their effect on self-healing performance with their extra silicon and calcium availability.

According to the results obtained from experiments conducted during the whole study can be summarized as:

- All CDW-based materials (concrete, glass, red clay brick, hollow brick and roof tile) can be utilized in alkali-activation. Clay originated materials are highly reactive for geopolymerization. The primary reason for this reasoned from their silica and alumina-rich chemical content. While their mineralogical structures are similar to fly-ash, which is the most popular and feasible material for alkali-activation, amorphous portions of them provide high solubility.
- For the alkali-activation of CDW-based materials, NaOH alone is sufficient as an alkaline-activator, provided that the samples are cured at high temperatures.
- While lower molarities of NaOH may be insufficient to dissolve aluminosilicate species completely, higher molarities may hinder strength development because of the silica coagulation. Also, it is seen that increasing

activator molarities may require an extended curing period to allow silica and alumina species to complete their reactions.

- Although curing temperature increment provides higher strength development, excessive temperatures may harm geopolymeric formations. It is seen that optimum curing temperatures for all precursors should be determined. 115 °C was seen as optimum curing temperature in almost all conditions (activator molarity, curing period, precursor design) for CDW-based precursors.
- Even though the mechanical properties of alkali-activated concrete waste has lower than clayey materials, recycled concrete aggregate has tremendous performance when utilized in developing geopolymer mortar. Scanning electron microscopy and line-mapping analysis exhibit that recycled concrete aggregate takes place in geopolymerization reactions on its surface.
- Polyethylene and nylon fibers are appropriate to obtain multiple crack formations. EGCs with PE and NM fiber content show excellent deflection hardening properties. For CDW-based materials used in this study, a combination of 1.25% PE and 0.75% NM is determined as the optimum fiber content.
- Unlike cementitious systems, the electrical properties of geopolymers are outrageously complex. Therefore evaluating self-healing with change in electrical impedance is challenging. Self-healing evaluation with water absorption is easier than electrical impedance. However, it should be known that the pore volume of geopolymers may increase in time and this situation may make water absorption misleading.
- Like geopolymers, EGCs also have an efflorescence tendency. Efflorescence causes misleading results in electrical impedance results when self-healing is evaluated. At later ages, fundamental healing products as sodium and potassium carbonate and continued geopolymerization reaction products take place in cracks rather than efflorescence.

- Self-healing of EGCs is highly dependent on sodium and calcium content. Sodium carbonate and calcium carbonate are clearly seen from scanning electron microscopy analyses. However, continued geopolymerization was also detected in healed cracks with EDX analyses. These findings were promoted by X-ray diffraction studies.
- A complete self-healing performance can be obtained in terms of flexural strength and deflection hardening behavior. In this context, narrow cracks are more advantageous than wider cracks. An increasing crack opening may decrease the density of material filling the crack. Consequently, adherence between this material and both fiber and the crack surface might fall.

Cracking tendency of geopolymers suppresses the widespread use of geopolymer. Researchers who concentrated on developing geopolymer structural members encounter this problem. In addition to early cracks, EGCs with construction and demolition waste content can be used to both suppress and heal cracks that may occur later. It is seen that clayey materials should be utilized in high amounts (totally 60% and higher) for main geopolymerization reactions as an aluminosilicate resource. Concrete waste, which is rich in calcium, promotes calcium carbonate formation. Thus, even if concrete waste is not preferred in geopolymer production, it should be used in a limited amount in EGC for self-healing capability. Like concrete waste, ground granulated blast furnace slag can be used as a calcium source to trigger calcium carbonate formation.

Although many studies in the literature concentrated on alkali-activation focus on high-temperature curing, EGCs developed in this study do not require elevated temperatures. Thus, EGCs will be highly preferable in this context. Electrical impedance measurements gave different results for different activator types and amounts in the early self-healing process. However, both NaOH alone and the combination of NaOH and Na<sub>2</sub>SiO<sub>3</sub> can be chosen as alkaline activators for EGC production and self-healing behavior.



Further works can focus on developing large structural members with EGCs. Cracks that will occur in large-sized structural members can exist in different patterns and widths. The optimum fiber content for large-sized structural members may be varied, taking into account both this situation and the workability requirements of large members. Multiple micro-cracking formations and strain-hardening capabilities should be examined. Evaluating the self-healing of large-sized structural members with transport properties would be challenging. However, self-healing can be evaluated by observing the change in the durability performance of EGCs for both small-sized and large-sized structural members.

When only the amount of carbon emissions is considered, geopolymers seem to be more advantageous than conventional concrete. However, when the environmental effects are considered, geopolymer may be disadvantageous compared to conventional concrete. Therefore, the environmental impact assessment for these binders should be made by considering not only the carbon footprint but also the environmental effects of the production and use of all materials involved in the production process of these binders. Especially the different raw material contents of geopolymers and a wide variety of curing processes (temperature and time) make this even more critical. Consequently, a comprehensive life cycle analysis (LCA) for geopolymers that incorporate CDW will be incredibly rewarding for the future of the material developed in this study.



## REFERENCES

- Abdel-Gawwad, H. A., Rashad, A. M., & Heikal, M. (2019). Sustainable utilization of pretreated concrete waste in the production of one-part alkali-activated cement. *Journal of Cleaner Production*, 232, 318–328. <https://doi.org/10.1016/j.jclepro.2019.05.356>
- Adamson, A. W. (1973). *A Textbook of Physical Chemistry*. Academic Press.
- Ahmari, S., Ren, X., Toufigh, V., & Zhang, L. (2012). Production of geopolymeric binder from blended waste concrete powder and fly ash. *Construction and Building Materials*, 35, 718–729. <https://doi.org/10.1016/j.conbuildmat.2012.04.044>
- Aldea, C., Song, W., & Popovics, J. S. (2000). Extent of healing of cracked normal strength concrete. *February*, 92–96.
- Allahverdi, A., Mehrpour, K., & Najafikani, E. (2008). Investigating the possibility of utilizing pumice-type natural pozzonal in production of geopolymer cement. *Ceramics - Silikaty*, 52(1), 16–23.
- Alonso, S., & Palomo, A. (2001). Alkaline activation of metakaolin and calcium hydroxide mixtures: Influence of temperature, activator concentration and solids ratio. *Materials Letters*, 47(1–2), 55–62. [https://doi.org/10.1016/S0167-577X\(00\)00212-3](https://doi.org/10.1016/S0167-577X(00)00212-3)
- Andrew, R. M. (2017). Global CO<sub>2</sub> emissions from cement production. *Earth System Science Data Discussions*, 1–52. <https://doi.org/10.5194/essd-2017-77>
- Arslan, H., Coşgun, N., & Salgın, B. (2012). Construction and Demolition Waste Management in Turkey. In M. Rebello, Luis, Fernando (Ed.), *Waste Management: An Integrated Vision* (p. 313).
- ASTM C1585 – 13. (2013). Standard Test Method for Measurement of Rate of Absorption of Water by Hydraulic Cement Concretes. *ASTM International*, 41(147), 1–6. <https://doi.org/10.1520/C1585-11.2>

- ASTM C1585 – 11. (2011). Standard Test Method for Measurement of Rate of Absorption of Water by Hydraulic-Cement Concretes. *ASTM International*
- Atış, C. D., Görür, E. B., Karahan, O., Bilim, C., Ilkentapar, S., & Luga, E. (2015). Very high strength (120 MPa) class F fly ash geopolymer mortar activated at different NaOH amount, heat curing temperature and heat curing duration. *Construction and Building Materials*, 96, 673–678. <https://doi.org/10.1016/j.conbuildmat.2015.08.089>
- Belitsky, I. V. (1993). Kinetics of hydration of slag in slag-alkaline cement. *3rd Beijing Int. Symp. On Cement and Concrete*, 1028–1031.
- Bernal, S. A., Rodríguez, E. D., Mejía de Gutiérrez, R., Provis, J. L., & Delvasto, S. (2012). Activation of metakaolin/slag blends using alkaline solutions based on chemically modified silica fume and rice husk ash. *Waste and Biomass Valorization*, 3(1), 99–108. <https://doi.org/10.1007/s12649-011-9093-3>
- Bădănoiu, A. I., Abood Al-Saadi, T. H., & Voicu, G. (2015). Synthesis and properties of new materials produced by alkaline activation of glass cullet and red mud. *International Journal of Mineral Processing*, 135, 1–10. <https://doi.org/10.1016/j.minpro.2014.12.002>
- Brew, D. R. M., & Mackenzie, K. J. D. (2007). Geopolymer synthesis using silica fume and sodium aluminate. *Journal of Materials Science*, 42(11), 3990–3993. <https://doi.org/10.1007/s10853-006-0376-1>
- Chen-Tan, N. W., Van Riessen, A., Ly, C. V., & Southam, D. C. (2009). Determining the reactivity of a fly ash for production of geopolymer. *Journal of the American Ceramic Society*, 92(4), 881–887. <https://doi.org/10.1111/j.1551-2916.2009.02948.x>
- Chindapasirt, P., Thaiwitcharoen, S., Kaewpirom, S., & Rattanasak, U. (2013). Controlling ettringite formation in FBC fly ash geopolymer concrete. *Cement and Concrete Composites*, 41, 24–28. <https://doi.org/10.1016/j.cemconcomp.2013.04.009>

- Clear, C. A. (1985). The Effects of Autogenous Healing upon the Leakage of Water through Cracks in Concrete. *Cement and Concrete Association*, 31.
- Coelho, A., & de Brito, J. (2013). Environmental analysis of a construction and demolition waste recycling plant in Portugal - Part II: Environmental sensitivity analysis. *Waste Management*, 33(1), 147–161. <https://doi.org/10.1016/j.wasman.2012.09.004>
- Criado, M., Palomo, A., & Fernandez-Jimenez, A. (2005). Alkali activation of fly ashes. Part 1: Effect of curing conditions on the carbonation of the reaction products. *Fuel*, 84(16), 2048–2054. <https://doi.org/10.1016/j.fuel.2005.03.030>
- Davidovits, J. (1982). *Mineral polymers and methods of making them* (Patent No. 4,349,386).
- Davidovits, J. (1994). *Properties of Geopolymer Cements, Alkaline Cements and Concretes*. 131–149.
- Detphan, S., & Chindaprasirt, P. (2009). Preparation of fly ash and rice husk ash geopolymer. *International Journal of Minerals, Metallurgy and Materials*, 16(6), 720–726. [https://doi.org/10.1016/S1674-4799\(10\)60019-2](https://doi.org/10.1016/S1674-4799(10)60019-2)
- Dias, D. P., & Thaumaturgo, C. (2005). Fracture toughness of geopolymeric concretes reinforced with basalt fibers. *Cement and Concrete Composites*, 27(1), 49–54. <https://doi.org/10.1016/j.cemconcomp.2004.02.044>
- Ding, Y., Dai, J. G., & Shi, C. (2016). Mechanical properties of alkali-activated concrete: A state-of-the-art review. *Construction and Building Materials*, 127, 68–79. <https://doi.org/10.1016/j.conbuildmat.2016.09.121>
- Djobo, J. N. Y., Elimbi, A., Tchakouté, H. K., & Kumar, S. (2017). Volcanic ash-based geopolymer cements/concretes: the current state of the art and perspectives. *Environmental Science and Pollution Research*, 24(5), 4433–4446. <https://doi.org/10.1007/s11356-016-8230-8>
- Duxson, P. (2009). Geopolymer precursor design. In John L Provis & J. S. J. van

- Deventer (Eds.), *Geopolymers, Structure, processing, properties and industrial applications* (p. 37). Woodhead Publishing Limited.
- Duxson, P., Fernandez-Jimenez, A., Provis, J. L., Lukey, G. C., Palomo, A., & Van Deventer, J. S. J. (2007). Geopolymer technology: The current state of the art. *Journal of Materials Science*, 42(9), 2917–2933. <https://doi.org/10.1007/s10853-006-0637-z>
- Duxson, P., Lukey, G. C., Separovic, F., & Van Deventer, J. S. J. (2005). Effect of alkali cations on aluminum incorporation in geopolymeric gels. *Industrial and Engineering Chemistry Research*, 44(4), 832–839. <https://doi.org/10.1021/ie0494216>
- Duxson, P., Lukey, G. C., & Van Deventer, J. S. J. (2007). Physical evolution of Na-geopolymer derived from metakaolin up to 1000 °C. *Journal of Materials Science*, 42(9), 3044–3054. <https://doi.org/10.1007/s10853-006-0535-4>
- Duxson, P., Mallicoat, S. W., Lukey, G. C., Kriven, W. M., & van Deventer, J. S. J. (2007). The effect of alkali and Si/Al ratio on the development of mechanical properties of metakaolin-based geopolymers. *Colloids and Surfaces A: Physicochemical and Engineering Aspects*, 292(1), 8–20. <https://doi.org/10.1016/j.colsurfa.2006.05.044>
- Duxson, P., Provis, J. L., Lukey, G. C., Mallicoat, S. W., Kriven, W. M., & Van Deventer, J. S. J. (2005). Understanding the relationship between geopolymer composition, microstructure and mechanical properties. *Colloids and Surfaces A: Physicochemical and Engineering Aspects*, 269(1–3), 47–58. <https://doi.org/10.1016/j.colsurfa.2005.06.060>
- Duxson, P., Provis, J.L., Lukey, G.C., van Deventer, G.C. (2007). The role of inorganic polymer technology in development of ‘green concrete’. *Cement and Concrete Research*, 37, 1590-1597.
- Edvardsen, C. K. (1996). Water permeability and self-healing of through-cracks in concrete. *DAfStb Bull*, 455.

- Fang, Y., & Kayali, O. (2013). The fate of water in fly ash-based geopolymers. *Construction and Building Materials*, 39, 89–94. <https://doi.org/10.1016/j.conbuildmat.2012.05.024>
- Fawer, M., Concannon, M., & Rieber, W. (1999). Life cycle inventories for the production of sodium silicates. *International Journal of Life Cycle Assessment*, 4(4), 207–212. <https://doi.org/10.1007/BF02979498>
- Glukhovsky, V. D. (1983). *Binder* (Patent No. 4410365).
- Glukhovsky, V. D. (1980). High strength slag- alkaline cements. *7th Int. Congr. on the Chemistry of Cement*, 164–168.
- Glukhovsky, V. D., & Pakhomov, V. A. (1978). *Slag-alkali cements and concretes*.
- Görhan, G., & Kürklü, G. (2014). The influence of the NaOH solution on the properties of the fly ash-based geopolymer mortar cured at different temperatures. *Composites Part B: Engineering*, 58, 371–377. <https://doi.org/10.1016/j.compositesb.2013.10.082>
- Guo, X., & Yang, J. (2020). Intrinsic properties and micro-crack characteristics of ultra-high toughness fly ash/steel slag based geopolymer. *Construction and Building Materials*, 230, 116965. <https://doi.org/10.1016/j.conbuildmat.2019.116965>
- Habert, G., d’Espinoise de Lacaillerie, J.B., Roussel, N. (2011) An environmental evaluation of geopolymer based concrete production: reviewing current research trends. *Journal of Cleaner Production*, 19(11), 1229–1238.
- Haddad, R. H., & Alshbuol, O. (2016). Production of geopolymer concrete using natural pozzolan: A parametric study. *Construction and Building Materials*, 114, 699–707. <https://doi.org/10.1016/j.conbuildmat.2016.04.011>
- Haha, M. Ben, Lothenbach, B., Le Saout, G., & Winnefeld, F. (2011). Influence of slag chemistry on the hydration of alkali-activated blast-furnace slag - Part I: Effect of MgO. *Cement and Concrete Research*, 41(9), 955–963.

<https://doi.org/10.1016/j.cemconres.2011.05.002>

Hajimohammadi, A., Ngo, T., & Kashani, A. (2018). Glass waste versus sand as aggregates: The characteristics of the evolving geopolymer binders. *Journal of Cleaner Production*, *193*, 593–603.  
<https://doi.org/10.1016/j.jclepro.2018.05.086>

Hajimohammadi, A., Provis, J. L., & Van Deventer, J. S. J. (2011). The effect of silica availability on the mechanism of geopolymerisation. *Cement and Concrete Research*, *41*(3), 210–216.  
<https://doi.org/10.1016/j.cemconres.2011.02.001>

Hanjitsuwan, S., Hunpratub, S., Thongbai, P., Maensiri, S., Sata, V., & Chindaprasirt, P. (2014). Effects of NaOH concentrations on physical and electrical properties of high calcium fly ash geopolymer paste. *Cement and Concrete Composites*, *45*, 9–14.  
<https://doi.org/10.1016/j.cemconcomp.2013.09.012>

Heiman, J. L., & Koerstz, P. (1991). Performance of polymer-modified cementitious repair mortars in chloride contaminated concrete. *Transactions of the Institution of Engineers*, *33*(3), 169–175.

Hong S Y. (1993). Studies on the hydration of alkali activated slag. *3rd Beijing Int. Symp. Cement and Concrete*, 1059–1063.

Hou, T. C. (2008). *Wireless and Electromechanical Approaches for Strain Sensing and Crack Detection in Fiber Reinforced Cementitious Materials*. University of Michigan.

Ibrahim, M., Megat Johari, M. A., Rahman, M. K., & Maslehuddin, M. (2017). Effect of alkaline activators and binder content on the properties of natural pozzolan-based alkali activated concrete. *Construction and Building Materials*, *147*, 648–660. <https://doi.org/10.1016/j.conbuildmat.2017.04.163>

Iler, R. K. (1979). *The Chemistry of Silica*. John Wiley and Sons Inc.



- Ismail, M., Toumi, A., François, R., & Gagné, R. (2004). Effect of crack opening on the local diffusion of chloride in inert materials. *Cement and Concrete Research*, 34(4), 711–716. <https://doi.org/10.1016/j.cemconres.2003.10.025>
- Jacobsen, S., Marchand, J., & Homain, H. (1995). SEM OBSERVATIONS OF THE MICROSTRUCTURE OF FROST DETERIORATED AND SELF-HEALED CONCRETES. *Cement and Concrete Research*, 25(8), 1781–1790.
- Jadhav, U. U., Lahoti, M., Chen, Z., Qiu, J., Cao, B., & Yang, E.-H. (2018). Viability of bacterial spores and crack healing in bacteria-containing geopolymer. *Construction and Building Materials*, 169, 716–723. <https://doi.org/10.1016/j.conbuildmat.2018.03.039>
- Jang, J. G., & Lee, H. K. (2016). Effect of fly ash characteristics on delayed high-strength development of geopolymers. *Construction and Building Materials*, 102, 260–269. <https://doi.org/10.1016/j.conbuildmat.2015.10.172>
- Jong, B., & Brown, G. E. (1980). Polymerization of Silicate and Aluminate Tetrahedra in Glasses, Melts, and Aqueous Solutions. *Geochimica et Cosmochimica Acta*, 44(3).
- Kan, L. li, Lv, J. wei, Duan, B. bei, & Wu, M. (2019). Self-healing of Engineered Geopolymer Composites prepared by fly ash and metakaolin. *Cement and Concrete Research*, 125(September), 105895. <https://doi.org/10.1016/j.cemconres.2019.105895>
- Ken, P. W., Ramli, M., & Ban, C. C. (2015). An overview on the influence of various factors on the properties of geopolymer concrete derived from industrial by-products. *Construction and Building Materials*, 77, 370–395. <https://doi.org/10.1016/j.conbuildmat.2014.12.065>
- Komnitsas, K., & Zaharaki, D. (2007). Geopolymerisation: A review and prospects for the minerals industry. *Minerals Engineering*, 20(14), 1261–1277. <https://doi.org/10.1016/j.mineng.2007.07.011>

- Komnitsas, K., Zaharaki, D., Vlachou, A., Bartzas, G., & Galetakis, M. (2015). Effect of synthesis parameters on the quality of construction and demolition wastes (CDW) geopolymers. *Advanced Powder Technology*, 26(2), 368–376. <https://doi.org/10.1016/j.appt.2014.11.012>
- Kucharczyk, S., Sitarz, M., Zajac, M., & Deja, J. (2018). The effect of CaO/SiO<sub>2</sub> molar ratio of CaO-Al<sub>2</sub>O<sub>3</sub>-SiO<sub>2</sub> glasses on their structure and reactivity in alkali activated system. *Spectrochimica Acta - Part A: Molecular and Biomolecular Spectroscopy*, 194, 163–171. <https://doi.org/10.1016/j.saa.2018.01.018>
- Lee, B. Y., Cho, C. G., Lim, H. J., Song, J. K., Yang, K. H., & Li, V. C. (2012). Strain hardening fiber reinforced alkali-activated mortar - A feasibility study. *Construction and Building Materials*, 37, 15–20. <https://doi.org/10.1016/j.conbuildmat.2012.06.007>
- Li, V. C., Lim, Y. M., & Chan, Y. W. (1998). Feasibility study of a passive smart self-healing cementitious composite. *Composites Part B: Engineering*, 29(6), 819–827. [https://doi.org/10.1016/S1359-8368\(98\)00034-1](https://doi.org/10.1016/S1359-8368(98)00034-1)
- Li, V. C., & Yang, E.-H. (2007). Self Healing in Concrete Materials. In S. van der Zwaag (Ed.), *Self-healing Materials: An Alternative Approach to 20 Centuries of Materials Science* (pp. 161–193).
- Li, Z., & Liu, S. (2007). Influence of Slag as Additive on Compressive Strength of Fly Ash-Based Geopolymer. *Journal of Materials in Civil Engineering*, 19(6), 470–474. [https://doi.org/10.1061/\(asce\)0899-1561\(2007\)19:6\(470\)](https://doi.org/10.1061/(asce)0899-1561(2007)19:6(470))
- Lin, T., Jia, D., He, P., Wang, M., & Liang, D. (2008). Effects of fiber length on mechanical properties and fracture behavior of short carbon fiber reinforced geopolymer matrix composites. *Materials Science and Engineering A*, 497(1–2), 181–185. <https://doi.org/10.1016/j.msea.2008.06.040>
- Lunevich, L., Sanciolò, P., Smallridge, A., & Gray, S. R. (2016). Silica scale formation and effect of sodium and aluminium ions -<sup>29</sup>Si NMR study.

- Environmental Science: Water Research and Technology*, 2(1), 174–185.  
<https://doi.org/10.1039/c5ew00220f>
- Ma, Y., Hu, J., & Ye, G. (2013). The pore structure and permeability of alkali activated fly ash. *Fuel*, 104, 771–780.  
<https://doi.org/10.1016/j.fuel.2012.05.034>
- Mahmoodi, O., Siad, H., Lachemi, M., Dadsetan, S., & Sahmaran, M. (2020a). Development of ceramic tile waste geopolymer binders based on pre-targeted chemical ratios and ambient curing. *Construction and Building Materials*, 258, 120297. <https://doi.org/10.1016/j.conbuildmat.2020.120297>
- Mahmoodi, O., Siad, H., Lachemi, M., Dadsetan, S., & Sahmaran, M. (2020b). Optimization of brick waste-based geopolymer binders at ambient temperature and pre-targeted chemical parameters. *Journal of Cleaner Production*, 268, 122285. <https://doi.org/10.1016/j.jclepro.2020.122285>
- Mahmoodi, O., Siad, H., Lachemi, M., Dadsetan, S., & Sahmaran, M. (2021). Development of normal and very high strength geopolymer binders based on concrete waste at ambient environment. *Journal of Cleaner Production*, 279, 123436. <https://doi.org/10.1016/j.jclepro.2020.123436>
- Manjunath, R., Narasimhan, M. C., & Umesha, K. M. (2019). Studies on high performance alkali activated slag concrete mixes subjected to aggressive environments and sustained elevated temperatures. *Construction and Building Materials*, 229, 116887. <https://doi.org/10.1016/j.conbuildmat.2019.116887>
- McIntosh, A., Lawther, S. E. M., Kwasny, J., Soutsos, M. N., Cleland, D., & Nanukuttan, S. (2015). Selection and characterisation of geological materials for use as geopolymer precursors. *Advances in Applied Ceramics*, 114(7), 378–385. <https://doi.org/10.1179/1743676115Y.0000000055>
- Mehta, P. K., & Monteiro, P. J. M. (2006). *Concrete Microstructure, Properties, and Materials* (3rd ed.). McGraw-Hill.

- Memon, F. A., Nuruddin, M. F., Demie, S., & Shafiq, N. (2011). Effect of Curing Conditions on Strength of Fly ash-based Self-Compacting Geopolymer Concrete. *International Journal of Civil and Environmental Engineering*, 5(8), 342–345. <https://doi.org/10.24200/sci.2017.2419>
- Mills, T. H., Showalter, E., & Jarman, D. (1999). A cost-effective waste management plan. *Cost Engineering*, 41(3), 35–43.
- Mo, B. H., Zhu, H., Cui, X. M., He, Y., & Gong, S. Y. (2014). Effect of curing temperature on geopolymerization of metakaolin-based geopolymers. *Applied Clay Science*, 99, 144–148. <https://doi.org/10.1016/j.clay.2014.06.024>
- Mohseni, E. (2018). Assessment of Na<sub>2</sub>SiO<sub>3</sub> to NaOH ratio impact on the performance of polypropylene fiber-reinforced geopolymer composites. *Construction and Building Materials*, 186, 904–911. <https://doi.org/10.1016/j.conbuildmat.2018.08.032>
- Moungam, L. M. B., Moohamed, H., Kamseu, E., Billong, N., & Melo, U. C. (2017). Properties of Geopolymers Made from Fired Clay Bricks Wastes and Rice Husk Ash (RHA)-Sodium Hydroxide (NaOH) Activator. *Materials Sciences and Applications*, 8(7).
- Mustafa Al Bakria, A. M., Kamarudin, H., Bin Hussain, M., Khairul Nizar, I., Zarina, Y., & Rafiza, A. R. (2011). The effect of curing temperature on physical and chemical properties of geopolymers. *Physics Procedia*, 22, 286–291. <https://doi.org/10.1016/j.phpro.2011.11.045>
- Myers, R. (2003). *The Basics of Chemistry*, 1st Edition, Greenwood Press, Westport, Connecticut.
- Oh, J. E., Monteiro, P. J. M., Jun, S. S., Choi, S., & Clark, S. M. (2010). The evolution of strength and crystalline phases for alkali-activated ground blast furnace slag and fly ash-based geopolymers. *Cement and Concrete Research*, 40(2), 189–196. <https://doi.org/10.1016/j.cemconres.2009.10.010>

- Ohno, M., & Li, V. C. (2014). A feasibility study of strain hardening fiber reinforced fly ash-based geopolymer composites. *Construction and Building Materials*, 57, 163–168. <https://doi.org/10.1016/j.conbuildmat.2014.02.005>
- Ouda, A. S., & Gharieb, M. (2020). Development the properties of brick geopolymer pastes using concrete waste incorporating dolomite aggregate. *Journal of Building Engineering*, 27(June 2019), 100919. <https://doi.org/10.1016/j.job.2019.100919>
- Palomo, A., Grutzeck, M. W., & Blanco, M. T. (1999). Alkali-activated fly ashes: A cement for the future. *Cement and Concrete Research*, 29(8), 1323–1329. [https://doi.org/10.1016/S0008-8846\(98\)00243-9](https://doi.org/10.1016/S0008-8846(98)00243-9)
- Pascual, A. B., Tognonvi, M. T., & Tagnit-hamou, A. (2014). WASTE GLASS POWDER-BASED ALKALI-ACTIVATED MORTAR. 15–19.
- Poulesquen, A., Frizon, F., & Lambertin, D. (2011). Rheological behavior of alkali-activated metakaolin during geopolymerization. *Journal of Non-Crystalline Solids*, 357(21), 3565–3571. <https://doi.org/10.1016/j.jnoncrysol.2011.07.013>
- Provis, J. L. (2009). Activating solution chemistry for geopolymers. In L. Provis, John & J. S. J. van Deventer (Eds.), *Geopolymers Structure, processing, properties and industrial applications* (pp. 53–55). Woodhead Publishing Limited.
- Provis, J. L., & Bernal, S. A. (2014). Geopolymers and related alkali-activated materials. *Annual Review of Materials Research*, 44, 299–327. <https://doi.org/10.1146/annurev-matsci-070813-113515>
- Provis, J. L., Fernandez-Jimenez, A., Kamseu, E., Leonelli, C., & Palomo, A. (2014). Binder Chemistry – Low-Calcium Alkali-Activated Materials. In Joh L Provis & van D. J. S. J (Eds.), *Alkali Activated Materials* (pp. 93–124).
- Provis, J. L., Lukey, G. C., & van Deventer, J. S. J. (2005). Do Geopolymers Actually Contain Nanocrystalline Zeolites? A Reexamination of Existing Results. *Chem.*

*Mater.*, 17(12), 3075–3085.

Provis, J. L., & van Deventer, J. S. J. (2007). Geopolymerisation kinetics. 2. Reaction kinetic modelling. *Chemical Engineering Science*, 62(9), 2318–2329. <https://doi.org/10.1016/j.ces.2007.01.028>

Provis, J. L., & van Deventer, J. S. J. (2009). *Geopolymers Structure, processing, properties and industrial applications*. Woodhead Publishing Limited.

Provis, J. L., Yong, C. Z., Duxson, P., & van Deventer, J. S. J. (2009). Correlating mechanical and thermal properties of sodium silicate-fly ash geopolymers. *Colloids and Surfaces A: Physicochemical and Engineering Aspects*, 336(1–3), 57–63. <https://doi.org/10.1016/j.colsurfa.2008.11.019>

Pu, X. C. (1991). Study on durability of alkali-slag concrete. *Int. Symp. on Concr. Engng*, 1144–1149.

Purdon, A. O. (1940). The action of alkalis on blast-furnace slag. *Journal of the Society of Chemical Industry*, 59, 191–202. <https://doi.org/10.1039/jr9270002819>

Qing-hua, C., Tagnit-hamou, A., & Sarkar, S. L. (1991). Strength and microstructural properties of water glass activated slag. *MRS Online Proceedings Library*, 245, 49–54.

Rattanasak, U., & Chindaprasirt, P. (2009). Influence of NaOH solution on the synthesis of fly ash geopolymer. *Minerals Engineering*, 22(12), 1073–1078. <https://doi.org/10.1016/j.mineng.2009.03.022>

Razak, R. A., Abdullah, M. M. A. B., Hussin, K., Ismail, K. N., Hardjito, D., & Yahya, Z. (2015). Optimization of NaOH molarity, LUSI mud/alkaline activator, and Na<sub>2</sub>SiO<sub>3</sub>/NaOH ratio to produce lightweight aggregate-based geopolymer. *International Journal of Molecular Sciences*, 16(5), 11629–11647. <https://doi.org/10.3390/ijms160511629>

Reig, L., Soriano, L., Borrachero, M. V., Monzó, J., & Payá, J. (2014). Influence of

the activator concentration and calcium hydroxide addition on the properties of alkali-activated porcelain stoneware. *Construction and Building Materials*, 63, 214–222. <https://doi.org/10.1016/j.conbuildmat.2014.04.023>

Reig, L., Tashima, M. M., Borrachero, M. V., Monzó, J., Cheeseman, C. R., & Payá, J. (2013). Properties and microstructure of alkali-activated red clay brick waste. *Construction and Building Materials*, 43, 98–106. <https://doi.org/10.1016/j.conbuildmat.2013.01.031>

Reinhardt, H. W., Jonkers, H., Van Tittelboom, K., Snoeck, D., De Belie, N., De Muynck, W., Verstraete, W., Wang, J., & Mechtcherine, V. (2013). Recovery against environmental action. In M. de Rooij, K. Van Tittelboom, N. De Belie, & E. Schlangen (Eds.), *Self-healing Phenomena in Cement-Based Materials* (p. 65).

Reinhardt, H. W., & Jooss, M. (2003). Permeability and self-healing of cracked concrete as a function of temperature and crack width. *Cement and Concrete Research*, 33(7), 981–985. [https://doi.org/10.1016/S0008-8846\(02\)01099-2](https://doi.org/10.1016/S0008-8846(02)01099-2)

Robayo-Salazar, R. A., Mejía-Arcila, J. M., & Mejía de Gutiérrez, R. (2017). Eco-efficient alkali-activated cement based on red clay brick wastes suitable for the manufacturing of building materials. *Journal of Cleaner Production*, 166, 242–252. <https://doi.org/10.1016/j.jclepro.2017.07.243>

Robayo-Salazar, R. A., Rivera, J. F., & Mejía de Gutiérrez, R. (2017). Alkali-activated building materials made with recycled construction and demolition wastes. *Construction and Building Materials*, 149, 130–138. <https://doi.org/10.1016/j.conbuildmat.2017.05.122>

Sahmaran, M., Li, M., & Li, V. C. (2007). Transport properties of engineered cementitious composites under chloride exposure. *ACI Materials Journal*, 104(6), 604–611. <https://doi.org/10.14359/18964>

Sahmaran, M., & Li, V. C. (2007). De-icing salt scaling resistance of mechanically loaded engineered cementitious composites. *Cement and Concrete Research*,

37(7), 1035–1046. <https://doi.org/10.1016/j.cemconres.2007.04.001>

Sahmaran, M., & Li, V. C. (2008). Durability of mechanically loaded engineered cementitious composites under highly alkaline environments. *Cement and Concrete Composites*, 30(2), 72–81. <https://doi.org/10.1016/j.cemconcomp.2007.09.004>

Sahmaran, M., Yücel, H. E., Demirhan, S., Arık, M. T., & Li, V. C. (2012). Combined Effect of Aggregate and Mineral Admixtures on Tensile Ductility of Engineered Cementitious Composites. *ACI Materials Journal*, 109(6), 627–638. <https://doi.org/10.14359/51684160>

Salas, D. A., Ramirez, A. D., Ulloa, N., Baykara, H., Boero, A. J. (2018). Life cycle assessment of geopolymer concrete. *Construction and Building Materials*, 190, 170–177

Shi, C. (1996). Strength, pore structure and permeability of alkali-activated slag mortars. *Cement and Concrete Research*, 26(12), 1789–1799. [https://doi.org/10.1016/S0008-8846\(96\)00174-3](https://doi.org/10.1016/S0008-8846(96)00174-3)

Shi, C., Krivenko, Pavel, V., & Roy, D. (2005). *Alkali-Activated Cements and Concretes*. Taylor & Francis.

Siad, H., Lachemi, M., Sahmaran, M., Mesbah, H. A., & Hossain, K. M. A. (2018). Use of recycled glass powder to improve the performance properties of high volume fly ash-engineered cementitious composites. *Construction and Building Materials*, 163, 53–62. <https://doi.org/10.1016/j.conbuildmat.2017.12.067>

Siddique, R. (2011). Effect of volcanic ash on the properties of cement paste and mortar. *Resources, Conservation and Recycling*, 56(1), 66–70. <https://doi.org/10.1016/j.resconrec.2011.09.005>

Silva, F. J., & Thaumaturgo, C. (2003). Fibre reinforcement and fracture response in geopolymeric mortars. *Fatigue and Fracture of Engineering Materials and Structures*, 26(2), 167–172. <https://doi.org/10.1046/j.1460-2695.2003.00625.x>



- Silva, G., Castañeda, D., Kim, S., Castañeda, A., Bertolotti, B., Ortega-San-Martin, L., Nakamatsu, J., & Aguilar, R. (2019). Analysis of the production conditions of geopolymer matrices from natural pozzolana and fired clay brick wastes. *Construction and Building Materials*, 215, 633–643. <https://doi.org/10.1016/j.conbuildmat.2019.04.247>
- Singh, B., Ishwarya, G., Gupta, M., & Bhattacharyya, S. K. (2015). Geopolymer concrete: A review of some recent developments. *Construction and Building Materials*, 85, 78–90. <https://doi.org/10.1016/j.conbuildmat.2015.03.036>
- Singh, S., Basavanagowda, S. N., Aswath, M. U., & Ranganath, R. V. (2016). Durability of Bricks Coated with Red mud Based Geopolymer Paste. *IOP Conference Series: Materials Science and Engineering*, 149(1). <https://doi.org/10.1088/1757-899X/149/1/012070>
- Sisomphon, K., Copuroglu, O., & Koenders, E. A. B. (2012). Self-healing of surface cracks in mortars with expansive additive and crystalline additive. *Cement and Concrete Composites*, 34(4), 566–574. <https://doi.org/10.1016/j.cemconcomp.2012.01.005>
- Sitarz, M., Urban, M., & Hager, I. (2020). Rheology and mechanical properties of fly ash-based geopolymer mortars with ground granulated blast furnace slag addition. *Energies*, 13(10). <https://doi.org/10.3390/en13102639>
- Somna, K., Jaturapitakkul, C., Kajitvichyanukul, P., & Chindaprasirt, P. (2011). NaOH-activated ground fly ash geopolymer cured at ambient temperature. *Fuel*, 90(6), 2118–2124. <https://doi.org/10.1016/j.fuel.2011.01.018>
- Spragg, R. P., Bu, Y., Snyder, K. A., Bentz, D. P., & Weiss, J. (2013). *Electrical Testing of Cement-Based Materials: Role of Testing Techniques, Sample Conditioning, and Accelerated Curing*. 23. <https://doi.org/10.5703/1288284315230>
- Suluguru, A. K., Surana, S. R., GuhaRay, A., Kar, A., & Muktinutalapati, J. (2019). Experimental Investigations on Building Derived Materials in Chemically

- Aggressive Environment as a Partial Replacement of Soil in Geotechnical Applications. *Geotechnical and Geological Engineering*, 37(2), 947–963. <https://doi.org/10.1007/s10706-018-0662-0>
- Sun, P., & Wu, H. C. (2008). Transition from brittle to ductile behavior of fly ash using PVA fibers. *Cement and Concrete Composites*, 30(1), 29–36. <https://doi.org/10.1016/j.cemconcomp.2007.05.008>
- Sun, Z., Cui, H., An, H., Tao, D., Xu, Y., Zhai, J., & Li, Q. (2013). Synthesis and thermal behavior of geopolymer-type material from waste ceramic. *Construction and Building Materials*, 49, 281–287. <https://doi.org/10.1016/j.conbuildmat.2013.08.063>
- Tashima, M. M., Soriano, L., Borrachero, M. V., Monzó, J., Cheeseman, C. R., & Payá, J. (2012). Alkali activation of vitreous calcium aluminosilicate derived from glass fiber waste. *Journal of Sustainable Cement-Based Materials*, 1(3), 83–93. <https://doi.org/10.1080/21650373.2012.742610>
- Tavira, J., Jiménez, J. R., Ledesma, E. F., López-Uceda, A., & Ayuso, J. (2020). Real-scale study of a heavy traffic road built with in situ recycled demolition waste. *Journal of Cleaner Production*, 248. <https://doi.org/10.1016/j.jclepro.2019.119219>
- UNEP Global Environmental Alert Service. (2012). Keeping Track of Our Changing Environment - From Rio to Rio +20 (1992-2012). *Environmental Development*, 3(May), 166–179. <https://doi.org/10.1016/j.envdev.2012.05.013>
- Vafaei, M., & Allahverdi, A. (2017). High strength geopolymer binder based on waste-glass powder. *Advanced Powder Technology*, 28(1), 215–222. <https://doi.org/10.1016/j.apt.2016.09.034>
- Vail, J. G., & Wills, J. H. (1952). *Soluble Silicates – Their Properties and Uses*. Reinhold Publishing Corporation.
- van Deventer, J. S. J., Provis, J. L., Duxson, P., & Lukey, G. C. (2007). Reaction

- mechanisms in the geopolymeric conversion of inorganic waste to useful products. *Journal of Hazardous Materials*, 139(3), 506–513. <https://doi.org/10.1016/j.jhazmat.2006.02.044>
- van Jaarsveld, J. G. S., van Deventer, J. S. J., & Lukey, G. C. (2002). The effect of composition and temperature on the properties of fly ash- and kaolinite-based geopolymers. *Chemical Engineering Journal*, 89, 63–73.
- Vásquez, A., Cárdenas, V., Robayo-Salazar, R. A., & de Gutiérrez, R. M. (2016). Geopolymer based on concrete demolition waste. *Advanced Powder Technology*, 27(4), 1173–1179. <https://doi.org/10.1016/j.apt.2016.03.029>
- Vijay, K., Murmu, M., & Deo, S. V. (2017). Bacteria based self healing concrete – A review. *Construction and Building Materials*, 152, 1008–1014. <https://doi.org/10.1016/j.conbuildmat.2017.07.040>
- Wahlstrom, M., Bergmans, J., Teittinen, T., Bacher, J., Smeets, A., & Paduart, A. (2020a). *Construction and Demolition Waste: challenges and opportunities in a circular economy*.
- Wahlstrom, M., Bergmans, J., Teittinen, T., Bacher, J., Smeets, A., & Paduart, A. (2020b). *Construction and Demolition Waste: challenges and opportunities in a circular economy*.
- Wang, R., Wang, J., Dong, T., & Ouyang, G. (2020). Structural and mechanical properties of geopolymers made of aluminosilicate powder with different SiO<sub>2</sub>/Al<sub>2</sub>O<sub>3</sub> ratio: Molecular dynamics simulation and microstructural experimental study. *Construction and Building Materials*, 240, 117935. <https://doi.org/10.1016/j.conbuildmat.2019.117935>
- Wang, S. D. (1991). Review of recent research on alkali-activated concrete in China. *Magazine of Concrete Research*, 43(154), 29–35. <https://doi.org/10.1680/mac.1992.44.159.137>
- Wang, S. D., Scrivener, K. L., & Pratt, P. L. (1994). Factors affecting the strength of

- alkali-activated slag. *Cement and Concrete Research*, 24(6), 1033–1043.  
[https://doi.org/10.1016/0008-8846\(94\)90026-4](https://doi.org/10.1016/0008-8846(94)90026-4)
- Weidema, B. (2000). Avoiding Co-Product Allocation in Life-Cycle Assessment. *Journal of Industrial Ecology*, 4(3), 11–33.
- Weil, M., Dombrowski, K., Buchwald, A. (2009). Life-cycle analysis of geopolymers. *Structures, Processing, Properties and Industrial Applications*, 194-210
- Xu, H., & Van Deventer, J. S. J. (2000). The geopolymerisation of alumino-silicate minerals. *International Journal of Mineral Processing*, 59(3), 247–266.  
[https://doi.org/10.1016/S0301-7516\(99\)00074-5](https://doi.org/10.1016/S0301-7516(99)00074-5)
- Yang, T., Yao, X., Zhang, Z., & Wang, H. (2012). Mechanical property and structure of alkali-activated fly ash and slag blends. *Journal of Sustainable Cement-Based Materials*, 1(4), 167–178.  
<https://doi.org/10.1080/21650373.2012.752621>
- Yip, C. K., Lukey, G. C., & Van Deventer, J. S. J. (2005). The coexistence of geopolymeric gel and calcium silicate hydrate at the early stage of alkaline activation. *Cement and Concrete Research*, 35(9), 1688–1697.  
<https://doi.org/10.1016/j.cemconres.2004.10.042>
- Yıldırım, G., Aras, G. H., Banyhussan, Q. S., Sahmaran, M., & Lachemi, M. (2015). Estimating the self-healing capability of cementitious composites through non-destructive electrical-based monitoring. *NDT and E International*, 76, 26–37.  
<https://doi.org/10.1016/j.ndteint.2015.08.005>
- Yunsheng, Z., Wei, S., Zongjin, L., Xiangming, Z., Eddie, & Chungkong, C. (2008). Impact properties of geopolymer based extrudates incorporated with fly ash and PVA short fiber. *Construction and Building Materials*, 22(3), 370–383.  
<https://doi.org/10.1016/j.conbuildmat.2006.08.006>
- Zeng, S., & Wang, J. (2016). Characterization of mechanical and electric properties

- of geopolymers synthesized using four locally available fly ashes. *Construction and Building Materials*, 121, 386–399.  
<https://doi.org/10.1016/j.conbuildmat.2016.06.011>
- Zhang, G., & Xu, J. (2010). Environmental and Uncertainty Assessment: Hazardous Industry Waste as Aggregate in Cement Production. *Advanced Materials Research*, 160–162, 373–378.  
<https://doi.org/10.4028/www.scientific.net/AMR.160-162.373>
- Zhang, J., Ding, L., Li, F., & Peng, J. (2020). Recycled aggregates from construction and demolition wastes as alternative filling materials for highway subgrades in China. *Journal of Cleaner Production*, 255, 120223.  
<https://doi.org/10.1016/j.jclepro.2020.120223>
- Zhang, M., Zhao, M., Zhang, G., El-Korchi, T., & Tao, M. (2017). A multiscale investigation of reaction kinetics, phase formation, and mechanical properties of metakaolin geopolymers. *Cement and Concrete Composites*, 78, 21–32.  
<https://doi.org/10.1016/j.cemconcomp.2016.12.010>
- Zhang, L. V., Suleiman, A. R., & Nehdi, M. L. (2020). Self-healing in fiber-reinforced alkali-activated slag composites incorporating different additives. *Construction and Building Materials*, 262(2020), 120059.  
<https://doi.org/10.1016/j.conbuildmat.2020.120059>
- Zhang, Z., Wang, H., Provis, J. L., & Reid, A. (2013). Efflorescence : A Critical Challenge for Geopolymer Applications ? *In Concrete Institute of Australia's Biennial National Conference*.
- Zhao, Q., Nair, B., Rahimian, T., & Balaguru, P. (2007). Novel geopolymer based composites with enhanced ductility. *Journal of Materials Science*, 42(9), 3131–3137. <https://doi.org/10.1007/s10853-006-0527-4>
- Zhao, X., Liu, C., Wang, L., Zuo, L., Zhu, Q., & Ma, W. (2019). Physical and mechanical properties and micro characteristics of fly ash-based geopolymers incorporating soda residue. *Cement and Concrete Composites*, 98(February),

125–136. <https://doi.org/10.1016/j.cemconcomp.2019.02.009>

Zhao, X., Liu, C., Zuo, L., Wang, L., Zhu, Q., & Wang, M. (2019). Investigation into the effect of calcium on the existence form of geopolymerized gel product of fly ash based geopolymers. *Cement and Concrete Composites*, *103*(October 2018), 279–292. <https://doi.org/10.1016/j.cemconcomp.2018.11.019>

Zhu, Y., Yang, Y., & Yao, Y. (2012). Autogenous self-healing of engineered cementitious composites under freeze-thaw cycles. *Construction and Building Materials*, *34*, 522–530. <https://doi.org/10.1016/j.conbuildmat.2012.03.001>

## CURRICULUM VITAE

### PERSONAL INFORMATION

Surname, Name : Ulugöl, Hüseyin  
Nationality : Turkish (TC)  
Date and Place of Birth : 17 June 1982, Kayseri  
Marital Status : Married  
Email : hu.ulugol@gmail.com

### EDUCATION

Degree	Institution	Year of Graduation
MS	Sakarya University Civil Engineering	2015
BS	Erciyes University Civil Engineering	2012
BS	Erciyes University Physics	2004
High School	Sümer High School, Kayseri	1999

### WORK EXPERIENCE

Year	Place	Enrollment
2015-Present	Hacettepe Uni. Dept. of Civil Eng.	Research Assistant
2012-2015	Sakarya Uni. Dept. of Civil Eng.	Research Assistant
2009 July	Limak Holding	Intern Eng. Student
2005-2008	Servus	Technician

### FOREIGN LANGUAGES

English

### PUBLICATIONS

1. Ulugöl H., Günel M.F., Yaman İ.Ö., Yıldırım G., Şahmaran M. "Effects of self-healing on the microstructure, transport, and electrical properties of 100% construction-and demolition-waste-based geopolymer composites" Cement & Concrete Composites, 121, 104081 (2021)
2. Ulugöl H., Kul A., Yıldırım G., Şahmaran M., Aldemir A., Figueira D., Ashour A. "Mechanical and microstructural characterization of geopolymers from assorted construction and demolition waste-based masonry and glass" Journal of Cleaner Production, 280, 124358 (2021)

3. Çelik D.N., Yıldırım G., Al-Dahawi, A., Ulugöl, H., Han, B., Şahmaran, M. “Self-monitoring of flexural fatigue damage in large-scale steel-reinforced cementitious composite beams” *Cement & Concrete Composites*, 123, 104183 (2021)
4. Yıldırım G., Öztürk O., Ulugöl H., Hatem H., Şahmaran M. “Determination of Autogenous Self-healing Capability of Cementitious Composites Through Non-destructive Testing” *RILEM Spring Convention and Conference*, 25-38 (2020)
5. Yıldırım G., Ulugöl H., Öztürk O., Şahmaran M., “Autogenous Self-healing Assessment of 1-Year-Old Cementitious Composites” *RILEM Spring Convention and Conference*, 39-48 (2020)
6. Bayer R., Ulugöl H., Demir İ., Yıldırım G., Şahmaran M. “Tasnif Edilmiş İnşaat Yıkıntı Atıklarından Elde Edilen Harman Tuğlası, Delikli Tuğla ve Çatı Kiremitinden Oluşan İkili Karışımların Geopolimer Hamur Üretiminde Değerlendirilmesi” *Çukurova Üniversitesi Mühendislik Fakültesi Dergisi*, 35 (1) 79 - 90 (2020)
7. Şahmaran M., Yıldırım G., Ulugöl H., Bozkurt H.B. “Otojen Kendini İyileştiren ECC Malzemelerde Tekrarlanabilirlik ve Tutarlılık” 10. Uluslararası Beton Kongresi, Bursa, 504-512, (2019)
8. Şahmaran M., Yıldırım G., Ulugöl H. “Effects of Hydrated Lime on Reproducibility and Extensiveness of Autogenous Self-healing Materials” *iSTE-CE'2019 İskenderun*, 895-904, (2019)
9. Ulugöl H., Yıldırım G., Coşkun O., Tolunay B., Şahmaran M. “Multi-functional Cementitious Composites with Autogenous Healing Functionality” 13<sup>th</sup> International Congress on Advances in Civil Engineering, İzmir, (2018)
10. İpek M., Yılmaz K., Gökçek, B., Ulugöl H., Akça K.R. “Bitüm Emdirilmiş Atık Mukavva Levhaların Asfalt Betonunda Kullanılabilirliğinin Araştırılması” *ISITES2015, Valencia*, 1832-1839 (2015)
11. Uysal M., Yılmaz K., Ulugöl H. “Betonarme Eleman Tipinin Sertleşmiş Betonun Dayanım Özelliklerine Etkisi” *ISITES2014, Karabük*, 989-998 (2014)
12. Uysal M., Yılmaz K., Ulugöl H. “Sıkıştırma İşleminin Betonarme Elemanların Sertleşmiş Betonun Dayanım Özelliklerine Etkisi” *ISITES2014, Karabük*, 979-988 (2014)